

UC Irvine

UC Irvine Electronic Theses and Dissertations

Title

Characterization of a Heme Degrading Enzyme from Mycobacterium tuberculosis

Permalink

<https://escholarship.org/uc/item/8vk0723j>

Author

Chao, Alex

Publication Date

2018

Supplemental Material

<https://escholarship.org/uc/item/8vk0723j#supplemental>

Copyright Information

This work is made available under the terms of a Creative Commons Attribution License, available at <https://creativecommons.org/licenses/by/4.0/>

Peer reviewed|Thesis/dissertation

UNIVERSITY OF CALIFORNIA,
IRVINE

Characterization of a Heme Degrading Enzyme from *Mycobacterium tuberculosis*

DISSERTATION

submitted in partial satisfaction of the requirements
for the degree of

DOCTOR OF PHILOSOPHY

in Biological Sciences

by

Alex Chao

Dissertation Committee:
Professor Celia W. Goulding, Chair
Professor Thomas L. Poulos
Professor Sheryl Tsai

2018

Chapter 2 was reproduced in part from Inorg. Chem. (2014). 10.1021/ic500033b
© American Chemical Society

Chapter 4 was reproduced in part from mBio (2016). 10.1128/mBio.01675-16
© American Society for Microbiology

All other materials © 2018 Alex Chao

TABLE OF CONTENTS

	Page
LIST OF FIGURES	iii
LIST OF TABLES	vi
ACKNOWLEDGMENTS	vii
CURRICULUM VITAE	viii
ABSTRACT OF THE DISSERTATION	xi
CHAPTER 1: Heme Uptake and Heme Degradation in <i>Mycobacterium tuberculosis</i> and Other Organisms	1
References	20
CHAPTER 2: The Role of Heme Ruffling in MhuD Heme Degradation	24
References	47
CHAPTER 3: A Single Mutation in the <i>Mycobacterium tuberculosis</i> Heme-Degrading Protein MhuD, Results in a Different Product	49
References	87
CHAPTER 4: Inhibition of In vivo <i>Mycobacterium tuberculosis</i> Infection with Tin-Protoporphyrin IX	91
References	104
CHAPTER 5: Towards the Identification and Characterization of MhuD Interaction Partners for Electron Donation and Product Release	106
References	125
CHAPTER 6: Closing Remarks and Future Directions - Understanding MhuD and its Role in Mtb Heme Uptake	130
References	134

LIST OF FIGURES

	Page	
Figure 1.1	Incidence map of extreme drug resistant Tuberculosis	3
Figure 1.2	Schematic of the <i>Serratia marscescences</i> heme uptake pathway	5
Figure 1.3	Schematic of the <i>Staphylococcus aureus</i> heme uptake pathway	6
Figure 1.4	Schematic of the proposed Mycobacterium tuberculosis (Mtb) heme uptake pathway	8
Figure 1.5	Structure of Heme oxygenase (HO) heme degradation product biliverdin	9
Figure 1.6	Reaction pathway for HO catalyzed heme degradation	10
Figure 1.7	Activation of HOs vs activation of P450s	11
Figure 1.8	Isomers of staphylobilin products from <i>S. aureus</i> heme degrading enzymes IsdG and IsdI	12
Figure 1.9	Structure of human heme oxygenase-1 (hHO-1)	13
Figure 1.10	Proposed mechanism for IsdG and IsdI heme degradation	14
Figure 1.11	Active site pockets of hHO-1 and of <i>S. aureus</i> heme degraders IsdG N7A and IsdI	15
Figure 1.12	Structures of mycobilin isomers from Mtb heme degrader MhuD	16
Figure 1.13	X-ray crystal structure of diheme form of MhuD	17
Figure 1.14	Proposed mechanism for MhuD heme degradation	18
Figure 2.1	A summary of reported enzymatic heme degradation	26
Figure 2.2	Electron distributions of the 2E_g and the $^2B_{2g}$ electronic states	28
Figure 2.3	X-ray crystal structure of MhuD-heme-CN	31
Figure 2.4	Degree of heme ruffling within heme degrading enzymes	32
Figure 2.5	Structural comparison of the active sites of MhuD-heme-CN and MhuD-diheme	33

Figure 2.6	Ribbon representation of the MhuD active site	34
Figure 2.7	Heme degradation assays with ascorbate as the electron donor	36
Figure 2.8	Heme degradation assays with cytochrome P450 reductase as the electron donor	36
Figure 2.9	Heme titration assays of wild type MhuD and its mutants	38
Figure 2.10	Heme off rate measurement of wild type MhuD and its mutants	39
Figure 2.11	Structural comparison of MhuD-heme-CN with IsdG N7A and IsdI	41
Figure 2.12	Relative energies molecular orbitals energies among different heme ruffling states	42
Figure 3.1	Structures of heme, biliverdin, and staphylobilin	51
Figure 3.2	Structures of MhuD heme degradation products mycobilin-a and mycobilin-b	52
Figure 3.3	Proximal view of MhuD active site	53
Figure 3.4	Heme degradation assays with heme orientating mutants	55
Figure 3.5	HPLC chromatogram from MhuD product purification	56
Figure 3.6	MhuD R26S degrades heme into biliverdin	58
Figure 3.7	Fragmentation spectra of MhuD R26S product	59
Figure 3.8	MhuD R26S does not produce carbon monoxide during heme degradation	60
Figure 3.9	MhuD R26S does not produce formic acid during heme degradation	61
Figure 3.10	MhuD R26S produces formaldehyde as its C1 product	62
Figure 3.11	Structure of MhuD R26S-diheme and of MhuD R26S-diMnPPiX	64
Figure 3.12	Structural comparison of the active sites of MhuD R26S-biliverdin with other MhuD structures	66
Figure 3.13	UV/vis spectra of MhuD WT and MhuD R26S	68
Figure 3.14	Comparison of resonance Raman spectra from MhuD WT and MhuD R26S monohemes	69

Figure 3.15	EPR spectroscopy of different heme degraders along with MhuD mutants	71
Figure 3.16	Proposed mechanism for MhuD R26S heme degradation	77
Figure 4.1	Administration of SnPPIX in conjunction with conventional antibiotic treatment accelerates pulmonary bacterial clearance in Mtb-infected mice	95
Figure 4.2	Tin-protoporphyrin IX (SnPPIX) inhibits hHO-1 heme degradation	97
Figure 4.3	MhuD cannot degrade SnPPIX	98
Figure 4.4	Tin-protoporphyrin IX (SnPPIX) does not inhibit MhuD heme degradation	99
Figure 5.1	Demonstration of the presence of a MhuD electron donor in mycobacterium	109
Figure 5.2	Sequence alignment of IruO with Mtb homolog TrxB2	110
Figure 5.3	Sequence alignment of NtrA with Mtb homolog Rv0306	110
Figure 5.4	TrxB2 is not a MhuD electron donor	111
Figure 5.5	Rv0306 does not appear to act as a MhuD electron donor	112
Figure 5.6	Expression study of LpqF in various different <i>E. coli</i> cells	113
Figure 5.7	Solubility test of LpqF in different purification buffers	114
Figure 5.8	Ni ²⁺ affinity purification of LpqF	115
Figure 5.9	Size exclusion chromatography of LpqF	116
Figure 5.S1	Sequence alignment of IruO with Mtb homolog Rv0628c	127
Figure 5.S2	Sequence alignment of IruO with Mtb homolog IpdB	127
Figure 5.S3	Sequence alignment of IruO with Mtb homolog Rv1432	128
Figure 5.S4	Sequence alignment of IruO with Mtb homolog GorA	128
Figure 5.S5	Sequence alignment of IruO with Mtb homolog Rv2997	129

LIST OF TABLES

		Page
Table 2.1	X-ray data collection and refinement statistics for the structural determination of MhuD-heme-CN	30
Table 2.2	Heme off rates of MhuD and mutants	39
Table 3.1	Estimated product yields from MhuD WT and mutants	59
Table 3.2	X-ray data collection and refinement statistics for the structural determination of MhuD R26S diheme, MhuD R26S di-MnPPIX, and MhuD R26S biliverdin	67
Table 3.3	Sign assignments from EPR spectroscopy of different heme degraders including MhuD mutants	71
Table 4.1	Examples of novel anti-TB host directed therapies	93
Table 5.1	Primers used in the expression vector construction of candidate electron donors and candidate product release protein	120

ACKNOWLEDGMENTS

I would like to thank everyone who have helped made this dissertation possible. In particular, I would like to thank my committee chair Professor Celia Goulding for the opportunity to do research in her lab as well as for her mentorship and guidance throughout my time in graduate school.

I would like to thank my other committee members, Professor Thomas L. Poulos and Professor Sheryl Tsai, for their input and insight.

I would like to thank everyone in the Goulding lab that has helped me progress through my research. Special thanks Dr. Nicholas Chim and Dr. Robert Morse for their mentorship on how to work with MhuD as well as for helping me understand X-ray crystallography.

I would like to acknowledge the Cellular and Molecular Biosciences Program as well as NSF Graduate Research Fellowship Program for their generous financial support for the duration of graduate school.

I would like to acknowledge the undergraduates that have assisted me in my research: Yugi Liu, Dan Nguyen, and Ervin Irimpan.

Finally, I would like to thank my friends and family for their support in graduate school.

CURRICULUM VITAE

Alex Chao

EDUCATION

University of California, Irvine (UCI) June 2018
Doctor of Philosophy, Biochemistry, 3.9 GPA
Cellular & Molecular Biosciences Gateway Program

Arizona State University (ASU) June 2012
Bachelor of Science, Chemistry, Minors in Biology & Mathematics, 3.9 GPA
Dean's List

PROFESSIONAL EXPERIENCE

NSF Graduate Research Fellow September 2012 – Present
University of California, Irvine, California

- Characterized unusual *Mycobacterium Tuberculosis* heme degrading enzyme MhuD and 4 mutants using various different biochemical, biophysical, and structural methods such as X-ray crystallography, Raman, EPR, reaction assays
- Determined the 5 co-crystal structures heme degrading enzymes with various ligands including heme and heme analogs and solved the structure of a novel iron uptake protein
- Mentored 4 graduate students and 3 undergraduate students as lab lead for various projects investigating *Mycobacterium Tuberculosis* iron and heme uptake pathways
- Ensured 100% compliance resulting in 0 mishaps over 5 years and performed routine maintenance for optimal performance of key lab instruments
- Lectured classes with 300+ students in biochemistry and molecular biology

Helios Scholar June 2012 – July 2012

Translational Genomics Research Institute, Phoenix, Arizona

- Developed novel phosphopeptide enrichment protocol for mass spectrometry-based proteomics for biomedical research
- Validated the effectiveness of an 3rd party instrument at tissue preservation for posttranslational modification studies

WSU Summer Undergraduate Research Fellow May 2011 – August 2011

Wayne State University, Detroit, Michigan

- Constructed viral vector for transfection into mammalian cells for experiments
- Identified insulin stimulated or suppressed phosphorylation sites via HPLC-MS/MS

Undergraduate Student Researcher

May 2009 – May 2012

Arizona State University, Tempe, Arizona

- Maintained L6 myotubes, HEK 293, and modified CHO mammalian cells for experiments
- Collected, organized, and maintained sensitive and confidential volunteer data for clinical studies
- Performed highly sensitive mass spectrometry-based proteomics experiments under the direction of PI and overseeing postdoctoral scholar
- Performed preliminary studies to validate the effect of insulin-stimulation on site specific protein phosphorylation
- Identified binding sites of glycosaminoglycan chondroitin-4-sulfate on novel cell surface adhesion protein from *Borrelia burgdorferi* using NMR techniques

PUBLICATIONS

- **Chao, A.**, Oswald, V.F., Goulding, C.W. Reduced heme ruffling in *Mycobacterium tuberculosis* heme degrading enzyme MhuD alters products. (Manuscript in preparation)
- **Chao, A.**, Sieminski, P.J., Goulding, C.W. Single mutation, different product for MhuD, the *Mycobacterium tuberculosis* heme-degrading protein. (Manuscript in preparation)
- **Chao, A.**, Sieminski, P.J., Owens, C.P., Goulding, C.W. Targeting iron uptake pathways for therapeutic intervention in TB. Chem. Rev. (In Review)
- Thakuri, B., Graves, A.B., **Chao, A.**, Johansen, S.L., Goulding, C.W., Liptak, M.D. Characterization of heme binding by heme degrading enzyme MhuD (In review)
- Costa, D.L., Namasivayam, S., Amaral, E.P., Arora, K., **Chao, A.**, Mittereder, L.R., Maiga, M., Boshoff, H.I., Barry, C.E., III, Goulding, C.W., Andrade, B.B., Sher, A. Pharmacological inhibition of host heme oxygenase-1 suppresses *Mycobacterium tuberculosis* infection in vivo by a mechanism dependent on T lymphocytes. mBio, 2016, 7(5), e01675-16.
- Graves, A., Morse, R.P., **Chao, A.**, Iniguez, A., Goulding, C.W., Liptak, M.D. Crystallographic and Spectroscopic Insights into Heme Degradation by *Mycobacterium tuberculosis* MhuD. Inorg Chem, 2014, 53(12), 5931-5940.
- Pham, K., Langlais, P., Zhang, X., **Chao, A.**, Zingsheim, M., Yi, Z. Insulin-stimulated phosphorylation of protein phosphatase 1 regulatory subunit 12B revealed by HPLC-ESI-MS/MS. Proteome Sci, 2012, 10(1), 52.
- **Chao, A.**, Zhang, X., Ma, D., Langlais, P., Luo, M., Mandarino, L.J., Zingshelm, M., Pham, K., Dillon, J., Yi, Z. Site-specific phosphorylation of protein phosphatase 1 regulatory subunit 12A stimulated or suppressed by insulin. J Proteomics, 2012, 75(11), 3342-3350.

AWARDS AND FELLOWSHIPS

National Science Foundation Graduate Research Fellowship

2013 - 2017

Cellular and Molecular Biosciences Fellowship, University of California, Irvine

2012 - 2013

Summa Cum Laude, Arizona State University

2012

WSU College of Pharmacy & Health Sciences Summer Undergraduate Research Fellowship

2011

School of Life Sciences Undergraduate Research (SOLUR) Program - Researcher

2009 – 2011

President's Scholarship

2008 – 2012

POSTER PRESENTATIONS

- **Chao, A.**, Morse, R.P., Mitra, K., Green, M.T., Goulding, C.W. Single mutation, different product for MhuD, the *Mycobacterium tuberculosis* heme-degrading protein. Spring 2016 Southern California BioInorganic Meeting (2017), Irvine, CA.

- **Chao, A.**, Goulding, C.W. Single mutation, different product for MhuD, the *Mycobacterium tuberculosis* heme-degrading protein. UCI Department of Molecular Biology and Biochemistry Department Retreat (2017), Lake Arrowhead, CA.
- **Chao, A.**, Morse, R., Goulding, C.W. Characterization of the *Mycobacterium tuberculosis* heme-degrading protein, MhuD. UCI Pharmaceutical Sciences-Ewha Women's University College of Pharmacy Joint Symposium (2016), Irvine, CA.
- **Chao, A.**, Morse, R., Chim, N., Iniguez, A., Goulding, C.W. Structural and Biochemical analysis of *Mycobacterium tuberculosis* heme degrading enzyme. UCI Department of Molecular Biology and Biochemistry Retreat (2014), Lake Arrowhead, CA.
- **Chao, A.**, Zingsheim, M., Thangiah, G., Pham, K., Yi, Z. Analysis of Protein Phosphatase 1 Regulatory Subunit 12A Phosphorylation. School of Life Sciences Undergraduate Research Symposium (2011), Tempe, AZ.
- **Chao, A.**, Zingsheim, M., Thangiah, G., Pham, K., Yi, Z. Phosphorylation of protein phosphatase 1 regulatory subunit 12A. Arizona Physiological Society (2010), Phoenix, AZ.
- **Chao, A.**, Dillon, J., Pham, K., Yi, Z. Use of HPLC-ESI-MS/MS to Identify Possible Novel IRS-1 interaction Partners. School of Life Sciences Undergraduate Research Symposium (2010), Tempe, AZ.

TEACHING EXPERIENCE

Graduate Teaching Assistant, University of California, Irvine, California

AIDS Fundamentals

Fall 2014

Molecular Biology Lab

Fall 2014/Winter 2015

Biochemistry Lecture

Winter 2015

Molecular Biology Lecture

Spring 2015

Microbiology Lab

Spring 2015

ABSTRACT OF THE DISSERTATION

Characterization of a Heme Degrading Enzyme from *Mycobacterium tuberculosis*

By

Alex Chao

Doctor of Philosophy in Biological Sciences

University of California, Irvine, 2018

Professor Celia W. Goulding, Chair

Iron is important for pathogen survival and pathogens such as *Mycobacterium tuberculosis* (Mtb) have evolved pathways to acquire host iron. One such mechanism Mtb has evolved is the acquisition of heme, where Mtb imports host heme for degradation and iron release. In the cytosol, the heme degrading enzyme MhuD is responsible for the cleavage of heme and the liberation iron for use by Mtb. In this work we document our ongoing efforts to better understand MhuD and its larger role in Mtb.

Although the structure of the inactive diheme form of MhuD was previously determined, the structure of its active monoheme form was unresolved. We were able to determine the crystal structure of the cyano-derivative of MhuD-monoheme to obtain insights into MhuD heme degradation and product uniqueness. Heme ruffling, proposed to be responsible for heme's reactivity within the active site of MhuD homologs, was observed in the MhuD-monoheme structure. Mutations to apparent heme ruffling residues Phe23 and Trp66 appear to abolish MhuD's heme degradation activity suggesting the importance of heme ruffling in MhuD activity. Residues were also identified potentially responsible for MhuD's unique degradation products. We found that mutation of one such residue, Arg26

into a serine, alters MhuD's heme degradation into biliverdin and formaldehyde. Efforts to biophysically and structurally characterize the MhuD R26S mutant suggests that there is a reduction in heme ruffling in the mutant which may lead to the altered degradation product.

We also explored the role MhuD plays in the pharmacological inhibition of Mtb growth of mice infected with Mtb by the heme analog tin-protoporphrin IX (SnPPIX). Despite its ability to inhibit the human heme degrader, heme oxygenase, SnPPIX did not appear to inhibit MhuD's ability to degrade heme. Lastly, we also carried out preliminary research towards the identification of a MhuD electron donor as well as of a potential protein partner for MhuD product release. To date, neither proposed MhuD interaction partners have been identified, however more candidate proteins remain to be purified and tested.

CHAPTER 1

Heme Uptake and Heme Degradation in *Mycobacterium tuberculosis* and Other Organisms

Tuberculosis

Tuberculosis (TB) is one of the most deadly, infectious diseases known to man. Prior to the advent of anti-TB drugs, a TB diagnosis was considered a death sentence¹. TB is caused by *Mycobacterium tuberculosis* (Mtb), a slow-growing, pathogenic bacterium¹. Mtb has evolved multiple mechanisms to evade host immune defenses, often times the bacterium moves into a latent dormant state within a host². In the early to mid-1900's, TB was a major public health concern with scores of patients sent to isolated resorts for quarantine and treatment¹. Inspired by the discovery of penicillin, the first anti-TB drug streptomycin was discovered in 1943 from *Streptomyces griseus*¹. Other anti-TB drugs would soon follow leading to the near eradication of TB¹. However, with the rise of AIDS in the 1980's, TB cases reemerged³. Today, TB is responsible for approximately 1.4 million deaths annually⁴. Additionally, it is estimated that one-third of the world's population is infected with latent TB, where patients are infected with Mtb, but do not present symptoms⁵.

Current treatments for TB

Following the development of streptomycin in 1943, an array of anti-TB drugs were developed. These drugs are administered together as a drug cocktail and in accordance with guidelines set forth by the World Health Organization (WHO)⁶. First line drugs such as isoniazid, rifampicin, pyrazinamide, ethambutol, and streptomycin are used in the standard cocktail to treat TB patients⁶. However, if the patient has a drug resistant TB infection, then second line drugs are administered⁶. Second line drugs are divided into five categories: group 1 (first-line oral agents), group 2 (injectable agents), group 3 (fluoroquinolones), group 4 (oral bacteriostatic second-line agents), and group 5 (agents with unclear roles in treatment of drug resistant-TB)⁶. The usual TB treatment regime lasts more than 6 months, and up to 18 months for drug resistant forms⁶. Unfortunately, many anti-TB drugs come with harsh side effects or cause medical complications (i.e. liver damage), which combined with the prolonged treatment time can result in therapeutic non-compliance by patients and the development of drug resistant strains⁶.

Emergence of drug resistant TB

Drug resistance in TB is on the rise. Cases of multidrug resistant TB (MDR-TB) that are resistant to first-line anti-TB drugs, isoniazid and rifampin, have emerged. More concerning, however, is the emergence of extensively drug resistant TB (XDR-TB), which like MDR-TB are resistant to isoniazid and rifampin, but also fluoroquinolone and a second-generation anti-TB drugs (such as amikacin, kanamycin, or capreomycin). According to the WHO, cases

of XDR-TB have been documented around the world in both industrialized and unindustrialized countries (**Figure 1.1**). This emergence and spread of MDR-TB and XDR-TB is a major concern, necessitating the development of new classes of anti-TB therapeutics.

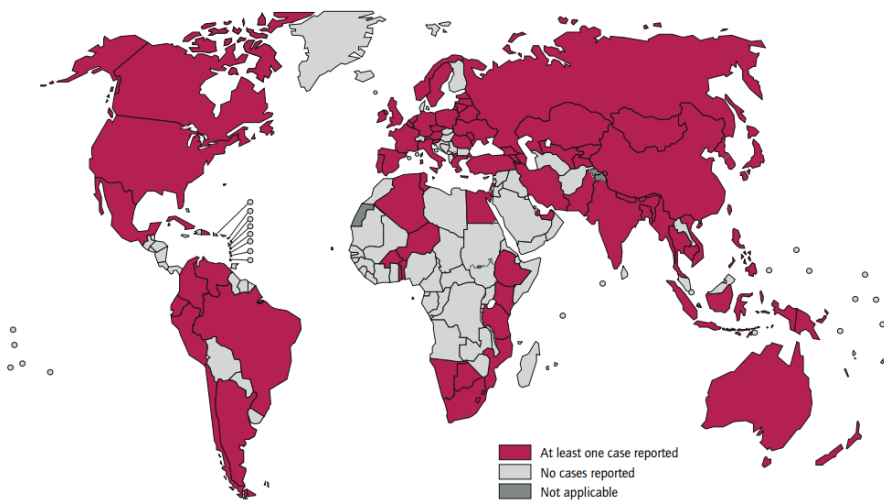


Figure 1.1 Incidence map of XDR-TB as of 2011 from the WHO⁷. Countries in magenta have reported to have at least one case of XDR-TB.

Targeting Iron Assimilation

Iron is essential for the survival of nearly all living organisms including pathogens⁸⁻¹⁰. Because of its unique catalytic properties, iron is a common cofactor for many enzymes¹¹. Iron is found in many protein families including oxidoreductases, hydrolases, lyases and isomerases¹². Iron-containing proteins are involved in many important metabolic processes such as ATP synthesis. Because of the importance of iron in essential biological functions, many bacteria have evolved pathways to acquire host iron. However, the majority of iron—80% of iron in the host—is in the form of heme. Consequently, in addition to evolving iron

acquisition pathways, pathogens have also evolved heme uptake pathways to access this large otherwise untapped reservoir of iron. Like many other pathogens, Mtb has the ability to acquire host heme-iron¹³. Thus, because of its role in Mtb iron acquisition, the Mtb heme uptake pathway is a potential target for novel anti-TB drugs.

Heme uptake in other bacteria

A number of different heme uptake pathways have been reported in both Gram-positive and Gram-negative bacteria such as *Staphylococcus aureus*, *Bacillus anthracis*, and *Serratia marscescences*¹⁴. One of the best characterized heme uptake pathways is that of the Gram-negative *S. marscescences*¹⁴. This pathway utilizes a bipartite heme acquisition system (Has) common throughout Gram-negative bacteria¹⁵. This system, encoded by the *has* operon (**Figure 1.2**), utilizes the hemophore HasA to scavenge heme from host hemoproteins in an affinity driven process¹⁵⁻¹⁷. Next, heme is transferred to TonB-dependent outer membrane transporter (HasR) and imported into the cytosol in a process involving a HasB/ExbB/ExbD import complex^{15, 18, 19}. In this proton motive force driven process, HasR transports heme across the outer membrane. The HasA TonB box of HasR interacts with the periplasmic domain of a TonB homolog HasB allowing for heme transfer to HasB^{15, 19}.

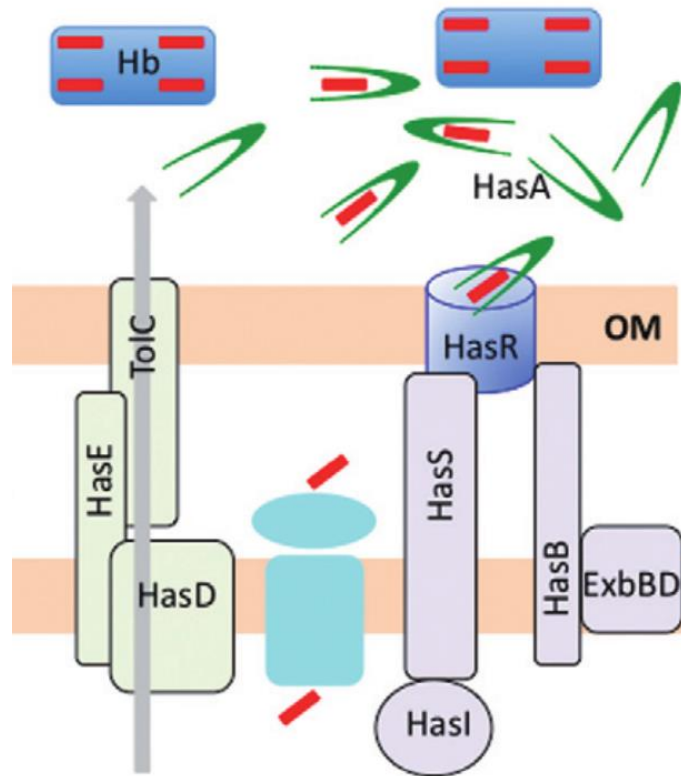


Figure 1.2 Schematic of the *S. marcescens* heme uptake pathway²⁰. Secreted hemophore HasA scavenges heme from host hemoproteins and transfers the heme to the TonB-dependent outer membrane transporter HasR, which imports heme across the outer membrane with the assistance of TonB analog HasB and auxiliary proteins ExbB and ExbD.

Another well-characterized heme uptake pathway is the *S. aureus* iron-regulated surface determinant (Isd) pathway (**Figure 1.3**)^{21, 22}. Many of the proteins in the Isd pathway (IsdA, IsdB, IsdC, IsdH) feature the Near Iron Transport domain fold (NEAT domain), which are immunoglobulin-like folds commonly found in heme uptake pathways of Gram-positive bacteria^{23, 24}. These NEAT domains mediate heme extraction from host heme proteins or heme transfer inside the bacteria^{23, 24}. In the *S. aureus* heme uptake pathway (**Figure 1.3**), NEAT domains on surface receptors IsdB and IsdH capture heme from host hemoglobin^{25, 26}. The captured heme is shuttled through the cell wall by a heme transfer cascade from IsdB

and IsdH onto IsdA and then IsdC via NEAT-NEAT interactions²⁷. Then IsdC transfer heme to IsdE, a membrane tethered lipoprotein²⁸. Heme is then transferred to the ABC permease, IsdF, for transport across the cell membrane using energy derived from ATP-hydrolysis²⁷. Once in the cytosol, heme is degraded by IsdG and IsdI into staphylobilin isomers (**Figure 1.8**)²⁹, formaldehyde³⁰, and ferrous iron. Recently, it has been shown that IruO, a FAD-containing NADPH-dependent reductase, provides electrons for *S. aureus* heme degradation³¹.

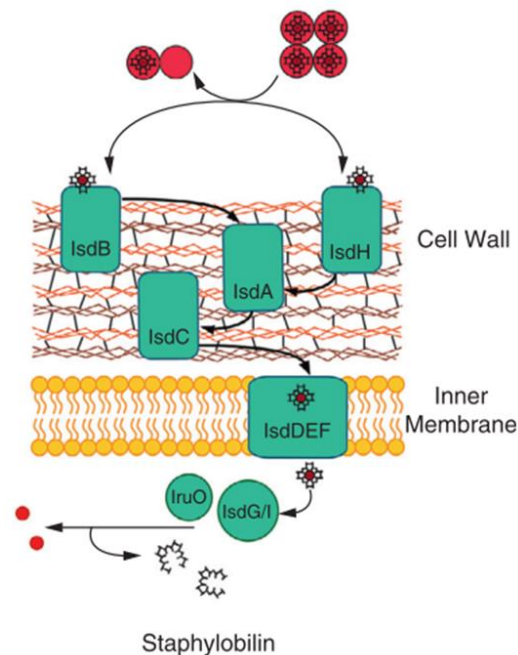


Figure 1.3 Schematic of the *S. aureus* heme uptake pathway¹⁴. Here, heme is captured from host heme proteins by IsdB and IsdH and transferred through the cell wall via IsdA and IsdC. Next, the heme is passed through the periplasmic space and the cell membrane in a process involving IsdDEF proteins. Finally, heme is degraded by IsdG and IsdI.

Mtb heme uptake pathway

Mtb has a heme uptake pathway, which could be a potential anti-TB drug target (**Figure 1.4**)¹³. The mechanism of mycobacterial heme uptake is still being unraveled; however, it is known to involve proteins encoded by the genomic region Rv0202c-Rv0207c¹³. In this pathway, it has been proposed that heme is acquired from host hemoproteins and involves the secreted hemophore Rv0203¹³. It is unknown how Rv0203-heme complex traverses the mycobacterial outer membrane; however Rv0203 can transfer its heme cargo onto the periplasmic soluble domains of the inner membrane transport proteins MmpL3 and MmpL11^{13, 32}. Once heme is imported across the inner member to the Mtb cytosol, heme is degraded by the mycobacterial heme utilization degrader (MhuD) into mycobilin isomers (**Figure 1.12**) and ferrous iron^{33, 34}.

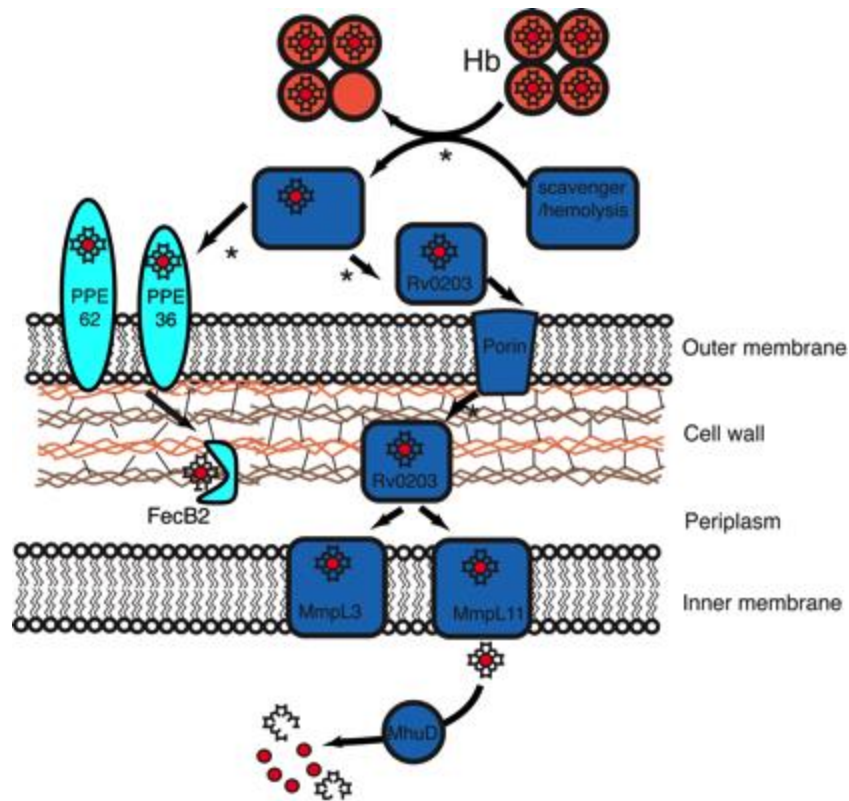


Figure 1.4 Schematic of the proposed Mtb heme uptake pathway.

More recently, Mitra et al. have identified several new proteins that may play a role in Mtb heme uptake (**Figure 1.4**)³⁵. These proteins, PPE36 (Rv2108), PPE62 (Rv3533c), and FecB2 (Rv0265c), were identified in transposon mutant screens by searching for mutants resistant to Ga(III)-protoporphyrin IX³⁵, a heme analog toxic to Mtb^{13, 35}. PPE36, PPE62, and FecB2 are thought to localize to the outer membrane, while Rv0265c is thought to localize to the periplasmic space³⁵. Initial characterization using surface plasmon resonance (SPR) suggest that these proteins are capable of binding heme albeit in the low millimolar to high micromolar range³⁵. The roles of these proteins in Mtb heme uptake are still being unraveled; however, based on predictions and experimental results, it is hypothesized that heme is captured by PPE36 for transport by outer membrane receptor PPE62³⁵. Periplasmic

siderophore binding protein FecB2 is thought to transport heme to an yet-to-be-identified heme receptor in the inner membrane³⁵. Together, PPE36 (Rv2108), PPE62 (Rv3533c), and FecB2 (Rv0265c) may play a role in Mtb heme uptake, however experimental verification is required³⁵.

Heme oxygenases

The canonical heme degrading protein, heme oxygenase (HO) (**Figure 1.9A**), has been extensively studied. In humans and several bacteria including *Corynebacterium diphtheriae* and *Neisseria Meningitidis*, heme oxygenase (HO) is responsible for the degradation of heme into biliverdin IX α (**Figure 1.5**), carbon monoxide (CO) and ferrous iron³⁶⁻³⁹.

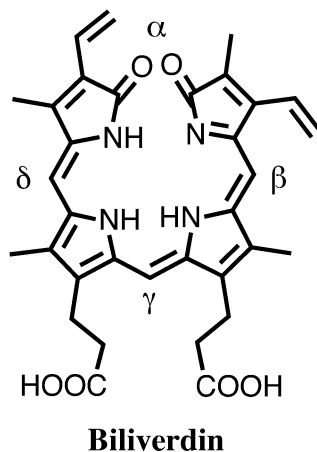


Figure 1.5 Structure of HO heme degradation product biliverdin.

The mechanism for heme degradation by HO occurs via three successive mono-oxygenation steps (**Figure 1.6**)⁴⁰. During HO heme degradation, first heme is hydroxylated at the α -meso carbon into α -mesohydroxyheme^{41, 42}, and then oxidized into α -verdoheme combined with

CO⁴³. This process has been shown to occur spontaneously even outside of HOs⁴⁴. In the third and final step, the α -verdoheme is oxidized to produce the final product biliverdin⁴⁵.

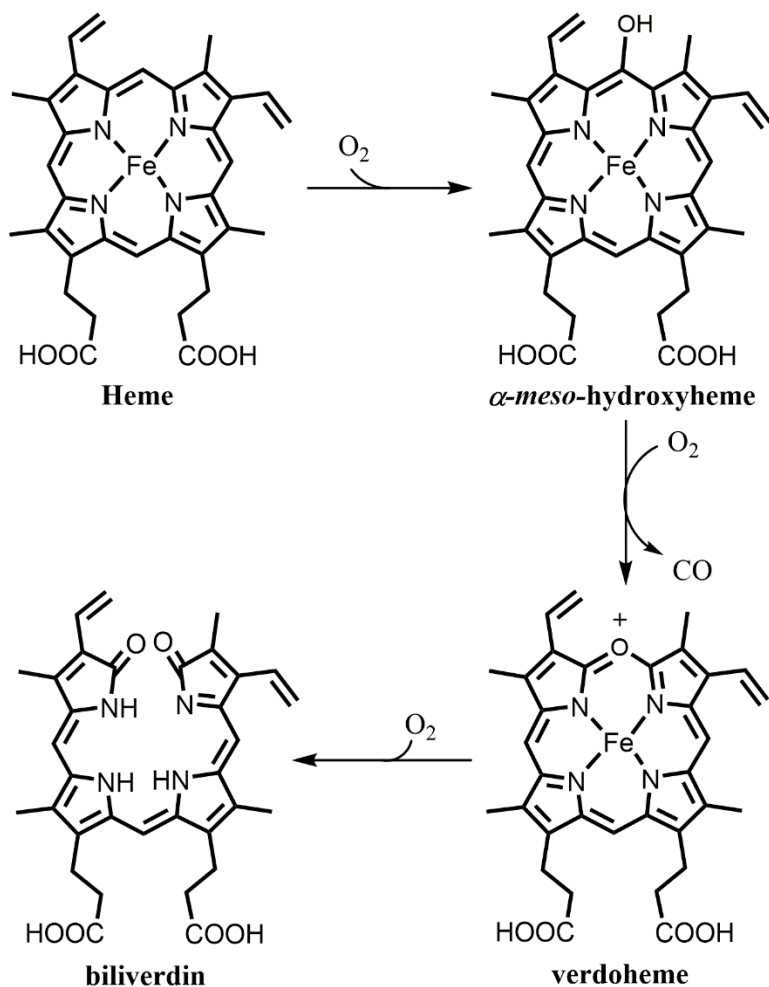


Figure 1.6 Reaction pathway for HO catalyzed heme degradation. The HO heme substrate is oxygenated into hydroxyheme, then into verdoheme, before finally into biliverdin, in a total of three successive oxygenation reactions.

Substrate hydroxylation in the first and third steps of heme degradation occur via activation of molecular oxygen by the substrate iron center⁴⁰. This is a process similar to P450 activation where the heme ferric iron center is reduced to its ferrous iron while coordinating molecular oxygen (**Figure 1.7**)^{40, 46}.

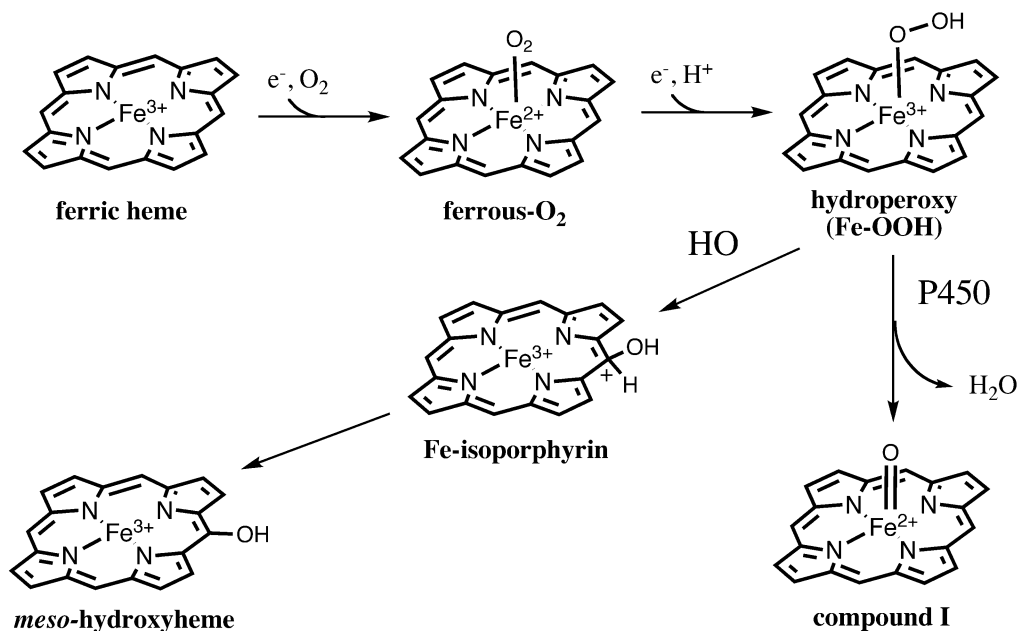


Figure 1.7 Activation of HO vs activation of P450s. Both P450s and HO generate a ferric hydroperoxyl [Fe(III)-OOH] species before diverging into their separate pathways.

In the second step of HO activation, ferrous-O₂ heme is further reduced into a ferric hydroperoxyl [Fe(III)-OOH] species⁴⁰. Cleavage of the hydroperoxyl [Fe(III)-OOH] species then occurs resulting in substrate hydroxylation in a yet-to-be-determined mechanism⁴⁰. Close examination of the human heme oxygenase-1 (hHO-1) crystal structure reported by Schuller et. al. reveals a distal network of water molecules that may stabilize the ferric hydroperoxyl [Fe(III)-OOH] species (**Figure 1.11A**)⁴⁷. Disruption of this network of water molecules within the vicinity of the HO active site via mutagenesis abolishes or diminishes the heme degrading properties of HO^{48, 49}. Further illustrating the importance of this network of water molecules, experiments by Davydov *et al* show that a water molecule is required for donating a proton to ferrous-O₂ heme allowing for substrate hydroxylation⁵⁰.

IsdG/I heme degradation

Other types of heme degrading enzymes have been reported in the literature. First among this non-canonical heme degrading enzymes and most characterized are the *S. aureus* IsdG and IsdI heme degraders, which degrade heme into staphylobilin isomers (**Figure 1.8**)²⁹, formaldehyde³⁰, and ferrous iron.

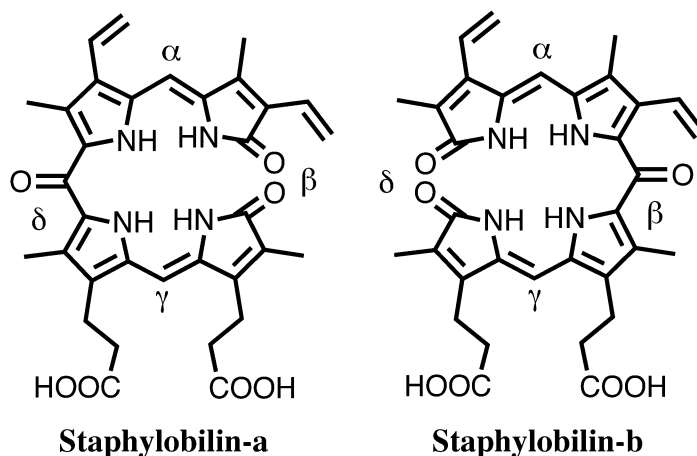


Figure 1.8 Isomers of staphylobilin products from *S. aureus* heme degrading enzymes IsdG and IsdI. IsdG and IsdI cleaves heme at either the β- or δ-meso carbon while oxidizing the other meso carbon.

These Isd-type heme degrading enzymes are structurally distinct from HO proteins^{51, 52}. While HO proteins are composed of solely α-helices (**Figure 1.9A**)⁴⁷, Isd-type proteins forms a homodimer with a ferredoxin-like α + β-barrel fold (**Figure 1.9B**)^{51, 52}.

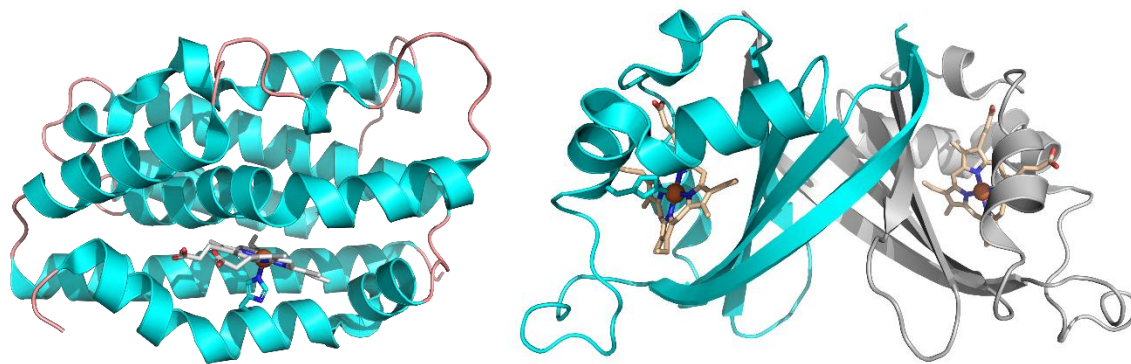


Figure 1.9 Structures of human heme oxygenase-1 (hHO-1, PDB: 1N45)⁴⁷ (A) and IsdI (PDB: 3LGN)⁵² (B). Despite both heme degrading enzymes, hHO-1 and IsdI share no structural homology.

The differences in protein structure and heme degradation products suggest that the Isd-type enzyme utilize a different degradation mechanism than that of HO. The details of IsdG/I heme degradation are still being worked out, however thus far, time resolved mass spectrometry experiments suggest that IsdG/I oxidizes heme into β/δ -meso-hydroxyheme and then into formyl-oxo-bilin⁵³. The formyl-oxo-bilin intermediate is converted into staphylobilin isomers through the spontaneous loss of formaldehyde (**Figure 1.10**)⁵³.

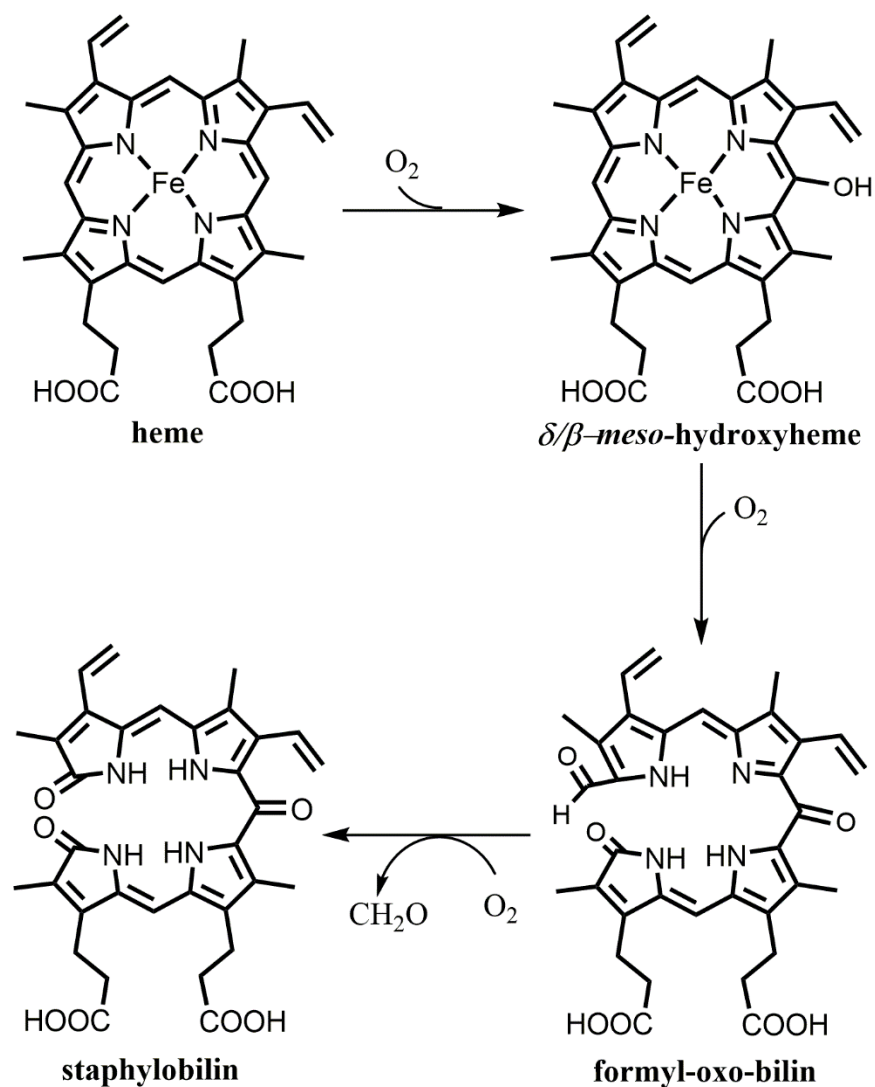


Figure 1.10 Proposed mechanism for IsdG and IsdI heme degradation⁵³.

Whereas HOs have a network of water molecules to assist in heme oxygenation⁴⁷, examination of IsdG/I structures reveal an absence of water molecules in the active site pocket suggesting an alternative mechanism for substrate oxidation than that of HOs⁵². Furthermore, both the IsdG/I structures reveals that bound heme is distorted or ruffled (**Figure 1.11**)⁵². While the heme in the rat HO structure is distorted only by 0.6 Å⁴⁷, the heme in the IsdG N7A and IsdI crystal structures are distorted by 1.9 and 2.3 Å, respectively⁵². NMR

experiments by Takayama et al. show that the observed heme ruffling appears to alter the electronic structure of heme, possibly sensitizing the heme meso-carbons to a nucleophilic attack⁵⁴. Density functional theory (DFT) calculations and hydrogen peroxide shunt experiments suggest this proposed nucleophilic attack occurs via the formation of a ferric-peroxo [Fe(III)-OO⁻] species and not the ferric-hydroperoxy [Fe(III)-OOH] species observed in HOs⁵⁵.

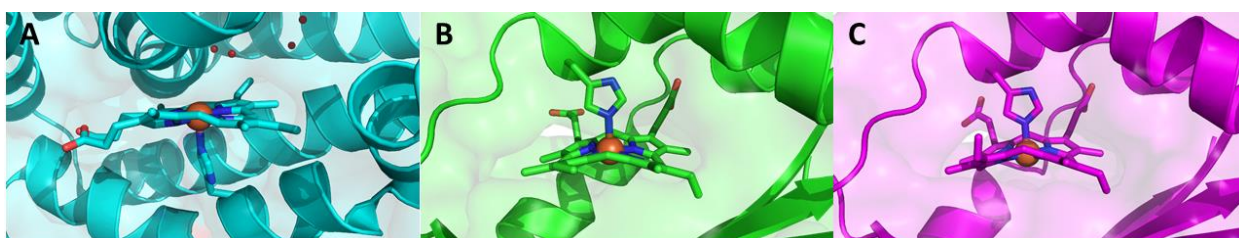


Figure 1.11 Active site pockets of hHO-1 (PDB: 1N45)⁴⁷ (A) and of *S. aureus* heme degraders IsdG N7A (PDB: 2ZDO) (B) and IsdI (PDB: 3LGN)⁵² (C). Distinct loss of heme planarity is observed in B and C.

The role of heme ruffling in IsdG/I heme degradation was further demonstrated via mutational studies. Mutation of the IsdG/I Trp-66, which makes a hydrophobic interaction with the heme protoporphyrin ring, resulted in a reduction of heme ruffling as well as a reduction in heme degradation activity⁵⁶. This loss in heme degradation activity is correlated to the bulkiness of the substituted residue⁵⁶. Additionally, mutation of Trp-66 also reverses alterations to the heme electronic structure⁵⁶. Together, this evidence suggests that heme ruffling in IsdG/I plays an important role in heme's reactivity in the active site⁵⁶.

MhuD heme degradation

Another Isd-type heme degrading protein is the Mtb heme degrading enzyme MhuD^{33, 57}. MhuD shares high sequence and structural homology with *S. aureus* IsdG/I heme degraders^{33, 57}, however, MhuD degrades heme into unique mycobilin isomers³⁴ (**Figure 1.12**) and free ferrous iron. Additionally, unlike IsdG-like proteins, MhuD is capable of binding two heme molecules in its active site, but is enzymatically inactive in its MhuD-diheme form³³. Thus far, only the structure of the diheme form of MhuD has been solved (**Figure 1.13**)³³

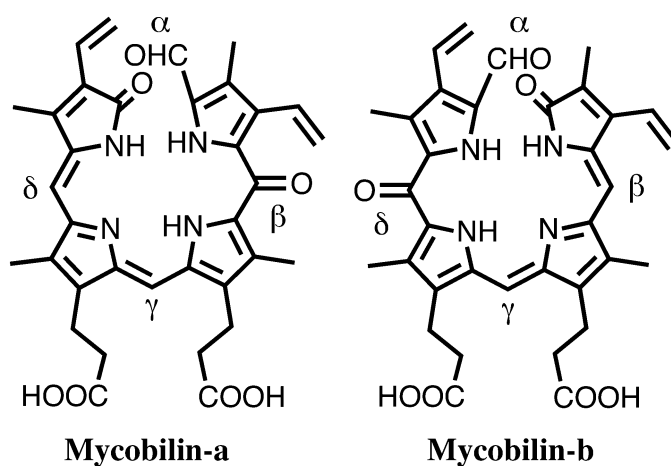


Figure 1.12 Structures of mycobilin isomers from Mtb heme degrader MhuD³⁴. MhuD cleaves and oxidizes heme at the α -meso carbon while also oxidizing the β - or δ -meso carbon.

Similar to IsdG/I, MhuD forms a homodimer with a ferredoxin-like $\alpha + \beta$ -barrel fold (**Figure 1.13**)^{33, 57}. In the MhuD-diheme structure, the two hemes are stacked one upon another with their propionate groups rotated approximately 80 degrees from one another³³. The iron of the solvent exposed heme is coordinated by His75 while the iron of the solvent protected heme is coordinated by a chloride ion³³. Minimal heme distortion was observed for both

hemes in the MhuD-diheme structure³³. While the hemes in IsdG N7A and IsdI crystal structures are distorted by 1.9 Å and 2.3 Å respectively⁵², the hemes in the MhuD-diheme structure were only distorted by 0.7 Å³³. This dramatic difference in heme ruffling may be responsible for inhibition of MhuD upon binding the second heme³³.

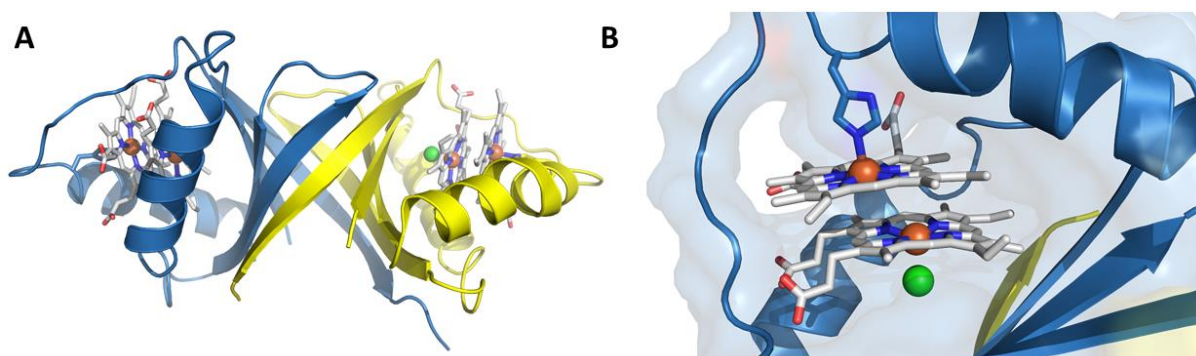


Figure 1.13 X-ray crystal structure of diheme form of MhuD (PDB: 3HX9)³³. (A) Ribbon representation of the dimeric MhuD-diheme. (B) Active site pocket MhuD-diheme.

Initial studies suggest that MhuD degrades heme in a similar mechanism to that of IsdI (Figure 1.14)⁵⁸. MhuD is proposed to oxidize heme into β/δ -meso-hydroxyheme intermediate via formation of a ferric-peroxo [Fe(III)-OO⁻] species⁵⁸. Then, the β/δ -meso-hydroxyheme is thought to undergo radical localization to the α -meso carbon before dioxygenation at the α -meso position into a dioxetane intermediate⁵⁸. Finally, dioxetane intermediate is proposed to spontaneously decompose into Fe-mycobilin⁵⁸.

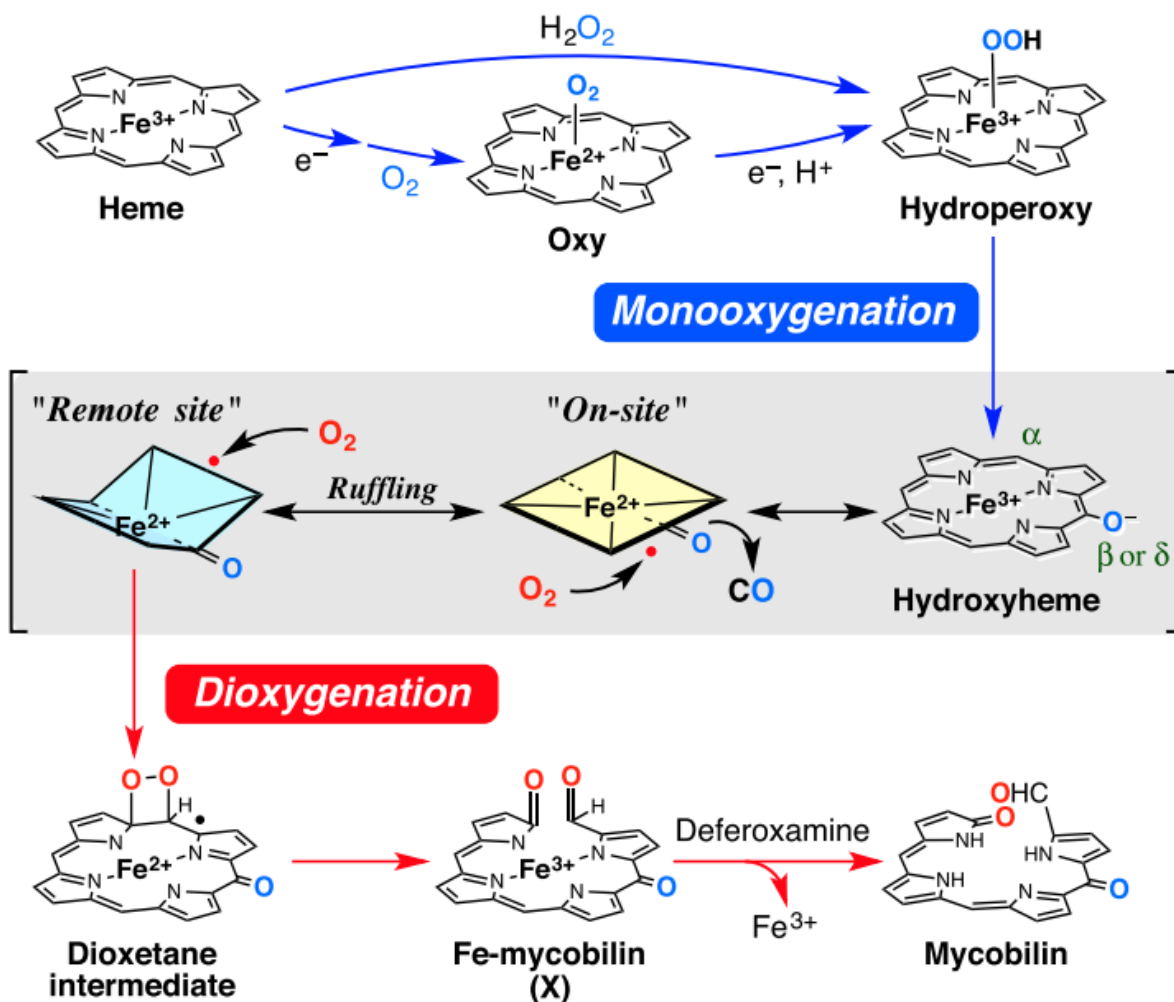


Figure 1.14 Proposed mechanism for MhuD heme degradation⁵⁸.

Although MhuD has been well characterized, much remains unknown about MhuD. The work presented herein details progress made toward a better understanding of MhuD. In Chapter 2, we describe the determination of cyanide inhibited MhuD-mono-heme structure, and discuss mutational analyses of residue that play a role in MhuD heme ruffling. In Chapter 3 we discuss a single mutation that produces a different heme degradation product. In Chapter 4, we examine the role of hHO-1 and MhuD in human Mtb infection. We demonstrate that adjunctive administration of the heme analog tin-protoporphyrin IX (SnPPiX) inhibits Mtb

growth in mice. In Chapter 5, we discuss preliminary work done towards identification of a MhuD electron donor as well as towards understanding of MhuD product release. Together, this work reveals factors important for MhuD heme degradation and product uniqueness as well as identifies potential MhuD protein partners.

References

- [1] Gazit, C. (2015) The Forgotten Plague, In *American Experience*, Boston, Ma.
- [2] Kiran, D., Podell, B. K., Chambers, M., and Basaraba, R. J. (2016) Host-directed therapy targeting the Mycobacterium tuberculosis granuloma: a review, *Semin Immunopathol* 38, 167-183.
- [3] Phillips, L. (2013) Infectious disease: TB's revenge, *Nature* 493, 14-16.
- [4] Organization, W. H. (2016) Global Tuberculosis Report, p 214, World Health Organization, Geneva, Switzerland.
- [5] Organization, W. H. (2017) Global Tuberculosis Report, p 262, World Health Organization, Geneva, Switzerland.
- [6] Organization, W. H. (2010) Treatment of tuberculosis Guidelines, 4th ed., World Health Organization, Geneva, Switzerland.
- [7] Organization, W. H. (2012) Global Tuberculosis Report 2012, p 100, World Health Organization, Geneva, Switzerland.
- [8] Cairo, G., Bernuzzi, F., and Recalcati, S. (2006) A precious metal: Iron, an essential nutrient for all cells, *Genes Nutr* 1, 25-39.
- [9] Skaar, E. P. (2010) The battle for iron between bacterial pathogens and their vertebrate hosts, *PLoS Pathog* 6, e1000949.
- [10] Doherty, C. P. (2007) Host-pathogen interactions: the role of iron, *J Nutr* 137, 1341-1344.
- [11] Outten, F. W., and Theil, E. C. (2009) Iron-based redox switches in biology, *Antioxid Redox Signal* 11, 1029-1046.
- [12] Andreini, C., Bertini, I., Cavallaro, G., Holliday, G. L., and Thornton, J. M. (2008) Metal ions in biological catalysis: from enzyme databases to general principles, *J Biol Inorg Chem* 13, 1205-1218.
- [13] Tullius, M. V., Harmston, C. A., Owens, C. P., Chim, N., Morse, R. P., McMath, L. M., Iniguez, A., Kimmey, J. M., Sawaya, M. R., Whitelegge, J. P., Horwitz, M. A., and Goulding, C. W. (2011) Discovery and characterization of a unique mycobacterial heme acquisition system, *Proc Natl Acad Sci U S A* 108, 5051-5056.
- [14] Contreras, H., Chim, N., Credali, A., and Goulding, C. W. (2014) Heme uptake in bacterial pathogens, *Curr Opin Chem Biol* 19, 34-41.
- [15] Ghigo, J. M., Letoffe, S., and Wandersman, C. (1997) A new type of hemophore-dependent heme acquisition system of *Serratia marcescens* reconstituted in *Escherichia coli*, *J Bacteriol* 179, 3572-3579.
- [16] Izadi, N., Henry, Y., Haladjian, J., Goldberg, M. E., Wandersman, C., Delepierre, M., and Lecroisey, A. (1997) Purification and characterization of an extracellular heme-binding protein, HasA, involved in heme iron acquisition, *Biochemistry* 36, 7050-7057.
- [17] Letoffe, S., Ghigo, J. M., and Wandersman, C. (1994) Iron acquisition from heme and hemoglobin by a *Serratia marcescens* extracellular protein, *Proc Natl Acad Sci U S A* 91, 9876-9880.
- [18] Letoffe, S., Deniau, C., Wolff, N., Dassa, E., Delepelaire, P., Lecroisey, A., and Wandersman, C. (2001) Haemophore-mediated bacterial haem transport: evidence for a common or overlapping site for haem-free and haem-loaded haemophore on its specific outer membrane receptor, *Mol Microbiol* 41, 439-450.

- [19] Benevides-Matos, N., Wandersman, C., and Biville, F. (2008) HasB, the *Serratia marcescens* TonB paralog, is specific to HasR, *J Bacteriol* 190, 21-27.
- [20] Wandersman, C., and Delepelaire, P. (2012) Haemophore functions revisited, *Mol Microbiol* 85, 618-631.
- [21] Skaar, E. P., and Schneewind, O. (2004) Iron-regulated surface determinants (Isd) of *Staphylococcus aureus*: stealing iron from heme, *Microbes Infect* 6, 390-397.
- [22] Mazmanian, S. K., Skaar, E. P., Gaspar, A. H., Humayun, M., Gornicki, P., Jelenska, J., Joachmiak, A., Missiakas, D. M., and Schneewind, O. (2003) Passage of heme-iron across the envelope of *Staphylococcus aureus*, *Science* 299, 906-909.
- [23] Andrade, M. A., Ciccarelli, F. D., Perez-Iratxeta, C., and Bork, P. (2002) NEAT: a domain duplicated in genes near the components of a putative Fe³⁺ siderophore transporter from Gram-positive pathogenic bacteria, *Genome Biol* 3, RESEARCH0047.
- [24] Grigg, J. C., Ukpabi, G., Gaudin, C. F., and Murphy, M. E. (2010) Structural biology of heme binding in the *Staphylococcus aureus* Isd system, *J Inorg Biochem* 104, 341-348.
- [25] Torres, V. J., Pishchany, G., Humayun, M., Schneewind, O., and Skaar, E. P. (2006) *Staphylococcus aureus* IsdB is a hemoglobin receptor required for heme iron utilization, *J Bacteriol* 188, 8421-8429.
- [26] Pilpa, R. M., Fadeev, E. A., Villareal, V. A., Wong, M. L., Phillips, M., and Clubb, R. T. (2006) Solution structure of the NEAT (NEAr Transporter) domain from IsdH/HarA: the human hemoglobin receptor in *Staphylococcus aureus*, *J Mol Biol* 360, 435-447.
- [27] Hammer, N. D., and Skaar, E. P. (2011) Molecular mechanisms of *Staphylococcus aureus* iron acquisition, *Annu Rev Microbiol* 65, 129-147.
- [28] Muryoi, N., Tiedemann, M. T., Pluym, M., Cheung, J., Heinrichs, D. E., and Stillman, M. J. (2008) Demonstration of the iron-regulated surface determinant (Isd) heme transfer pathway in *Staphylococcus aureus*, *J Biol Chem* 283, 28125-28136.
- [29] Reniere, M. L., Ukpabi, G. N., Harry, S. R., Stec, D. F., Krull, R., Wright, D. W., Bachmann, B. O., Murphy, M. E., and Skaar, E. P. (2010) The IsdG-family of haem oxygenases degrades haem to a novel chromophore, *Mol Microbiol* 75, 1529-1538.
- [30] Matsui, T., Nambu, S., Ono, Y., Goulding, C. W., Tsumoto, K., and Ikeda-Saito, M. (2013) Heme degradation by *Staphylococcus aureus* IsdG and IsdI liberates formaldehyde rather than carbon monoxide, *Biochemistry* 52, 3025-3027.
- [31] Loutet, S. A., Kobylarz, M. J., Chau, C. H., and Murphy, M. E. (2013) IruO is a reductase for heme degradation by IsdI and IsdG proteins in *Staphylococcus aureus*, *J Biol Chem* 288, 25749-25759.
- [32] Owens, C. P., Chim, N., Graves, A. B., Harmston, C. A., Iniguez, A., Contreras, H., Liptak, M. D., and Goulding, C. W. (2013) The *Mycobacterium tuberculosis* secreted protein Rv0203 transfers heme to membrane proteins MmpL3 and MmpL11, *J Biol Chem* 288, 21714-21728.
- [33] Chim, N., Iniguez, A., Nguyen, T. Q., and Goulding, C. W. (2010) Unusual diheme conformation of the heme-degrading protein from *Mycobacterium tuberculosis*, *J Mol Biol* 395, 595-608.
- [34] Nambu, S., Matsui, T., Goulding, C. W., Takahashi, S., and Ikeda-Saito, M. (2013) A new way to degrade heme: the *Mycobacterium tuberculosis* enzyme MhuD catalyzes heme degradation without generating CO, *J Biol Chem* 288, 10101-10109.

- [35] Mitra, A., Speer, A., Lin, K., Ehrt, S., and Niederweis, M. (2017) PPE Surface Proteins Are Required for Heme Utilization by *Mycobacterium tuberculosis*, *MBio* 8.
- [36] Tenhunen, R., Marver, H. S., and Schmid, R. (1969) Microsomal heme oxygenase. Characterization of the enzyme, *J Biol Chem* 244, 6388-6394.
- [37] Schmitt, M. P. (1997) Utilization of host iron sources by *Corynebacterium diphtheriae*: identification of a gene whose product is homologous to eukaryotic heme oxygenases and is required for acquisition of iron from heme and hemoglobin, *J Bacteriol* 179, 838-845.
- [38] Wilks, A., and Schmitt, M. P. (1998) Expression and characterization of a heme oxygenase (Hmu O) from *Corynebacterium diphtheriae*. Iron acquisition requires oxidative cleavage of the heme macrocycle, *J Biol Chem* 273, 837-841.
- [39] Zhu, W., Wilks, A., and Stojiljkovic, I. (2000) Degradation of heme in gram-negative bacteria: the product of the hemO gene of *Neisseriae* is a heme oxygenase, *J Bacteriol* 182, 6783-6790.
- [40] Matsui, T., Unno, M., and Ikeda-Saito, M. (2010) Heme oxygenase reveals its strategy for catalyzing three successive oxygenation reactions, *Acc Chem Res* 43, 240-247.
- [41] Wilks, A., Torpey, J., and Ortiz de Montellano, P. R. (1994) Heme oxygenase (HO-1). Evidence for electrophilic oxygen addition to the porphyrin ring in the formation of alpha-meso-hydroxyheme, *J Biol Chem* 269, 29553-29556.
- [42] Davydov, R. M., Tadashi, Y., Ikeda-Saito, M., and Hoffman, B. M. (1999) Hydroperoxy-Heme Oxygenase Generated by Cryoreduction Catalyzes the Formation of α -meso-Hydroxyheme as Detected by EPR and ENDOR, *Journal of the American Chemical Society* 121, 10656-10657.
- [43] Yoshida, T., Noguchi, M., and Kikuchi, G. (1982) The step of carbon monoxide liberation in the sequence of heme degradation catalyzed by the reconstituted microsomal heme oxygenase system, *J Biol Chem* 257, 9345-9348.
- [44] Morishima, I., Fujii, H., Shiro, Y., and Sano, S. (1995) Studies on the Iron(II) meso-Oxyporphyrin π -Neutral Radical as a Reaction Intermediate in Heme Catabolism, *Inorganic Chemistry* 34, 1528-1535.
- [45] Saito, S., and Itano, H. A. (1982) Verdohemochrome IX alpha: preparation and oxidoreductive cleavage to biliverdin IX alpha, *Proc Natl Acad Sci U S A* 79, 1393-1397.
- [46] Poulos, T. L. (2005) Structural biology of heme monooxygenases, *Biochem Biophys Res Commun* 338, 337-345.
- [47] Schuller, D. J., Wilks, a., Ortiz de Montellano, P. R., and Poulos, T. L. (1999) Crystal structure of human heme oxygenase-1, *Nature structural biology* 6, 860-867.
- [48] Liu, Y., Koenigs Lightning, L., Huang, H., Moenne-Loccoz, P., Schuller, D. J., Poulos, T. L., Loehr, T. M., and Ortiz de Montellano, P. R. (2000) Replacement of the distal glycine 139 transforms human heme oxygenase-1 into a peroxidase, *J Biol Chem* 275, 34501-34507.
- [49] Lightning, L. K., Huang, H., Moenne-Loccoz, P., Loehr, T. M., Schuller, D. J., Poulos, T. L., and de Montellano, P. R. (2001) Disruption of an active site hydrogen bond converts human heme oxygenase-1 into a peroxidase, *J Biol Chem* 276, 10612-10619.
- [50] Davydov, R., Kofman, V., Fujii, H., Yoshida, T., Ikeda-Saito, M., and Hoffman, B. M. (2002) Catalytic mechanism of heme oxygenase through EPR and ENDOR of

- cryoreduced oxy-heme oxygenase and its Asp 140 mutants, *J Am Chem Soc* 124, 1798-1808.
- [51] Wu, R., Skaar, E. P., Zhang, R., Joachimiak, G., Gornicki, P., Schneewind, O., and Joachimiak, A. (2005) Staphylococcus aureus IsdG and IsdI, heme-degrading enzymes with structural similarity to monooxygenases, *J Biol Chem* 280, 2840-2846.
- [52] Lee, W. C., Reniere, M. L., Skaar, E. P., and Murphy, M. E. (2008) Ruffling of metalloporphyrins bound to IsdG and IsdI, two heme-degrading enzymes in Staphylococcus aureus, *J Biol Chem* 283, 30957-30963.
- [53] Streit, B. R., Kant, R., Tokmina-Lukaszewska, M., Celis, A. I., Machovina, M. M., Skaar, E. P., Bothner, B., and DuBois, J. L. (2016) Time-resolved Studies of IsdG Protein Identify Molecular Signposts along the Non-canonical Heme Oxygenase Pathway, *J Biol Chem* 291, 862-871.
- [54] Takayama, S. J., Ukpabi, G., Murphy, M. E., and Mauk, A. G. (2011) Electronic properties of the highly ruffled heme bound to the heme degrading enzyme IsdI, *Proc Natl Acad Sci U S A* 108, 13071-13076.
- [55] Takayama, S. J., Loutet, S. A., Mauk, A. G., and Murphy, M. E. (2015) A Ferric-Peroxo Intermediate in the Oxidation of Heme by IsdI, *Biochemistry* 54, 2613-2621.
- [56] Ukpabi, G., Takayama, S. J., Mauk, A. G., and Murphy, M. E. (2012) Inactivation of the heme degrading enzyme IsdI by an active site substitution that diminishes heme ruffling, *J Biol Chem* 287, 34179-34188.
- [57] Graves, A. B., Morse, R. P., Chao, A., Iniguez, A., Goulding, C. W., and Liptak, M. D. (2014) Crystallographic and spectroscopic insights into heme degradation by Mycobacterium tuberculosis MhuD, *Inorg Chem* 53, 5931-5940.
- [58] Matsui, T., Nambu, S., Goulding, C. W., Takahashi, S., Fujii, H., and Ikeda-Saito, M. (2016) Unique coupling of mono- and dioxygenase chemistries in a single active site promotes heme degradation, *Proc Natl Acad Sci U S A*.

CHAPTER 2

The Role of Heme Ruffling in MhuD Heme Degradation

Abstract

Mycobacterium heme utilization degrader (MhuD) is a heme-degrading protein from *Mycobacterium tuberculosis* (Mtb) responsible for extracting the essential nutrient iron from host-derived heme. MhuD has been previously shown to produce unique organic products compared to those of canonical heme oxygenases (HOs) as well as those of the IsdG/I heme-degrading enzymes from *Staphylococcus aureus*. Here, we report the X-ray crystal structure of cyanide-inhibited MhuD (MhuD-heme-CN). There is no evidence for an ordered network of water molecules on the distal side of the heme substrate in the X-ray crystal structure, as was previously reported for canonical HOs. The degree of heme ruffling in the crystal structure of MhuD is greater than that observed for HO and less than that observed for IsdI. Furthermore, the degree of heme ruffling in MhuD is consistent with changes in relative energies between the $^2B_{2g}$ ground electronic state, which has a $(d_{xz}, d_{yz})^4(d_{xy})^1$ electronic configuration, and the 2E_g excited electronic state, which has a $(d_{xy})^2(d_{xz}, d_{yz})^3$ electronic configuration. Mutation of residues Trp-66 and Phe-23 thought to play a role in MhuD heme ruffling abolishes MhuD heme activity. Together, the data suggest that out of plane distortion of the heme in MhuD changes the electronic structure of heme and is essential to MhuD's heme degradation properties.

Introduction

Although MhuD from *Mycobacterium tuberculosis* (Mtb) degrades heme to non-heme iron and organic by-products, the enzyme has features that distinguish it from human heme oxygenases (hHOs)^{1,2}. Whereas hHOs adopt an all α -helical fold^{3,4}, the catalytically-inactive, diheme-bound form of MhuD (MhuD-diheme) has a ferredoxin-like β -barrel fold⁵. The structure of MhuD-diheme is more similar to heme degrading enzymes from *Staphylococcus aureus*, IsdG and IsdI⁶. However, MhuD is also distinct from these enzymes. The organic by-products of MhuD-catalyzed heme degradation are unique (**Figure 2.1**). MhuD cleaves the porphyrin ring of heme at the α -meso carbon, and this carbon is retained as an aldehyde group in the final “mycobilin” product⁷. In humans, the porphyrin ring is converted to biliverdin and carbon monoxide (CO) by hHOs, while *S. aureus*, IsdG and IsdI convert the porphyrin ring to staphylobilins⁸, and formaldehyde⁹. Since MhuD generates unique enzymatic products as compared to hHOs, IsdG, or IsdI, the reaction must proceed via a unique mechanism.

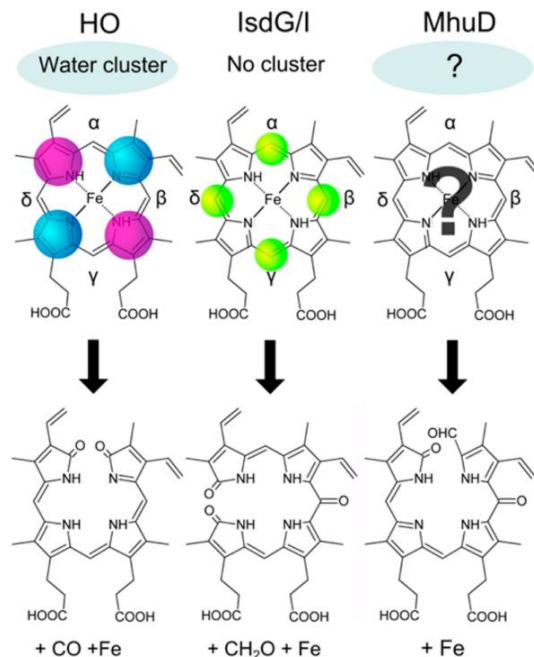


Figure 2.1 HO has an ordered network of active site water molecules on the distal side of the heme substrate and is believed to stabilize a 2E_g electronic state, where spin density is delocalized onto the porphyrin pyrrole rings (violet and blue circles represent the two components of this degenerate state), producing biliverdin, CO, and iron as products. *S. aureus* IsdI has been proposed to stabilize a ${}^2B_{2g}$ state, with spin density delocalized onto the α -, β -, γ -, and δ -meso carbons (green circles), without a defined network of water molecules en route to staphylobilin and formaldehyde formation. *M. tuberculosis* MhuD degrades heme to mycobilin and iron, but prior to this work, the active site and electronic structures were unknown.

Based upon Raman, electron paramagnetic resonance (EPR), UV/Vis absorption (Abs), and nuclear magnetic resonance (NMR) spectroscopy results, Ikeda-Saito has proposed that MhuD-catalyzed heme degradation proceeds through hydroperoxyheme and α -meso hydroxyheme intermediates, but bypasses verdoheme, en route to "mycobilin" formation⁷. The first steps of this proposed mechanism (binding of molecular oxygen, reduction to hydroperoxy, and hydroxylation of the α -meso carbon) are identical to the generally accepted mechanism of hHO-catalyzed heme degradation¹⁰. For hHOs, EPR and Mössbauer spectroscopic data¹¹, and density functional theory (DFT)-based hybrid quantum mechanical/molecular mechanical (QM/MM) calculations¹², have led researchers to

conclude that the enzyme active site stabilizes an $S = 1/2$, $(d-xy)^2(dxz,dyz)^3$ Fe(III)-hydroperoxy state (**Figure 2.1**). An ordered network of active site water molecules on the distal side of the heme substrate, first characterized in solution by NMR spectroscopy^{13, 14}, stabilizes the hydroperoxy ligand allowing for the stepwise homolytic cleavage of the hydroperoxy O–O bond followed by barrier-free attack of the α -meso carbon by the resulting hydroxyl radical.

There remain at least two mechanistic questions regarding the MhuD-catalyzed transformation of heme to α -mesohydroxyheme. First, in the generally accepted mechanism of hHO-catalyzed O–O bond cleavage, the homolysis proceeds through a $(dxy)^2(dxz,dyz)^3$ (2E_g) state^{11, 12}. However, Murphy and Mauk have proposed that the heme degradation reaction catalyzed by *S. aureus* IsdI, structurally more similar to MhuD than hHO, proceeds through a $(dxz,dyz)^4(dxy)^1$ (${}^2B_{2g}$) state^{15, 16}. These 2E_g and ${}^2B_{2g}$ states have different electron and spin density distributions and, thus, different reactivities (**Figure 2.2**). Second, there is no evidence for an ordered network of active site water molecules on the distal side of heme to control the regioselectivity of porphyrin hydroxylation in the available X-ray crystal structures of heme-bound IsdG or IsdI¹⁵⁻¹⁷. These data have led to their proposal that *S. aureus* IsdI compensates for the missing network of water molecules by stabilizing the ${}^2B_{2g}$ state.

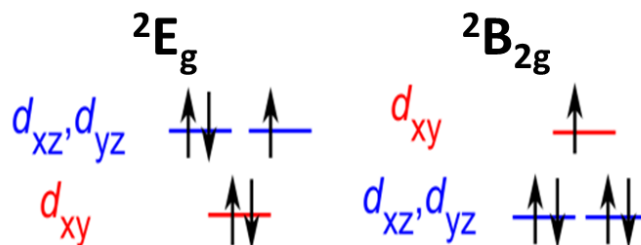


Figure 2.2 Electron distributions of the 2E_g and the ${}^2B_{2g}$ electronic states.

Here, we investigate the initial steps of Mtb MhuD-catalyzed heme degradation using a combined crystallographic and spectroscopic approach to clarify the geometric and electronic structure of the single heme-bound MhuD (MhuD-heme) species. We report the first X-ray crystal structure of a monoheme form of Mtb MhuD. This structure reveals that the MhuD active site stabilizes a ruffled His-ligated heme substrate without an organized network of water molecules on the distal side of heme. Work by our collaborators establish that the MhuD heme ruffling rearranges the heme electronic state sensitizing the meso-carbons to hydroxylation in the MhuD active site. Lastly, mutagenesis of purported heme ruffling residues abolished MhuD heme degradation demonstrating the importance of heme ruffling in MhuD enzymatic activity.

Results

MhuD heme-CN structure

We have previously determined the crystal structure of MhuD-diheme, which revealed two stacked heme molecules in the MhuD active site. However, no heme degradation activity is observed by MhuD-diheme and only the monoheme complex is capable of degrading heme⁵. To observe MhuD in its active conformation, we determined the structure of MhuD-heme-

CN to 1.9 Å resolution (**Table 2.1**), with one homodimer in the asymmetric unit. MhuD-heme-CN retains its ferredoxin-like $\alpha + \beta$ -barrel fold as observed for MhuD-diheme⁵; however only one bound molecule of heme is observed in each active site (**Figure 2.3A**). Within the active site, His-75 coordinates the iron of MhuD-heme-CN on its proximal side (2.1 Å, **Figure 2.3B**), and the His-75 imidazole ring is hydrogen (H)-bonded to the backbone carbonyl of Ala-71. A fully occupied cyano group was modeled into the electron density observed on the distal side of the heme iron (2.1 Å). The bound CN atoms refine with B-factors of approximately 22 Å², similar to those of the heme irons. The CN ligands are observed in a bent coordinating mode, with Fe–C–N angles of 118 and 120° for chains A and B, respectively, whereas the Fe–C–N bonds are nearly perpendicular to the porphyrin plane in the IsdI-heme-CN structure with Fe–C–N angles of 171° and 158°¹⁵. In the MhuD-heme-CN active site, the CN ligand H-bonds to Asn7 NH1. Furthermore, the CN-inhibited heme substrate is stabilized by hydrophobic interactions with Ile-9, Phe-23, Phe-39, Val-53, Thr-55, Phe-63, and Trp-66; H-bonds between propionate 6 and Arg-22 NH1 and the Val-83 backbone amide; and H-bonds between the bent propionate 7 and a water molecule, which in turn H-bonds to Arg-26.

Table 2.1 X-ray data collection and refinement statistics for the structural determination of MhuD-heme-CN

	MhuD heme-CN
Space group	P2 ₁ 2 ₁ 2 ₁
Unit cell dimensions (Å)	40.97 × 60.40 × 78.46
pH of crystallization conditions	6.0
Data Set	
wavelength (Å)	1.0
resolution range	39.23-1.90
unique reflections (total)	15989 (103418)
completeness (%) ^a	99.6 (99.9)
Redundancy	6.5 (6.7)
R _{merge} ^{a,b}	6.4 (35.5)
I/σ	17.3 (4.9)
NCS copies	2
Model Refinement	
resolution range (Å)	39.23-1.90
no. of reflections (working/free)	15935 (1595)
no. of protein atoms	1505
no. of water molecules	94
no. of heme dimer	2
no. of cyanide dimer	2
missing residues	103-105
R _{work} /R _{free} (%) ^c	17.3/22.4
Average B-factor (Å ²)	
protein	31.9
heme and cn	27.0
Water	37.6
rms deviations	
bond lengths (Å)	0.010
bond angles (degrees)	1.098
Ramachandran Plot	
most favorable region (%)	95.43
additional allowed region (%)	4.06
disallowed region	0.51
PDB ID code	4NL5

^aStatistics for the highest-resolution shell are given in brackets.
^b $R_{\text{merge}} = \sum |I - \langle I \rangle| / \sum I$
^c $R_{\text{work}} = \sum |F_{\text{obs}} - F_{\text{calc}}| / \sum F_{\text{obs}}$. R_{free} was computed identically to that of R_{work} except for where all reflections belong to a test set of 10% randomly selected data.

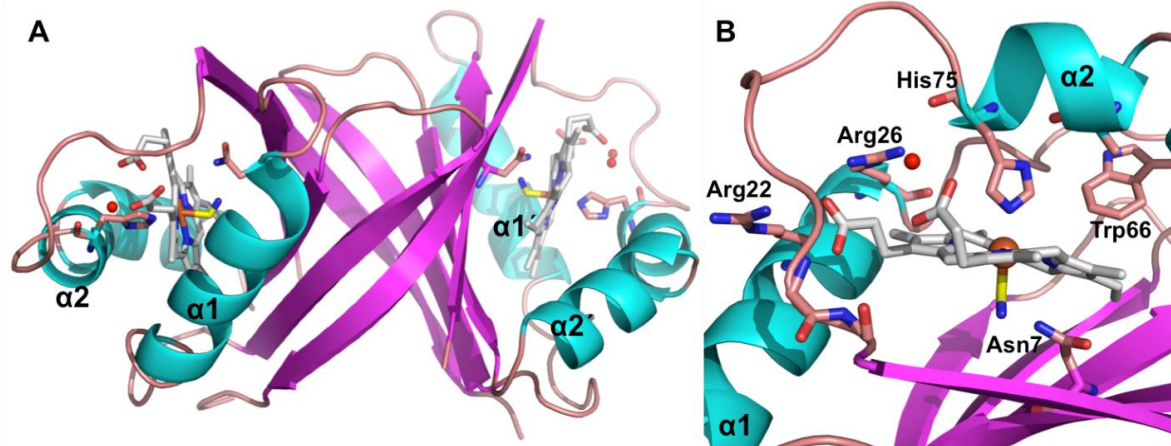


Figure 2.3 X-ray crystal structure of MhuD-heme-CN (PDB: 4NL5). Panel A: Ribbon representation of the dimeric MhuD-heme-CN complex. Panel B: Ribbon representation of the MhuD-heme-CN heme-binding pocket. α -helices and β -strands are depicted in cyan and magenta, respectively. Loops and sidechain carbons are shown in salmon. All α -helices are labeled, with the second polypeptide chain differentiated by a prime symbol ('). Heme-CN, one per active site, is represented as a stick model where nitrogen, oxygen, heme carbon, and cyano carbon atoms are in blue, red, white, and yellow, respectively. Iron atoms and ordered water molecules are depicted as orange and red spheres, respectively.

MhuD-diheme and MhuD-heme-CN structures superimpose with a root-mean-square deviation (rmsd) of 0.29 Å over all C α atoms¹⁸. Within the active site pocket, the heme substrate overlays with the solvent-protected heme from the MhuD-diheme structure, however the modeled heme is rotated 180° about the α - γ axis (**Figure 2.4**). Additionally, there is an increase in heme ruffling.

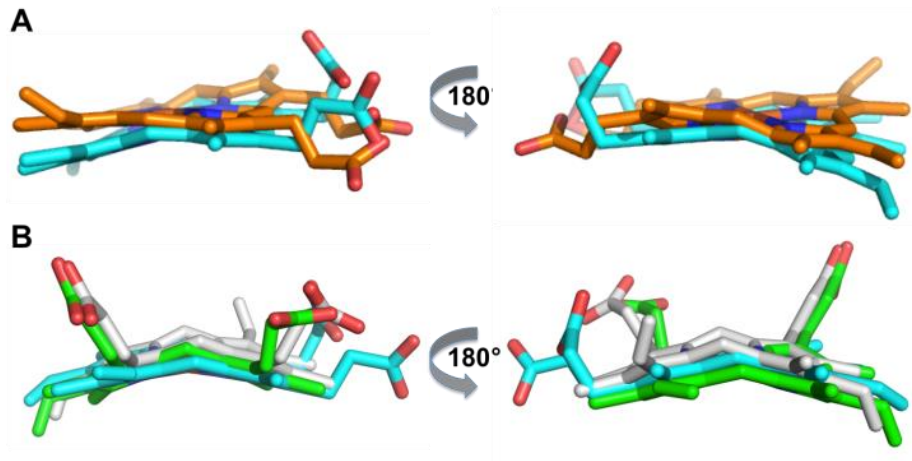


Figure 2.4 Degree of heme ruffling within heme degrading enzymes. Panel A: Overlay of MhuD-heme-CN (cyan) and HO-1 heme (orange, PDB: 1N45). The right panel shows HO-1 heme being mostly planar, while the left one shows that it is ruffled in one pyrrolic group. Panel B: Overlay of hemes from MhuD-heme-CN (cyan, PDB: 4NL5), N7A IsdG (white, PDB: 2ZDO) and IsdI-heme-CN (green, PDB: 3QGP) following structural overlay.

The distortions of the hemes in MhuD-heme-CN (1.4 and 1.5 Å) are more severe than those in MhuD-diheme (0.7 Å), as analyzed by normal-coordinate structural decomposition¹⁹. It was suggested that Phe-22 contributes to heme ruffling in IsdG by contacting the γ -meso carbon^{8, 17}; however, the corresponding residue, Phe-23, overlays in MhuD-diheme and MhuD-heme-CN. The most notable structural differences are within the α 2 helix and the subsequent loop region surrounding the active site (**Figure 2.5A**). In MhuD-heme-CN, the α 2 helix is kinked after residue Asn-68, while in the MhuD-diheme structure this helix (α 2) is extended. This kink results in the movement of His-75 (4.5 Å) so that it may coordinate with heme iron in the MhuD-heme-CN structure (**Figure 2.5B**). Furthermore, there is one notable altered sidechain conformation, Arg-26, between the MhuD-heme-CN and MhuD-diheme structures. In the MhuD-diheme structure, Arg-26 forms an H-bond with propionate 7 from the solvent-exposed heme, but not with the solvent-protected heme molecule (**Figure 2.5C**).

However, in MhuD-heme-CN Arg-26 is flipped into the reduced volume heme active site where it H-bonds to an active site water molecule, which in turn H-bonds to the carbonyl oxygen of His75 and heme propionate 7, whose orientation is rotated toward the active site water (Figure 2.5B). One could speculate that the ordered water and alternative conformation of the Arg26 sidechain may stabilize the otherwise flexible loop to form a stable monoheme active site. The position of this water molecule is conserved in both active sites of the MhuD dimer, however in one of two active sites of the dimer there is a second water molecule that also H-bonds with Arg-26.

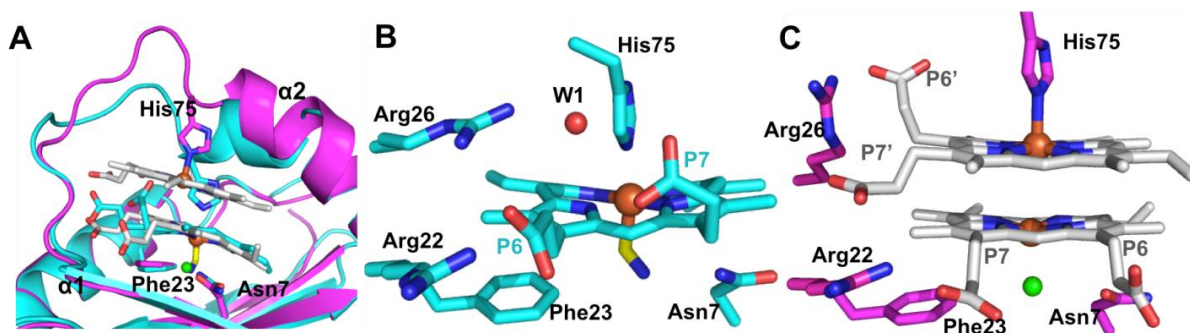


Figure 2.5 Structural comparison of the active sites of MhuD-heme-CN and MhuD-diheme. Panel A: Superposition of MhuD-heme-CN (PDB: 4NL5, cyan) with MhuD-diheme (PDB: 3HX9, pink) shows that $\alpha 2$ in MhuD-heme-CN is kinked while it is extended in the MhuD-diheme structure. This kink results in MhuD-heme-CN His75 moving 4.5 Å to coordinate heme iron (orange spheres). Panels B and C: The orientations of most residues within the MhuD-heme-CN (B) and MhuD-diheme (C) active sites are unchanged, but Arg26 in the MhuD-heme-CN structure flips into the reduced volume active site. Heme propionates 6 and 7 are denoted by P6 and P7, respectively, and the solvent-exposed heme propionates (MhuD-diheme) are differentiated with a prime symbol ('). Heme molecules are in stick representation, with carbon atoms depicted in cyan and white for MhuD-heme-CN and MhuD-diheme, respectively, and nitrogen, oxygen and cyano carbon atoms in blue, red, and yellow, respectively. Iron atoms, an ordered Cl⁻ atom (MhuD-diheme) and water molecule (MhuD-heme-CN) are depicted as orange, green, and red spheres, respectively.

Mutational studies on proposed heme ruffling residues

Previous studies have shown that mutation of the IsdG/I Trp-66, which makes a hydrophobic interaction with the heme protoporphyrin ring, resulted in a reduction of heme ruffling as

well as a loss of or reduction in heme degradation. This loss in heme degradation activity is correlated to the bulkiness of the replacement residue. Similar to IsdG/I, the Trp-66 residue (**Figure 2.6**) in MhuD may also play a role in heme ruffling through the same hydrophobic interaction previously observed in IsdG/I. In addition to Trp-66, we also propose that the Phe-23 residue (**Figure 2.6**) also plays an important role in MhuD heme ruffling by stabilizing the ruffled heme via a π -stacking interaction with the protoporphyrin.

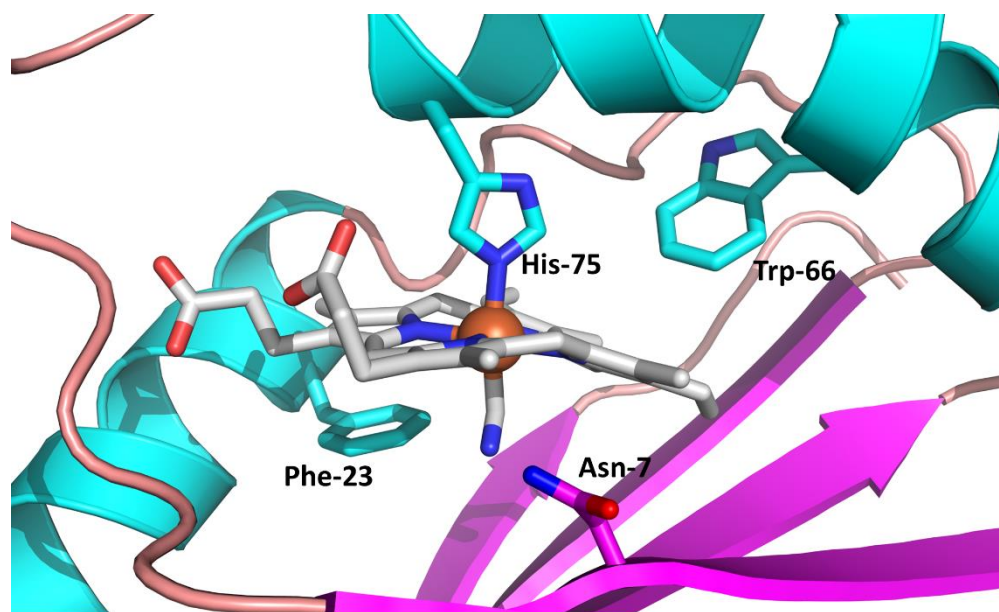


Figure 2.6 Ribbon representation of the MhuD active site. Residues Trp-66 and Phe-23 appear to stabilize the ruffled heme state via hydrophobic interaction and π - π stacking interaction respectively

To determine if Phe-23 and Trp-66 play an important role in MhuD activity, alanine mutants of these residues were generated for biochemical characterization. Heme degradation assays were initially performed to assess the effect of the aforementioned residues on MhuD heme degradation. In these assays, heme degradation by MhuD-mono-heme and its mutants were initiated with sodium ascorbate and were monitored spectrophotometrically between 300 and 700 nm. To avoid non-enzymatic heme degradation, catalase from *Aspergillus niger* was

included in each reaction. Similar heme degradation experiments were performed using cytochrome P450 reductase as an electron donor and NADPH as an electron source.

As previously reported, wild type MhuD degraded heme as indicated by a decrease in the Soret peak near 410 nm⁵. While MhuD WT was shown to degrade heme, no Soret peak decrease was observed in the MhuD W66A and F23A variants indicating that these mutants do not degrade heme upon the addition of ascorbate (**Figures 2.7A-2.7C**). Similarly, MhuD W66A mutant was also shown to be enzymatically inactive when using cytochrome P450 reductase as an electron donor and NADPH as an electron source (**Figures 2.8A-2.8B**). These results suggest that these mutants are functionally inactive and that the mutated residues play an important role in MhuD heme degradation activity and in heme ruffling as previously postulated.

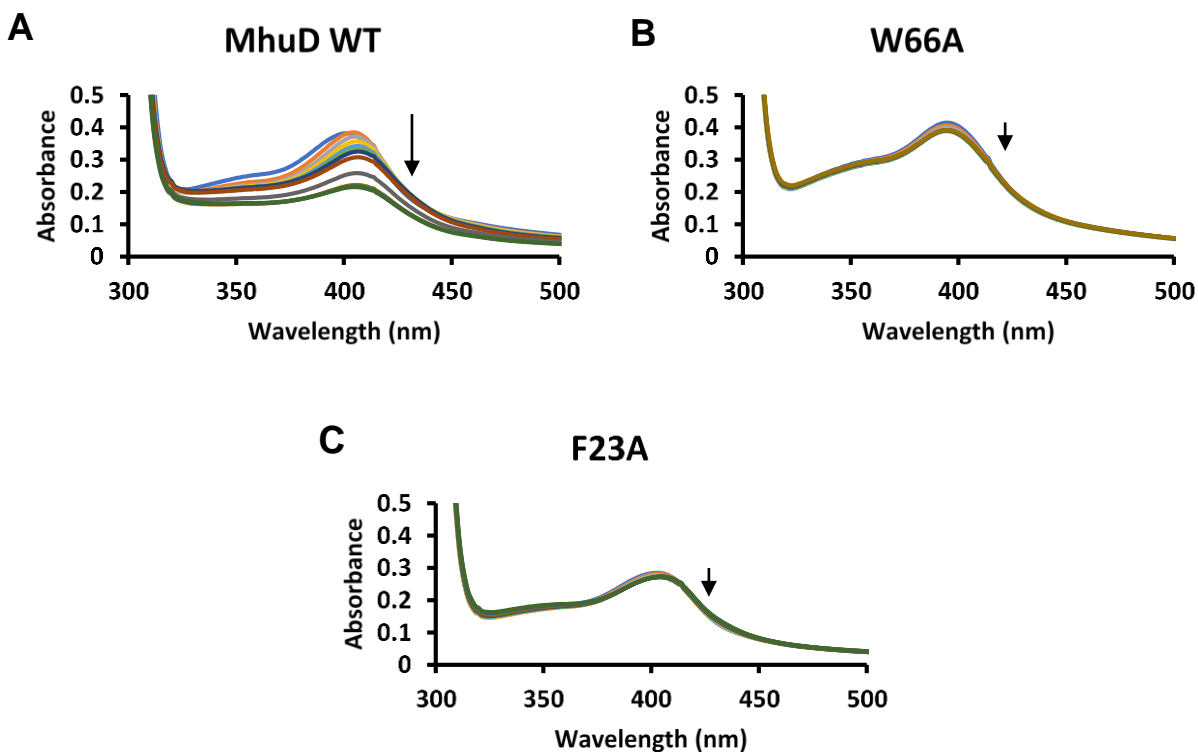


Figure 2.7 Heme degradation assays of wild type (A), W66A (B), and F23A (C) monoheme forms of MhuD in the presence of 0.5:1 molar ratio of catalase to MhuD-mono-heme using ascorbate (10 μ M) as the electron donor. UV/vis spectra were collected between 300 to 700 nm in 5 minute intervals. A decrease in the soret peak (arrow) near 410 nm was observed for MhuD WT indicating that heme was being degraded. No soret peak decrease were observed in heme degradation assays for the W66A and F23A variants.

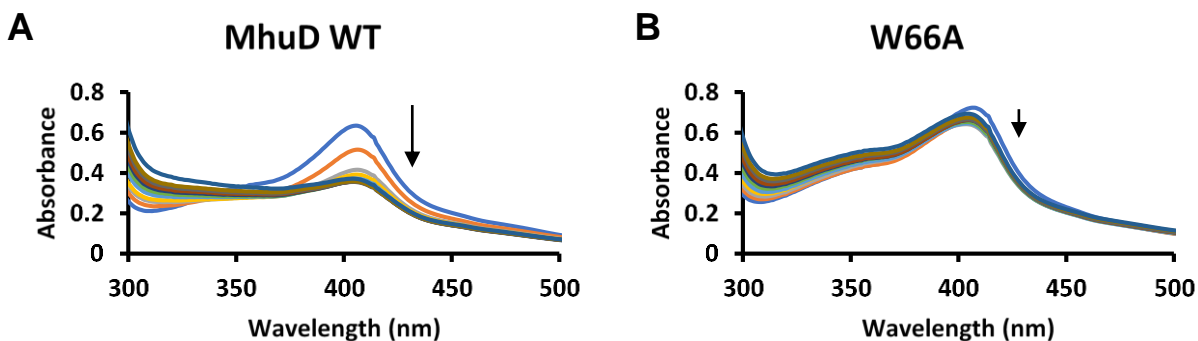


Figure 2.8 Heme degradation assays of wild type (A) and W66A (B) monoheme forms of MhuD in the presence of 0.3:1 molar ratio of catalase to MhuD-mono-heme using cytochrome P450 reductase as an electron donor and NADPH as an electron source. NADPH was titrated in 1 μ M increments up to 10 μ M final concentration and spectral changes between 300 and 700 nm were monitored after each titration. MhuD WT degrades heme as indicated by a decrease in the soret peak, and the W66A variant does not.

To eliminate the possibility that the inactivity of MhuD F23A and W66A variants is due to reduced heme affinity, heme titration experiments and heme off assays were performed to measure the affinity of the MhuD variants for heme. In the heme titration experiments, absorbance spectra between 300 and 700 nm were collected following the titration of heme into either 5 μ M apo-MhuD or buffer for a difference spectra. The absorbance difference at 412 nm was plotted against the titrated heme concentration. The change in absorbance attributed to MhuD WT interacting with heme plateaus after titrating of two molar equivalents of heme indicating that MhuD WT can bind up to two hemes (**Figures 2.9A**). Similarly, both MhuD F23A and W66A appear to saturate following the addition of two molar equivalents of heme indicating that these variants retained the ability to bind two hemes (**Figures 2.9B-2.9C**).

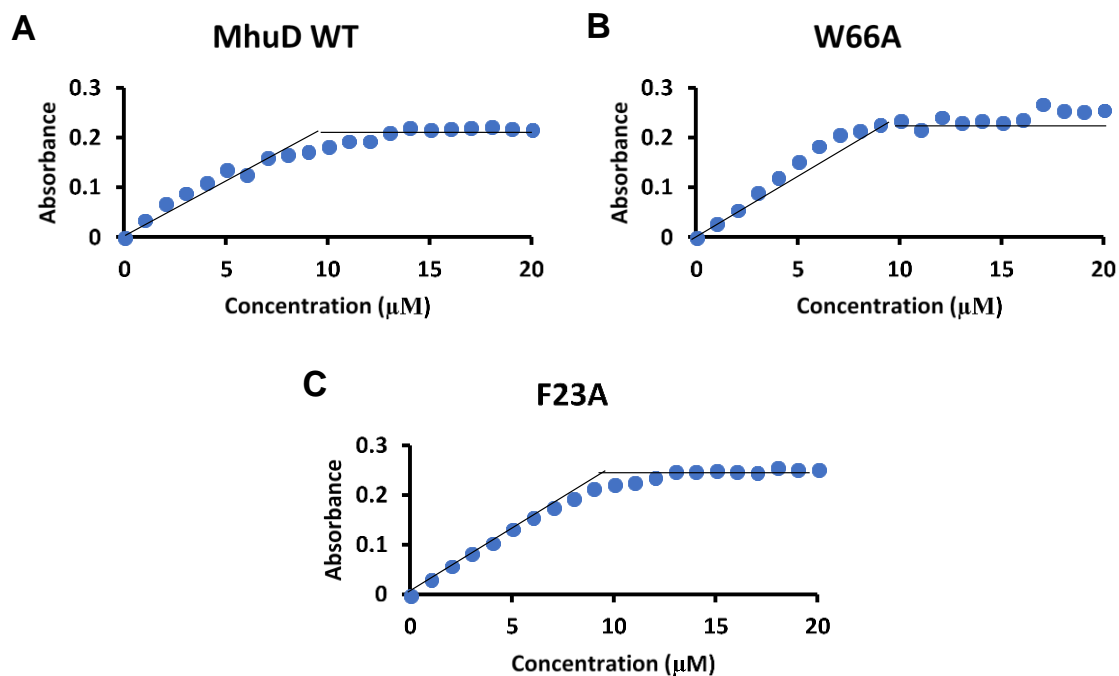


Figure 2.9 Difference absorption spectroscopy of heme added to wild type (A), W66A (B), and F23A (C) MhuD. Here, spectral changes at 412 or 413 nm were monitored upon additions of 1 μM heme titrations to 5 μM apo-MhuD. Heme binding saturates after titration of two-molar equivalents of heme for the MhuD variants tested indicating that the MhuD WT and the mutants are capable of binding up to two hemes per active site.

The heme off rates from MhuD-mono-heme and its variants were determined by monitoring absorbance changes over time upon the addition of apo-H64Y/V68F-myoglobin²⁰, which has a high affinity for heme ($k_{\text{heme-off}} = 6.6 \times 10^{-4} \text{ min}^{-1}$). Increased heme off rates were observed for the MhuD W66A and F23A variants indicating that these MhuD mutations reduced heme affinity (**Figure 2.10**). However, these MhuD variants are still capable of binding heme indicating that the W66A and F23A mutations render MhuD functionally inactive. These experiments demonstrate the importance of Phe-23 and Trp-66 in MhuD heme degradation activity and suggest that heme ruffling is important for MhuD function.

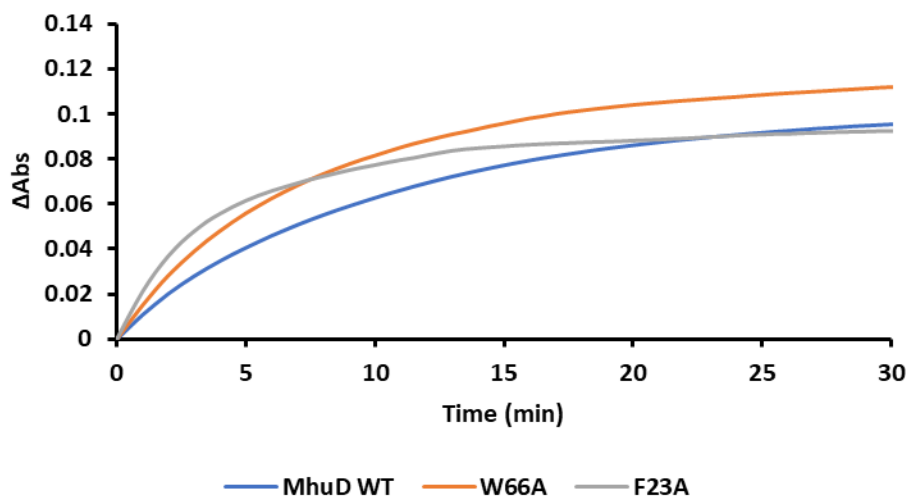


Figure 2.10 Time course of heme transfer from wild type (blue), W66A (orange), and F23A (gray) MhuD to a 5-fold excess of apo-H64Y/V68F-Mb. Heme transfer was monitored at 412 nm and conducted in triplicate.

Table 2.2 Heme off rates of MhuD and mutants determined via single-exponential fitting of time course heme transfer data from **Figure 2.9**.

	Rate (min ⁻¹)
WT	0.091 ± 0.002
W66A	0.126 ± 0.003
F23A	0.536 ± 0.004

Discussion

Geometric Structure of MhuD-heme-CN

It has been suggested that the heme ruffling observed in structures of Isd-like heme degrading proteins is required for their activity. The C α atoms of the MhuD-heme-CN structure superimpose with those of N7A IsdG (PDB ID 2ZDO) and IsdI-heme-CN (PDB: 3QGP) with rmsds of 1.59 and 1.24 Å, respectively (**Figure 2.11**)^{15, 17}. The 1.4 Å distortion of heme from planarity in the MhuD-heme-CN structure is less than that observed for N7A IsdG

and IsdI-heme-CN, which show heme distortions of 1.9 and 2.3 Å, respectively (**Figure 2.4**). This intermediate degree of heme ruffling confers a distinct electronic structure on the MhuD heme which may play a role in MhuD's unique degradation products. Experiments by the Liptak group at University of Vermont found that while electronic state of MhuD-heme-CN was similar to that of IsdI-heme-CN with a $^2B_{2g}$ ground state and a 2E_g excited state, the relative energy difference between the two states is in MhuD-heme-CN reduced due to the reduction of heme ruffling compared to in IsdI-heme-CN (**Figure 2.12**)²¹. The overall distortion of heme in MhuD-heme-CN is greater than that observed in hHO (1.2 Å, PDB: 1N45, **Figure 2.4**)³. Furthermore, distortion of the hHO heme is localized to a single pyrrolic group, while the MhuD-heme-CN heme is distorted throughout its tetrapyrrole ring. Finally, while the bound hemes of MhuD-heme-CN, IsdG, and IsdI occupy similar positions within their respective structures, the heme propionate groups of IsdG and IsdI are rotated approximately 90° about the axis normal to the tetrapyrrole ring compared to the MhuD-bound heme. The positional difference within the heme molecules is dictated by the α 1 helix and the loop region directly following the α 2 helix. Within MhuD-heme-CN, the C-terminus of the α 1 helix has an additional turn as compared to that of heme-bound IsdG/I, which enables Arg-26 to form a H-bonding network with a water molecule, His-75, and propionate 7. The last turn of this α 1 helix is a loop region in both the IsdG and IsdI structures and, thus, the IsdG/I Arg-26 C α is displaced \sim 6 Å from the heme molecule, with its sidechain solvent accessible instead of participating within the active site, as observed for Arg26 in of the MhuD-heme-CN structure. Furthermore, the structural variance in the loop region directly following the α 2 helix combined with that of the α 1 helix results in the MhuD heme propionates pointing towards this loop region, whereas the corresponding propionates in

IsdG/I point towards the $\alpha 1$ helix, reducing their solvent accessibility compared to those of MhuD (**Figure 2.11**). This heme rotation may play a role in the variant location of tetrapyrrole ring cleavage during the heme degradation reaction of MhuD and Isd proteins, whereby the two products of IsdI suggest cleavage at the β - and δ -meso carbons and the products of MhuD suggest cleavage at the α -meso carbon^{7,8}. The kink observed in the $\alpha 2$ helix of MhuD-heme-CN is reminiscent of the corresponding helix in the *S. aureus* IsdG and IsdI heme-degrading proteins¹⁷.

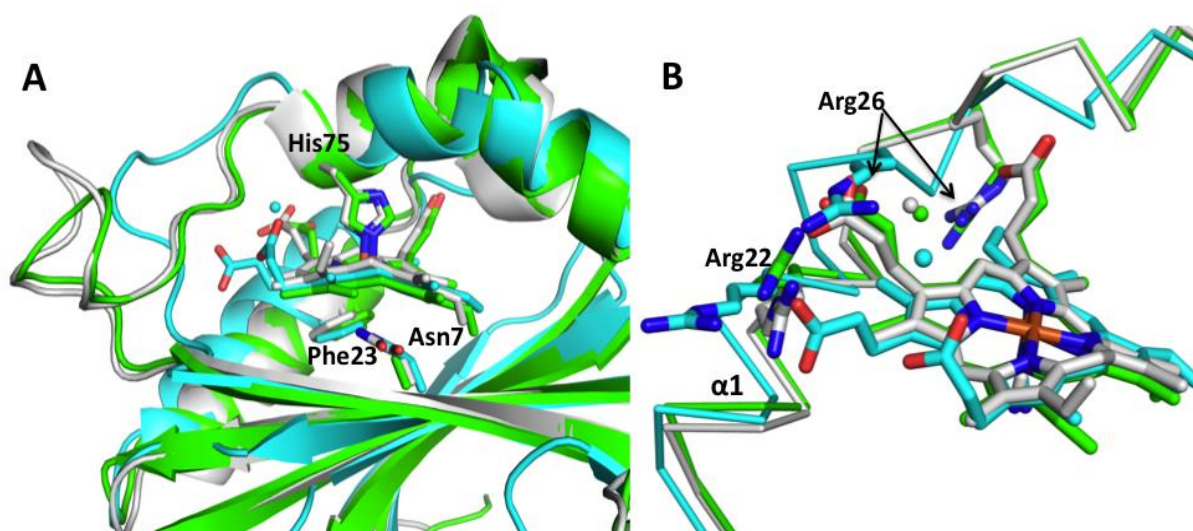


Figure 2.11 Structural comparison of MhuD-heme-CN with IsdG N7A and IsdI. Panel A: Superposition of MhuD-heme-CN (cyan, PDB: 4NL5) with N7A IsdG (green, PDB: 2ZD0) and IsdI-heme-CN (white, PDB: 3QGP) shows that the orientation of heme within the active site of MhuD is different compared to that of IsdG and IsdI, whereby the heme propionates in MhuD are rotated 90° around the axis normal to the heme plane. Panel B: The final turn of the $\alpha 1$ helix of MhuD (contains Arg-26) is a loop region in the IsdG and IsdI structures, enabling Arg-26 to flip from within the active site as observed in MhuD to be surface exposed in both IsdG and IsdI. Residue sidechains and heme molecules are represented as sticks, with oxygen, nitrogen, and iron atoms colored red, blue, and orange, respectively. Ordered water molecules are represented as spheres.

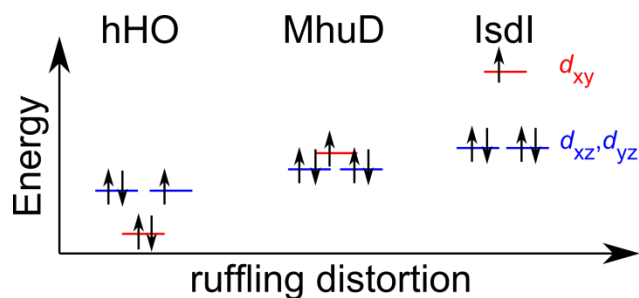


Figure 2.12 Porphyrin ruffling alters the relative energies of the Fe $3d_{xy}$, $3d_{xz}$, and $3d_{yz}$ -based MOs. As the degree of ruffling increases from 0.7 Å (hHO-heme-CN) to 1.4 Å (IsdI-heme-CN) the electronic ground state changes from 2E_g to ${}^2B_{2g}$. MhuD-heme-CN exhibits an intermediate degree of ruffling (2.3 Å) and, consequently, a thermal mixture of these two states is observed.

Residues Trp-66 and Phe-23 are important for MhuD heme degradation

Previous experiments by Ukpabi et al. have shown that the Trp-66 residue in IsdI plays an important role in IsdI heme ruffling and therefore IsdI heme degradation¹⁶. Mutation of the IsdI Trp-66, which makes a hydrophobic interaction with the heme protoporphyrin ring, resulted in a reduction of heme ruffling and a more negative measured heme reduction potential as well as a loss of or reduction in heme degradation. This loss in heme degradation activity is correlated to the bulkiness of the replacement residue and is thought to be due to the more negative heme reduction potential arising from decreased heme ruffling. The same residue in the Mtb heme degrading enzyme MhuD also appears to play a similar role in MhuD heme degradation. Replacement of Trp-66 with an alanine abolishes MhuD heme degradation activity (**Figures 2.7A, 2.7B, 2.8A, & 2.8B**). A similar loss of activity was observed upon mutation of the Phe-23 residue, which appears to stabilize the ruffled MhuD-mono-heme via a π - π stacking interaction, into an alanine (**Figures 2.7A & 2.7C**). Heme titration (**Figures 2.9A-2.9C**) and heme off experiments (**Figures 2.10**) show that the loss of heme degradation activity of the W66A and F23A variants are due to enzymatic inactivity

and not to a lack of heme binding. Furthermore, NMR and UV/vis experiments of the W66A variant by Graves et al. indicate that mutation of the Trp-66 similarly reduces ruffling of the MhuD-mono-heme²², which, similar to in IsdI, may decrease the reduction potential of the heme. Together, these results suggest that Trp-66 and Phe-23 are both heavily involved in MhuD heme ruffling which is thought to be crucial for MhuD heme degradation activity, highlighting the importance of heme ruffling in MhuD heme degradation activity.

Materials and Methods

Expression and purification of wild type Mtb MhuD and its mutants

Generation of pET22b vector for his-tagged wild type Mtb MhuD expression was achieved as previously described⁵. Site directed mutagenesis using MhuD-W66A-fwd (5' - CAT TCC AGG CGG CGG CAA ACG GGC C - 3') and MhuD-W66A-rev (5' - GGC CCG TTT GCC GCC GCC TGG AAT G - 3') primers was used to introduce the W66A mutation. The MhuD F23A construct was produced via site directed mutagenesis using primers MhuD-F23A-fwd (5' - CTG GAG AAG CGG GCG GCT CAC CGC GC - 3') and MhuD-F23A-rev (5' - GCG CGG TGA GCC GCC CGC TTC TCC AG - 3'). The MhuD mutants were expressed and purified in the same manner as reported for the wild type variant⁵. In brief, *E. coli* B21-Gold (DE3) cells transformed with pET22b-MhuD vector were grown in LB medium containing µg/mL ampicillin at 37 C. Overexpression was induced at OD₆₀₀ of ~ 0.6 using 1 mM IPTG. The cells were harvested 4 hours post induction and resuspended in lysis buffer (50 mM Tris/HCl pH 7.4, 350 mM NaCl and 10 mM imidazole). Cells were lysed via sonication and the resulting lysate was centrifuged at 14 krpm and passed through a 1 µm filter. The cell supernatant was loaded

onto a Ni²⁺-charged HiTrap chelating column (5 mL) and washed with lysis buffer. Bound protein was eluted from the column with increasing concentrations of imidazole. Next, MhuD, which elutes at 50 and 100 mM imidazole, was concentrated (Amicon, 5 kDa molecular mass cutoff) and was further purified on a S75 gel filtration column in 20 mM Tris, pH 8, and 10 mM NaCl. A final purification step was performed on an ion exchange column (HiTrap Q HP, 5 mL) with the pure MhuD eluting at 150 mM NaCl.

Crystallization of the cyanide inhibited MhuD-mono heme

A hemin solution was prepared by dissolving 3.3 mg of heme in 300 μ L 1 M NaOH before dilution into sodium phosphate buffer (50 mM NaPO₄ pH 7.4, 150 mM NaCl). After adjusting the pH of the hemin solution to pH 7.4, a few KCN crystals were added to derivatize the heme into heme-CN. Purified apo-MhuD was bound to heme-CN in sodium phosphate buffer in a 1.1:1.0 heme-CN/MhuD ratio. Excess heme was removed via a PD-10 desalting column. MhuD-heme-CN was crystallized using the hanging drop-vapor diffusion method. Hanging drops consisted of 1 μ L of MhuD heme-CN at 10 mg/mL and 1 μ L of mother liquor containing 0.1 M sodium acetate, pH 6.0, 1.9 M ammonium sulfate, and 0.2 M NaCl. Crystals were collected by flash freezing after soaking in a cryoprotectant containing a 1:1 mixture of 40% (v/v) glycerol and mother liquor. A native diffraction dataset was collected at a wavelength of 1.0 Å at 70 K. The MhuD heme-CN structure was solved to 1.9 Å resolution using molecular replacement against the heme-deplete MhuD-diheme structure (PDB: 3HX9).

Preparation of MhuD-monoHEME

Reconstitution of wild type MhuD and its mutants with heme was achieved as previously described⁵. Briefly, a heme solution was prepared by dissolving 4 mg of heme in 500 μ L 0.1 M NaOH. After the addition of 500 μ L 1 M tris, pH 7.4, the solution was diluted into 15 mL of 50 mM tris, pH 7.4, 150 mM NaCl. Heme was gradually titrated into 100 μ M apo-MhuD in a 0.9 heme: 1 MhuD ratio. The samples were incubated overnight at 4°C before being passed through a desalting column to remove unbound heme. Protein and heme concentrations of the eluted samples were determined via Lowry²³ and Hemochromogen²⁴ assays respectively.

Single turnover heme degradation assays

Single turnover heme degradation assays of 5 μ M MhuD-monoHEME were performed in 50 mM tris, pH 7.4, 150 mM NaCl^{25, 26}. To eliminate the possibility of non-enzymatic heme degradation, 2.5 μ M catalase from *Aspergillus niger* (Sigma Aldrich) was added to each reaction. Heme degradation reaction was initiated with 10 mM sodium ascorbate and the reaction was monitored spectrophotometrically (DU800, Beckman Coulter) between 300 and 700 nm for an hour with scans taken at 5-minute intervals.

Heme titration experiments

Heme was titrated in 1 μM increments into 5 μM apo-MhuD or buffer at room temperature. Spectra were collected between 300 and 700 nm after each titration after a 5-minute incubation period and the difference spectra obtained to determine absorbance change.

Heme off rate measurement

For the heme off rate measurements, MhuD-mono-heme of the wild type and its mutants were prepared as described above using the following heme to protein ratios: 1.2 heme:1 MhuD (wild type), 1.2 heme:1 MhuD (W66A), and 1.2 heme:1 MhuD (F23A). Preparation of apo-H64Y/V68F-Mb was achieved as previously reported²⁰. Hemochromogen²⁴ and Lowry²³ assays were used to determine heme and protein concentration to ensure a near 1 to 1 heme protein ratio. To measure heme dissociation, 5 μM MhuD-mono-heme was mixed with a 5-fold excess of apo-H64Y/V68F-Mb. The reaction was monitored spectrophotometrically (DU800, Beckman Coulter) at 412 nm to completion.

References

- [1] Tenhunen, R., Marver, H. S., and Schmid, R. (1969) Microsomal heme oxygenase. Characterization of the enzyme, *J Biol Chem* 244, 6388-6394.
- [2] Maines, M. D., Trakshel, G. M., and Kutty, R. K. (1986) Characterization of Two Constitutive Forms of Rat Liver Microsomal Heme Oxygenase: Only One Molecular Species of the Enzyme is Inducible, *Journal of Biological Chemistry* 261, 411-419.
- [3] Schuller, D. J., Wilks, a., Ortiz de Montellano, P. R., and Poulos, T. L. (1999) Crystal structure of human heme oxygenase-1, *Nature structural biology* 6, 860-867.
- [4] Bianchetti, C. M., Yi, L., Ragsdale, S. W., and Phillips, G. N., Jr. (2007) Comparison of apo- and heme-bound crystal structures of a truncated human heme oxygenase-2, *J Biol Chem* 282, 37624-37631.
- [5] Chim, N., Iniguez, A., Nguyen, T. Q., and Goulding, C. W. (2010) Unusual diheme conformation of the heme-degrading protein from Mycobacterium tuberculosis, *J Mol Biol* 395, 595-608.
- [6] Wu, R., Skaar, E. P., Zhang, R., Joachimiak, G., Gornicki, P., Schneewind, O., and Joachimiak, A. (2005) Staphylococcus aureus IsdG and IsdI, heme-degrading enzymes with structural similarity to monooxygenases, *J Biol Chem* 280, 2840-2846.
- [7] Nambu, S., Matsui, T., Goulding, C. W., Takahashi, S., and Ikeda-Saito, M. (2013) A new way to degrade heme: the Mycobacterium tuberculosis enzyme MhuD catalyzes heme degradation without generating CO, *J Biol Chem* 288, 10101-10109.
- [8] Reniere, M. L., Ukpabi, G. N., Harry, S. R., Stec, D. F., Krull, R., Wright, D. W., Bachmann, B. O., Murphy, M. E., and Skaar, E. P. (2010) The IsdG-family of haem oxygenases degrades haem to a novel chromophore, *Mol Microbiol* 75, 1529-1538.
- [9] Matsui, T., Nambu, S., Ono, Y., Goulding, C. W., Tsumoto, K., and Ikeda-Saito, M. (2013) Heme degradation by Staphylococcus aureus IsdG and IsdI liberates formaldehyde rather than carbon monoxide, *Biochemistry* 52, 3025-3027.
- [10] Matsui, T., Unno, M., and Ikeda-Saito, M. (2010) Heme oxygenase reveals its strategy for catalyzing three successive oxygenation reactions, *Acc Chem Res* 43, 240-247.
- [11] Garcia-Serres, R., Davydov, R. M., Matsui, T., Ikeda-Saito, M., Hoffman, B. M., and Huynh, B. H. (2007) Distinct reaction pathways followed upon reduction of oxy-heme oxygenase and oxy-myoglobin as characterized by Mossbauer spectroscopy, *J Am Chem Soc* 129, 1402-1412.
- [12] Chen, H., Moreau, Y., Derat, E., and Shaik, S. (2008) Quantum mechanical/molecular mechanical study of mechanisms of heme degradation by the enzyme heme oxygenase: the strategic function of the water cluster, *J Am Chem Soc* 130, 1953-1965.
- [13] Li, Y., Syvitski, R. T., Chu, G. C., Ikeda-Saito, M., and Mar, G. N. (2003) Solution ¹H NMR investigation of the active site molecular and electronic structures of substrate-bound, cyanide-inhibited HmuO, a bacterial heme oxygenase from Corynebacterium diphtheriae, *J Biol Chem* 278, 6651-6663.
- [14] Syvitski, R. T., Li, Y., Auclair, K., Ortiz De Montellano, P. R., and La Mar, G. N. (2002) ¹H NMR detection of immobilized water molecules within a strong distal hydrogen-bonding network of substrate-bound human heme oxygenase-1, *J Am Chem Soc* 124, 14296-14297.

- [15] Takayama, S. J., Ukpabi, G., Murphy, M. E., and Mauk, A. G. (2011) Electronic properties of the highly ruffled heme bound to the heme degrading enzyme IsdI, *Proc Natl Acad Sci U S A* 108, 13071-13076.
- [16] Ukpabi, G., Takayama, S. J., Mauk, A. G., and Murphy, M. E. (2012) Inactivation of the heme degrading enzyme IsdI by an active site substitution that diminishes heme ruffling, *J Biol Chem* 287, 34179-34188.
- [17] Lee, W. C., Reniere, M. L., Skaar, E. P., and Murphy, M. E. (2008) Ruffling of metalloporphyrins bound to IsdG and IsdI, two heme-degrading enzymes in *Staphylococcus aureus*, *J Biol Chem* 283, 30957-30963.
- [18] Chim, N., Torres, R., Liu, Y., Capri, J., Batot, G., Whitelegge, J. P., and Goulding, C. W. (2015) The Structure and Interactions of Periplasmic Domains of Crucial MmpL Membrane Proteins from *Mycobacterium tuberculosis*, *Chem Biol* 22, 1098-1107.
- [19] Jentzen, W., Song, X. Z., and Shelnut, J. A. (1997) Structural characterization of synthetic and protein-bound porphyrins in terms of the lowest-frequency normal coordinates of the macrocycle, *J Phys Chem B* 101, 1684-1699.
- [20] Hargroves, M. S., Singleton, E. W., Quilling, M. L., Ortizfl, L. A., Phillips, G. N., John, S., and Mathews, A. J. (1993) His64(E7)-->Tyr apomyoglobin as a reagent for measuring rates of hemin dissociation, *Journal of Biological Chemistry* 269, 4207-4214.
- [21] Graves, A. B., Morse, R. P., Chao, A., Iniguez, A., Goulding, C. W., and Liptak, M. D. (2014) Crystallographic and spectroscopic insights into heme degradation by *Mycobacterium tuberculosis* MhuD, *Inorg Chem* 53, 5931-5940.
- [22] Graves, A. B., Graves, M. T., and Liptak, M. D. (2016) Measurement of Heme Ruffling Changes in MhuD Using UV-vis Spectroscopy, *J Phys Chem B* 120, 3844-3853.
- [23] Lowry, O. H., Rosebrough, N. J., Farr, A. L., and Randall, R. J. (1951) Protein measurement with the Folin phenol reagent, *J Biol Chem* 193, 265-275.
- [24] Anson, M. L., and Mirsky, A. E. (1928) On Hemochromogen, *J Gen Physiol* 12, 273-288.
- [25] Wilks, A., and Schmitt, M. P. (1998) Expression and characterization of a heme oxygenase (Hmu O) from *Corynebacterium diphtheriae*. Iron acquisition requires oxidative cleavage of the heme macrocycle, *J Biol Chem* 273, 837-841.
- [26] Zhu, W., Wilks, A., and Stojiljkovic, I. (2000) Degradation of heme in gram-negative bacteria: the product of the hemO gene of *Neisseriae* is a heme oxygenase, *J Bacteriol* 182, 6783-6790.

CHAPTER 3

A Single Mutation in the *Mycobacterium tuberculosis* Heme-Degrading Protein MhuD, Results in a Different Product

Abstract

Mycobacterium tuberculosis MhuD degrades heme into mycobilin isomers and free iron, unlike canonical heme degrading enzymes, heme oxygenases (HOs), which degrade heme into biliverdin, carbon monoxide (CO), and ferric iron. Within the MhuD heme binding active site, Arg26 stabilizes one of the heme propionates. In this work, we report that the R26S mutation alters the end-product of MhuD from mycobilin into biliverdin. Surprisingly, unlike in HOs, our novel R26S MhuD variant produces formaldehyde instead of CO as its C1 product. Attempts to crystalize and solve the complex structure of MhuD R26S in its monoheme form proved unsuccessful. Instead these efforts resulted in crystal structures of the R26S variant in the di-metalloprotoporphyrin form, suggesting the active site of the mutant is more flexible compared to that of the wild type. Electron paramagnetic resonance (EPR) analysis suggests that the presence of mixed ruffling states in the MhuD R26S complex in which heme ruffling is probably diminished in one of the states compared to the heme in MhuD WT. Together, this suggest that the heme in the MhuD R26S mutant is in a different heme ruffling state compared to that of wild type MhuD thus resulting in an altered heme degradation product.

Introduction

In living organisms, heme (iron-protoporphyrin IX) degradation is known to play a variety of crucial functions including iron homeostasis¹, cell signaling², and antioxidant defense³. The most well-studied heme-degradation enzyme, mammalian heme oxygenase (HO), catalyzes the regiospecific breakdown of heme (iron-protoporphyrin IX, **Figure 3.1**) into biliverdin IX α (**Figure 3.1**), the C1-product carbon monoxide (CO) and ferrous iron⁴⁻⁶. HO-like enzymes have also been found in prokaryotes such as HmuO in *Corynebacterium diphtheriae* and nm-HO in *Neisseria meningitidis* that share structural homology with HOs and produce the same heme degradation products⁷⁻¹¹. Other heme-degrading enzymes have been reported in the literature with no homology to HOs^{12, 13}. These non-canonical heme-degrading enzymes produce chromophores distinct from biliverdin¹⁴⁻¹⁶. For example, *Staphylococcus aureus* heme-degrading proteins, IsdG and IsdI, break down heme to liberate iron, staphylobilin isomers (**Figure 3.1**), and formaldehyde^{14, 17}. The IsdG-like heme degrading enzymes are structurally distinct from HOs and have a ferredoxin-like $\alpha + \beta$ fold¹². Whereas HOs and HO-like enzymes are composed exclusively of alpha helices¹⁸, the structure of IsdG/I-like enzymes are dimeric and are composed of an eight-stranded β -barrel decorated with α -helices¹². The *Mycobacterium tuberculosis* heme degrading enzyme MhuD falls into this category of heme-degrading proteins as, it has high structural homology to IsdG/I proteins^{13, 19}. Despite this high homology to IsdG/I, MhuD yields two unique mycobilin isomers (**Figure 3.2**) upon heme degradation¹⁵. Mycobilins differ from the staphylobilin isomers as ring cleavage occurs at the α -meso carbon instead of the β -meso or δ -meso carbons, and there is no loss of vicinal C–O moiety in mycobilins^{14, 15}. Additionally, mycobilin is oxygenated at either the β -meso or δ -meso carbons by MhuD depending on the isomer¹⁵.

In addition to generating an unique heme degradation product, another way MhuD also differs from IsdG/I is that MhuD is capable of binding two hemes per active site¹³. However, accommodation of the additional heme into the active site renders the enzyme inactive¹³. Most recently, LaMattina et al have reported a new type of heme degrading enzyme, ChuW in *E. coli* O157:H7¹⁶. ChuW degrades heme in an oxygen-independent manner via a radical-mediated mechanism¹⁶, whereas HOs and IsdG-type enzymes degrade heme in an oxygen dependent manner^{6, 14}.

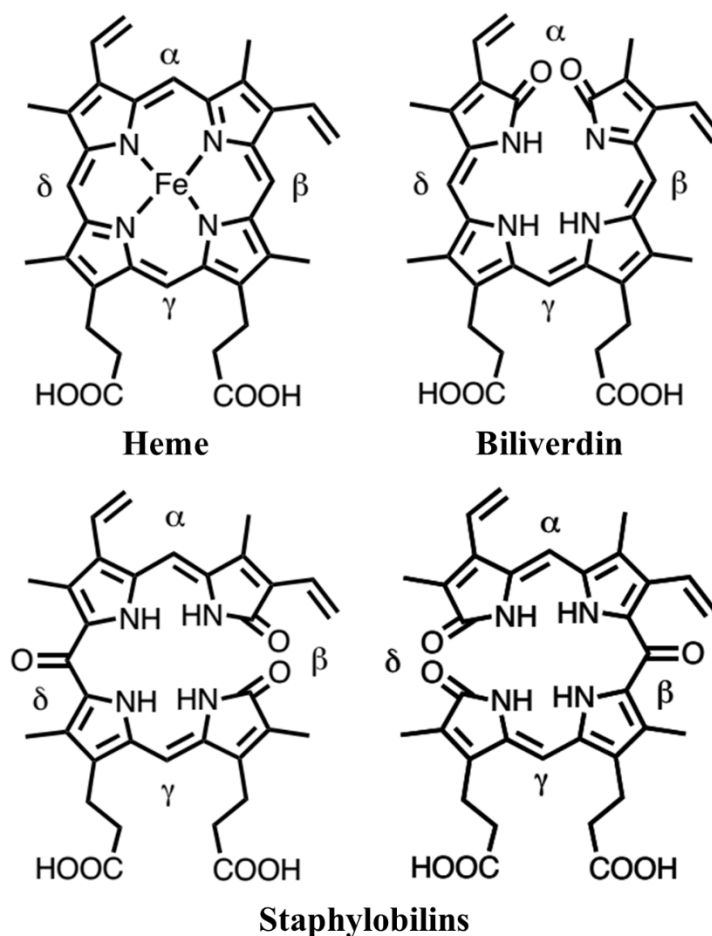


Figure 3.1 Structures of heme, biliverdin, and staphylobilins.

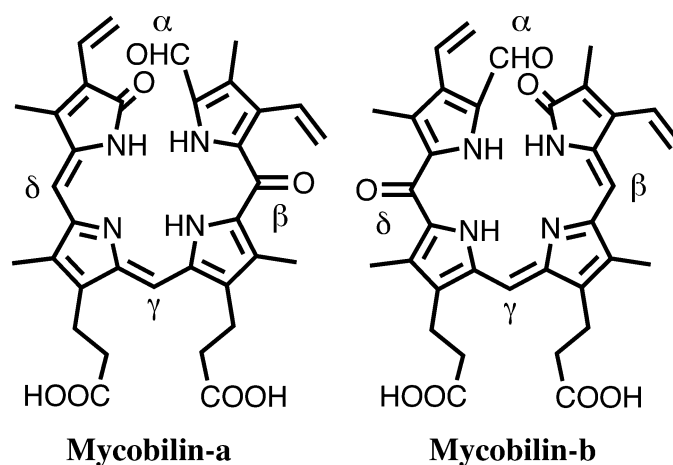


Figure 3.2 Structures of MhuD heme degradation products mycobilin-a and mycobilin-b.

Superposition of the structures of MhuD heme-CN and IsdG/I reveal that the heme molecule in the MhuD active site is rotated $\sim 90^\circ$ about the tetrapyrrole plane from the heme molecules in both IsdG and IsdI^{13, 20}. This difference in heme orientation probably accounts for the variation in the resulting product between IsdG/I and MhuD heme degradation reactions. Previously, the effect of heme orientation on product specificity has been observed in a HO from *Pseudomonas aeruginosa* (*pa*-HO)²¹. Structural determination of *pa*-HO revealed that the *pa*-HO heme molecule, as a result of differential residue contacts, is rotated $\sim 100^\circ$ from the canonical orientation of heme in other HOs²¹. As a consequence, heme cleavage by *pa*-HO occurs at the β -meso or δ -meso carbon instead of at the α -meso carbon producing β - and δ -biliverdin products instead of the typical α -biliverdin product²¹. Mutation to the HO active site has also been shown to alter the HO degradation products. Work by Wang et al. has shown that the hHO Arg183Glu variant results in the generation of δ -biliverdin and trace amounts of β -biliverdin in addition to the canonical α -biliverdin product when ascorbate is used as an electron donor²². Unexpectedly, the heme molecule in the hHO-1 R183E binding

pocket retains the same orientation as wild-type hHO; however, it was proposed that differences in heme degradation products are attributed to changes in the electrostatic environment in the hHO R183E variant active site²².

Close examination of the MhuD active site revealed two residues, Arg22 and Arg26, which could aid in the orientation of the heme molecule via hydrogen-bonding interactions with the heme propionates (**Figure 3.3**). Thus, these residues may be responsible for MhuD's unique degradation products by controlling the site of heme cleavage. In this work, we explore the roles of the Arg22 and Arg26 residues in MhuD's product uniqueness.

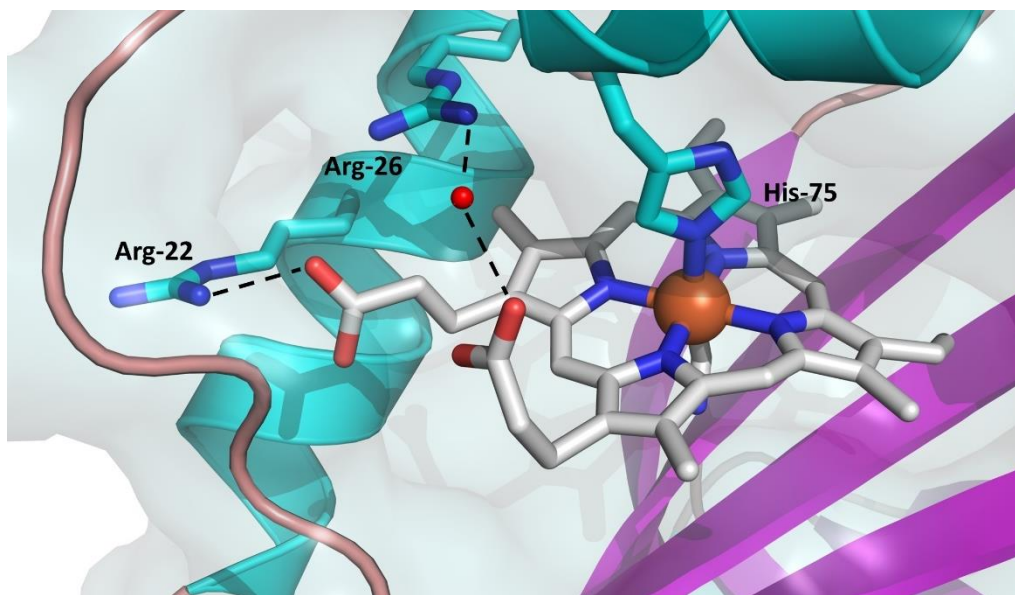


Figure 3.3 Proximal view of MhuD active site. MhuD heme appears to be orientated by Arg-22 and Arg-26 residues.

Results

Heme off tests

To further test that the MhuD mutations did not affect heme binding, the heme off rates for heme to WT MhuD and the R22S and R26S variants were determined. The heme off rates for MhuD-mono-heme and its variants were determined by monitoring absorbance changes over time upon the addition of apo-H64Y/V68F-myoglobin, a high-affinity heme scavenger ($k_{\text{heme-off}} = 1.1 \times 10^{-5} \text{ s}^{-1}$). The reaction was monitored spectrophotometrically and a single-exponential fit was used to determine the heme off rates for wild type (WT) MhuD and its mutants. While little change in the heme off rate was observed for the R26S variant ($k_{\text{heme-off}} = 1.68 \times 10^{-3} \pm 0.08 \times 10^{-3} \text{ min}^{-1}$) compared to wild type MhuD ($k_{\text{heme-off}} = 1.5 \times 10^{-3} \pm 0.03 \times 10^{-3} \text{ min}^{-1}$). There was a noticeable decrease in heme off rate for MhuD R22S ($k_{\text{heme-off}} = 3.87 \times 10^{-3} \pm 0.03 \times 10^{-3} \text{ min}^{-1}$). Despite this, the change in heme off rate in the R22S variant was not substantial enough to prevent heme binding.

Heme degradation assays

To test that the MhuD mutants did not abolish heme degradation activity, the activity of WT MhuD and variants was assessed. MhuD WT and variants were incubated with an electron donor sodium ascorbate to determine heme-degradation. Catalase was added to each heme degradation reaction to rule out non-enzymatic heme degradation. A noticeable decrease in the Soret peak at 401 nm was observed when MhuD WT mono-heme was incubated with sodium ascorbate indicating heme degradation (**Figure 3.4A**). Heme degradation assays

performed using the MhuD variants and indicated that the MhuD R22S and R26S variants did not inhibit MhuD heme degradation (**Figures 3.4B & 3.4C**).

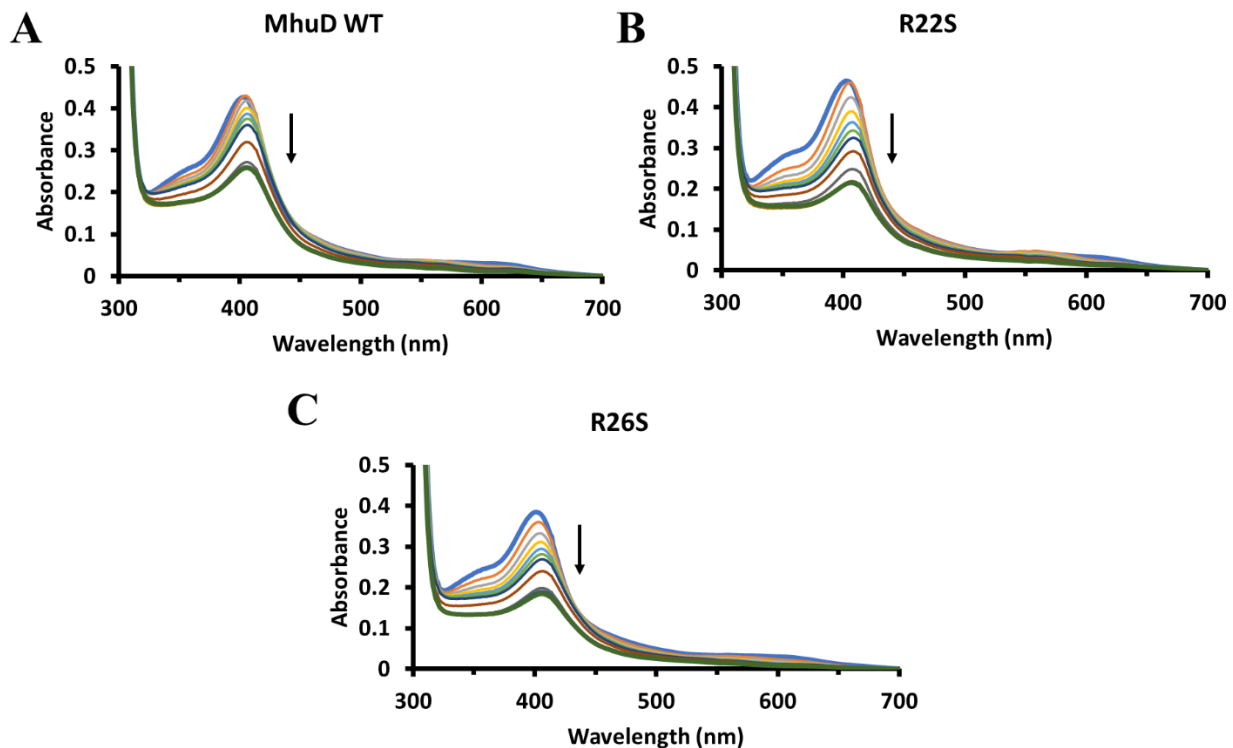


Figure 3.4 Heme degradation assays of wild type (A), R22S (B), and R26S (C) monoheme forms of MhuD in the presence of 0.5:1 molar ratio of catalase to monoheme-MhuD (5 μ M) using ascorbate (10 mM) as the electron donor. UV/vis spectra were collected between 300 to 700 nm in 5-minute intervals. A decrease in the Soret peak (arrow) at 401 nm was observed for MhuD WT indicating that heme was being degraded. The same Soret peak decrease was observed for the R22S and R26S variants of MhuD.

Product purification of MhuD mutants

After initial characterization of the MhuD R22S and R26S variants, product purification from MhuD WT and its variants was carried out as outlined in Nambu et al¹⁵. In brief, to extract the degradation products heme degradation was performed in the presence of an iron chelator. Upon reaction completion, the protein was denatured and the degradation products were extracted using a reverse phase column. HPLC was used to analysis as well as

to further separate the products. Previous characterization found that the wild type MhuD degrades heme into novel chromophores, mycobilin-a and mycobilin-b¹⁵. Product purification from MhuD R22S yielded two primary chromatogram peaks, which elute at the same time as mycobilin-a and mycobilin-b, suggesting that MhuD R22S also produces mycobilin isomers during heme degradation (**Figure 3.5**).

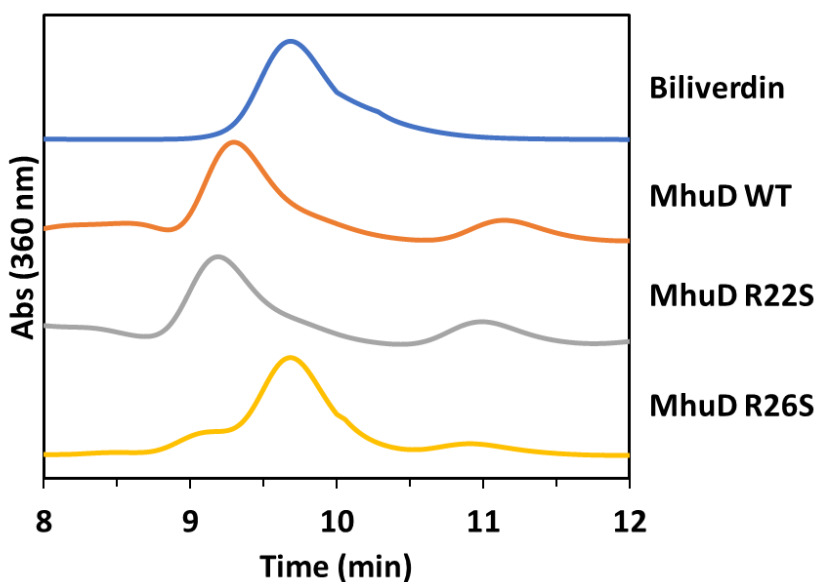


Figure 3.5 HPLC chromatogram of biliverdin (blue) and of heme degradation products from WT (orange), R22S (gray), and R26S (yellow) MhuD-mono heme. Peaks corresponding to MhuD products mycobilin-a and -b appear to elute near 9 min and 11 min respectively for WT and R22S forms of MhuD. Biliverdin and the main R26S product elutes near 10 min.

Furthermore, the UV/vis spectrum of the two HPLC products both have Soret peak maxima at 345nm and Q-band peaks at 555 nm and 565 nm, which are consistent with mycobilin isomer products (**Figure 3.6**). Moreover, the ESI-MS analyses of the MhuD-R22S products, both resulting 611 m/z, further supports that the products are mycobilin-a and mycobilin-b (**Figure 3.6**). While the data suggest that MhuD R22S produces both mycobilin isomers, MhuD R26S appears to produce a product distinct from mycobilin-a or mycobilin-b. Unlike

MhuD WT and MhuD R22S, only one primary peak appears on the chromatogram with an elution time distinct from those of either mycobilin isomers (**Figure 3.5**). HPLC retention times, m/z ratio, and UV/vis spectra suggest that the MhuD R26S variant predominately degrades the protoporphyrin ring to biliverdin. UV/vis analysis shows that the R26S primary product has a Soret peak at 377 nm like biliverdin (**Figure 3.6**) and unlike mycobilin-a and -b that has Soret peaks at 345 nm and 336 nm, respectively (**Figure 3.6**). Furthermore, mass spectrometry found that the molecular mass of the R26S product (m/z 583) is equivalent to that of biliverdin (**Figure 3.6**) and not of mycobilin-a and -b (m/z 611). ESI-MS/MS was performed to verify that our R26S variant produces α -biliverdin as its degradation product. Fragmentation of α -biliverdin control yielded a daughter-ion species at m/z 297 as previously reported in literature (**Figure 3.7**)²³. The same 297 m/z daughter-ion species was observed in the fragmentation spectra of the R26S product showing that α -biliverdin is produced by MhuD R26S (**Figure 3.7**). Lastly, two minor peaks with similar retention times to the mycobilin isomers were also observed, which were identified as mycobilin-a and -b (**Table 3.1**). These results demonstrate that α -biliverdin is primarily generated upon heme degradation by the MhuD R26S variant and thus highlights the importance of Arg26 in MhuD product uniqueness and perhaps mechanism of action.

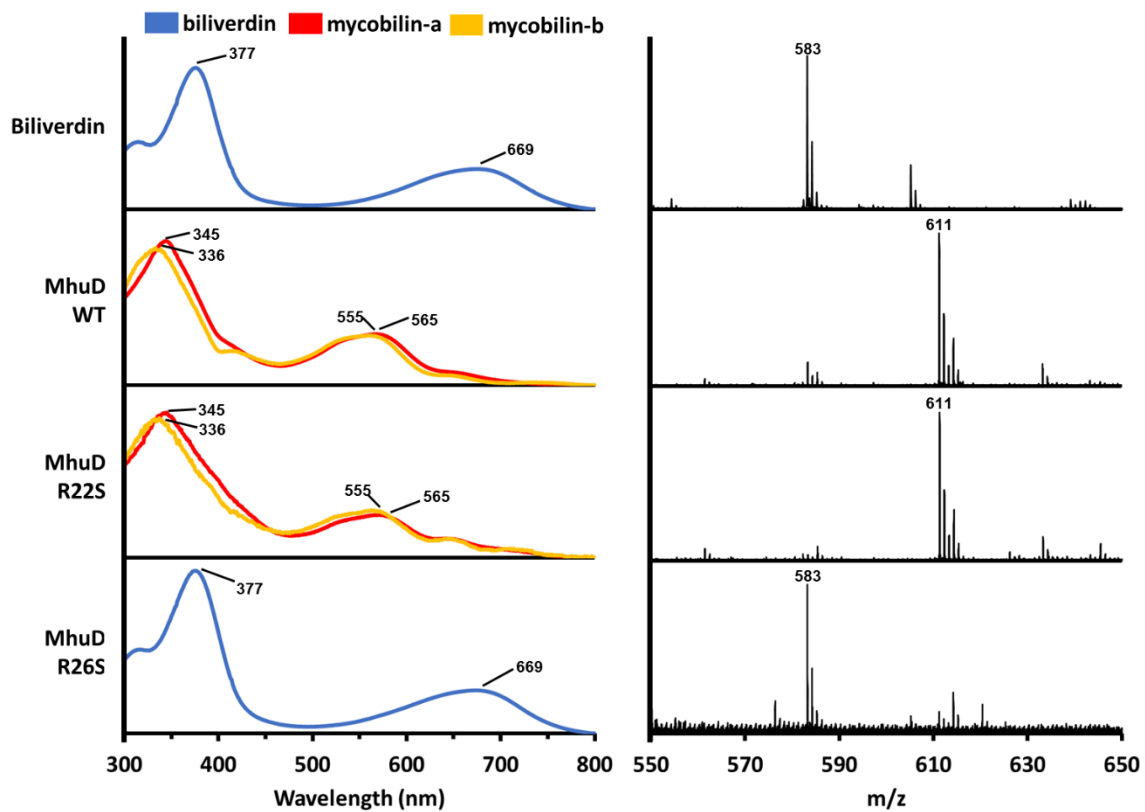


Figure 3.6 UV/vis spectra (left) and ESI-MS spectra (right) of biliverdin and degradation products from the wild type, R22S, and R26S variants of MhuD. Products from MhuD R22S share the same UV/vis and mass spectra as wildtype MhuD's mycobilin products, while MhuD R26S products share the same spectra as biliverdin.

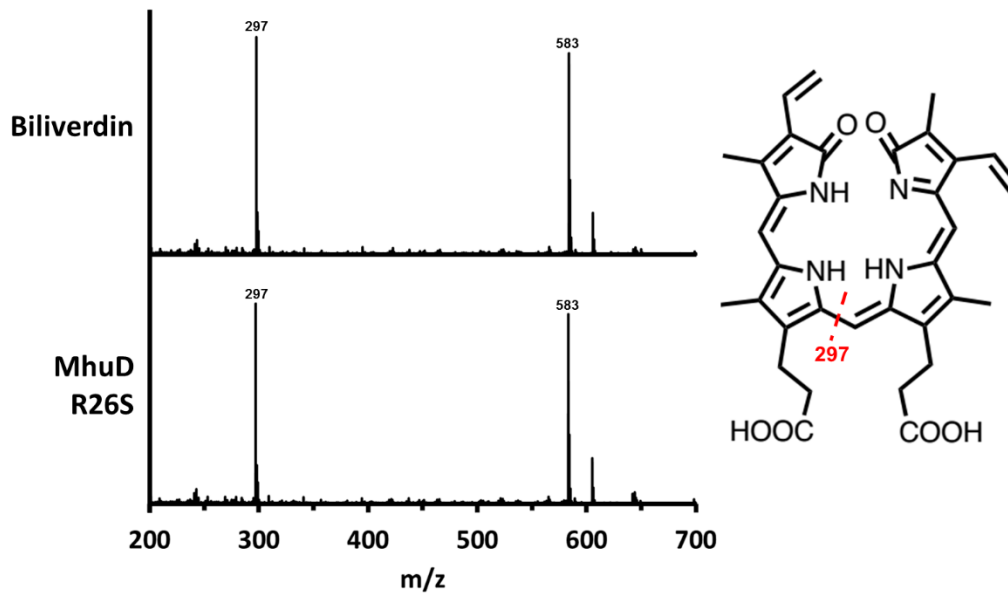


Figure 3.7 Fragmentation spectra of α -biliverdin (top) and MhuD R26S heme degradation product (bottom). Fragmentation profiles of both α -biliverdin and the MhuD R26S product share the same 297 m/z daughter-ion. Structure of α -biliverdin with predicted fragmentation also shown (right).

Table 3.1 Estimated product yields from MhuD WT and mutants

	Mycobilin-a	Mycobilin-b	Biliverdin
MhuD WT	87.0%	12.8%	0.0%
MhuD R22S	80.3%	19.7%	0.0%
MhuD R26S	10.7%	7.7%	81.6%

Identification of MhuD-R26S C1 product

Since CO is generated when HO degrades heme into biliverdin, we tested if the MhuD R26S variant also produces CO as its C1 product upon heme degradation. CO production was detected using a H64L variant of myoglobin (Mb) with high CO affinity as outlined in Nambu et al¹⁵. In this assay, spectral changes upon the addition of reduced myoglobin were compared between MhuD-mono heme samples where heme degradation was initiated and samples without initiation of heme degradation. Consistent with prior reports, CO

generation was detected during HO-1 heme degradation, but not observed during MhuD WT heme degradation (**Figure 3.8**). Despite degrading heme into biliverdin, no CO production was detected during heme degradation by the MhuD R26S variant (**Figure 3.8**).

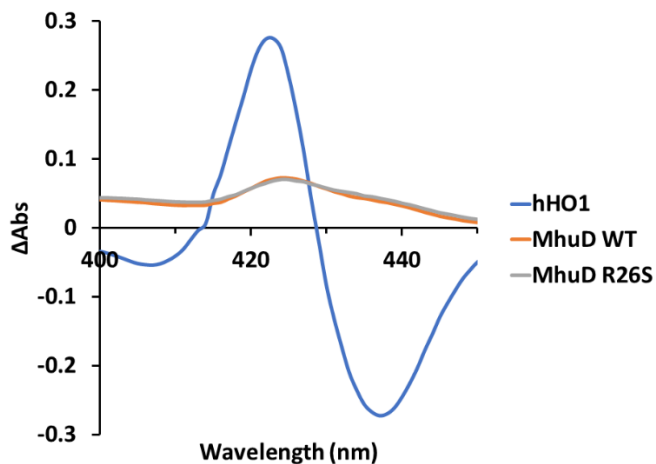


Figure 3.8 CO detection assay of known CO producer human heme oxygenase-1 (hHO-1) (blue), MhuD WT (orange), and MhuD R26S (gray). While hHO-1 produces CO during heme degradation as indicated by the peak near 420 nm, MhuD WT and R26S do not.

MhuD R26S was also tested for the production of alternate C1 products. Another C1 candidate may be formic acid and previously, it was shown that MhuD homologs IsdG/I generate formaldehyde upon heme degradation¹⁷.

To test for formic acid production, formic acid dehydrogenase was used to consume formic acid and generate NADH, which can be quantified via HPLC. No formic acid production was detected for MhuD WT or the R26S variant (**Figure 3.9**).

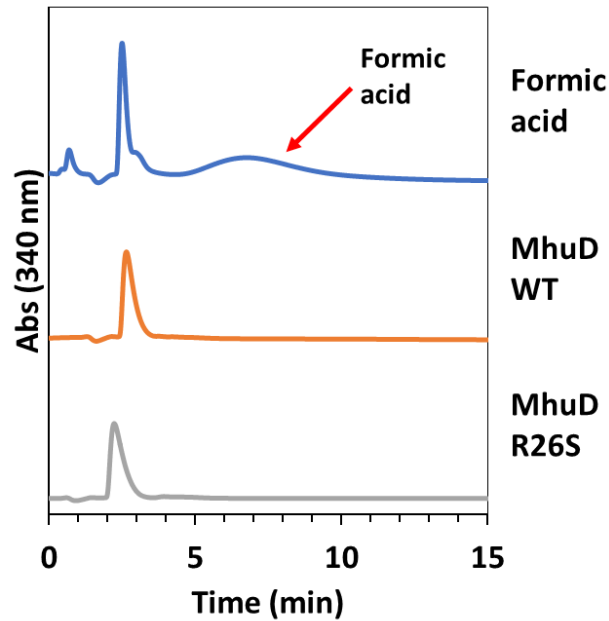


Figure 3.9 Formic acid detection assay of MhuD WT (orange) and MhuD R26S (gray) as well as a formic acid standard (blue). Neither MhuD WT nor MhuD R26S produce formic acid in the heme degradation process.

To test for formaldehyde production, Nash's reagent was used to convert the generated formaldehyde into a yellow pigment quantifiable via HPLC. As expected, formaldehyde production was detected during IsdG heme degradation, while no formaldehyde was observed for WT MhuD heme degradation (**Figure 3.10**).

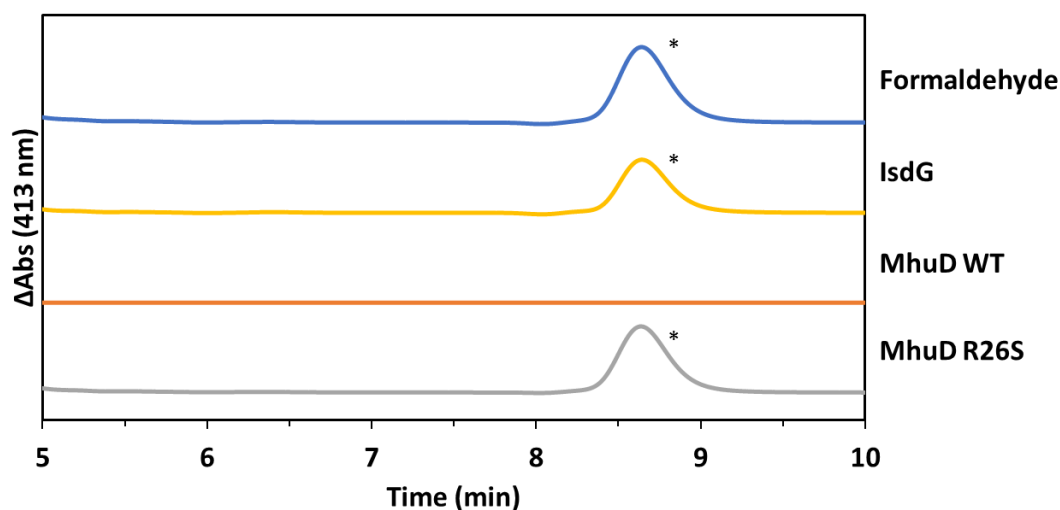


Figure 3.10 Formaldehyde detection assay of known formaldehyde generator IsdG (yellow), MhuD WT (orange), and MhuD R26S (gray). A formaldehyde standard (blue) was also included. Product signal marked with asterisks. While MhuD WT does not produce formaldehyde during heme degradation, the R26S variant does.

While MhuD WT doesn't generate formaldehyde, tests showed that like IsdG/I, the MhuD R26S variant produces formaldehyde during heme degradation (**Figure 3.10**).

Crystallization of MhuD R26S

Previous studies of MhuD and IsdG/I have found that the hemes in these heme degrading enzymes are distorted or ruffled as opposed to the more planar hemes observed in canonical HOs^{19, 20}. Because the MhuD R26S produces biliverdin like HOs, it was suspected that like in HOs the heme MhuD R26S was also more planar than in the MhuD WT. To determine the degree of heme ruffling in our R26S variant, we attempted to solve the structure of MhuD-mono-heme-R26S via X-ray crystallography. Initially, crystallization trials were set up with

MhuD R26S with cyanide derivatized heme. Despite using substoichiometric ratios of heme-CN, only the diheme form of MhuD R26S was crystallized and solved. The crystal structure of diheme MhuD R26S was refined to a resolution of 1.9 Å and is highly similar to that of the wild type MhuD-diheme with a rmsd of 0.759 Å. MhuD R26S diheme retains the ferredoxin-like $\alpha + \beta$ -barrel fold previously observed in both wild type MhuD-diheme and wild type cyanide inhibited MhuD monoheme (**Figure 3.11A & 3.11B**). Like in the wild type MhuD diheme, the hemes of the MhuD R26S diheme are planar and solvent exposed heme is rotated 90° degrees from the solvent protected heme. One notable difference is that Ser26 residues are oriented away from the heme molecules and does not in any way interact with heme. Moving on, it is also unclear, based on the electron density, whether the solvent protected hemes are coordinated by cyanide or chloride ions, despite having derivatizing heme with cyanide. While cyanide is a stronger ligand compared to chloride, it is plausible that the cyanide may have been protonated under the slightly acidic conditions of the crystallization condition.

Attempts were also made to crystalize MhuD R26S in its monoheme form with heme analogs Mn-protoporphyrin IX (Mn-PPIX), Co-protoporphyrin IX, and Zn-protoporphyrin IX. Bright red crystals formed of MhuD R26S with substoichiometric ratios of Mn-PPIX. As with heme, MhuD R26S was crystallized in its diheme form with two Mn-PPIX per active site (**Figure 3.11C & 3.11D**). The MhuD R26S di-Mn-PPIX structure was solved to a resolution of 2.4 Å and had a rmsd of 0.638 Å to MhuD-diheme. However, as with the MhuD R26S-diheme structure, the Ser26 residue is orientated away from the heme.

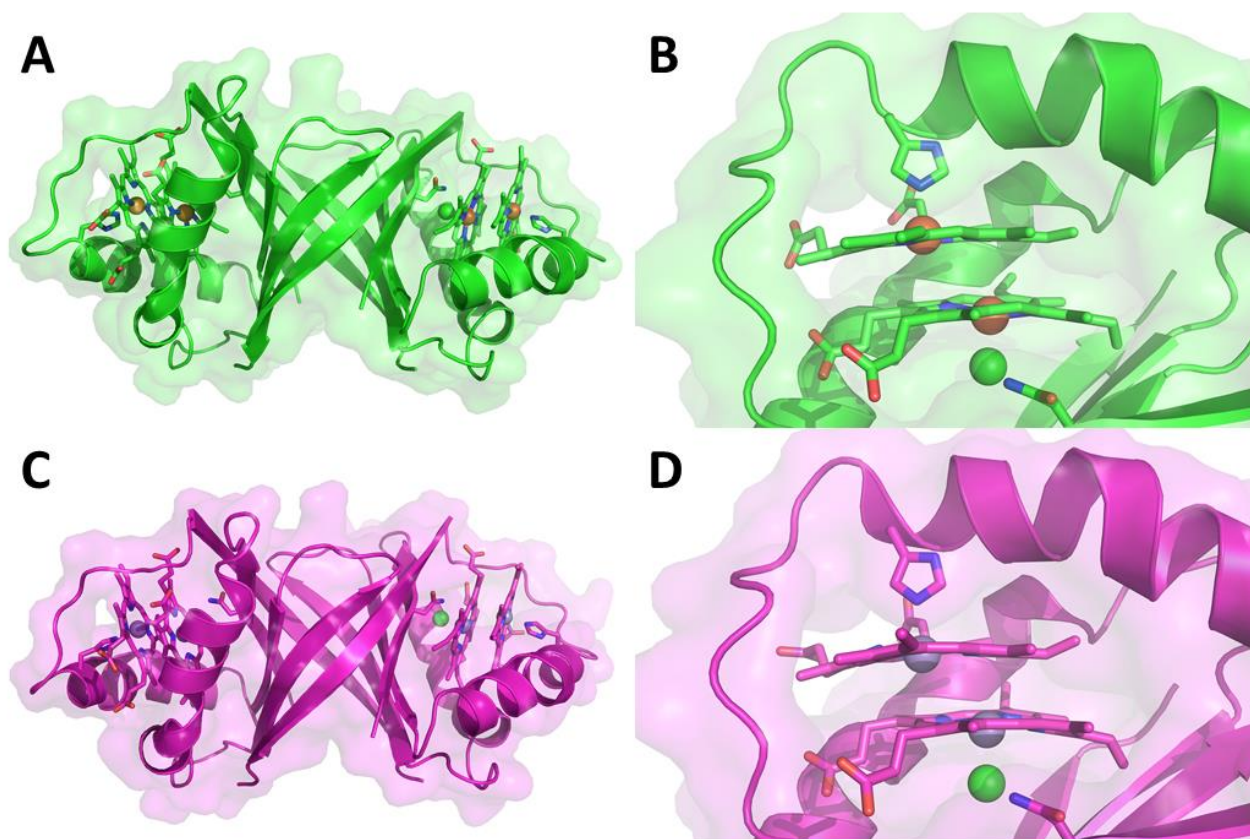


Figure 3.11 Ribbon representations of the full MhuD R26S-diheme structure (**A**) and a close up view of its binding site (**B**). Ribbon representations of the full MhuD R26S-diMnPIX structure (**C**) and a close up view of its binding site (**D**). In both structures, each MhuD R26S monomer has either two hemes or two Mn-PIX in its active site.

We also crystallized and solved the structure of MhuD R26S in complex with its biliverdin product to a resolution of 2.5 Å. The asymmetric unit of the MhuD-biliverdin consist of two MhuD monomers connected at their active sites by five partially π -stacked biliverdin molecules (**Figure 3.12A**). The MhuD-biliverdin structure is highly similar to that of the MhuD heme-CN and the MhuD-diheme structures. The solvent protected biliverdin adopts a similar orientation as the monoheme in MhuD heme-CN and the solvent protected heme in the MhuD-diheme structure (**Figure 3.12B & 3.12C**). As seen in the MhuD heme-CN structure, the $\alpha 2$ helix is kinked at the Asn68 residue in the MhuD-biliverdin structure but is

ends a few residues earlier than in the MhuD heme-CN structure (**Figure 3.12B**). Despite structural similarity of the MhuD-biliverdin with other MhuD structures, MhuD-biliverdin contains an additional α -helix at residues 76-80 not observed in either the MhuD heme-CN or the MhuD-diheme structures. We suspect that the absence of a metal for the His75 residue to coordinate is primarily responsible for the previously mentioned shortening of the α 2 helix as well as the formation of this new α 3 helix in the MhuD-biliverdin structure.

Recently, the structure of apo-MhuD has been crystallized and solved (5UQ4). The apo-MhuD structure shares high structural homology with the MhuD-biliverdin structure, however, two notable differences can be observed between the two structures (**Figure 3.12D**). First, α 1 helix of apo-MhuD-WT is extended by two helical turns. This can be attributed to the absence of a ligand in the binding pocket that would otherwise sterically hinder. Secondly, residues 73-85 are missing in the apo-MhuD structure indicating that this region is highly disordered when MhuD is in its unbound state.

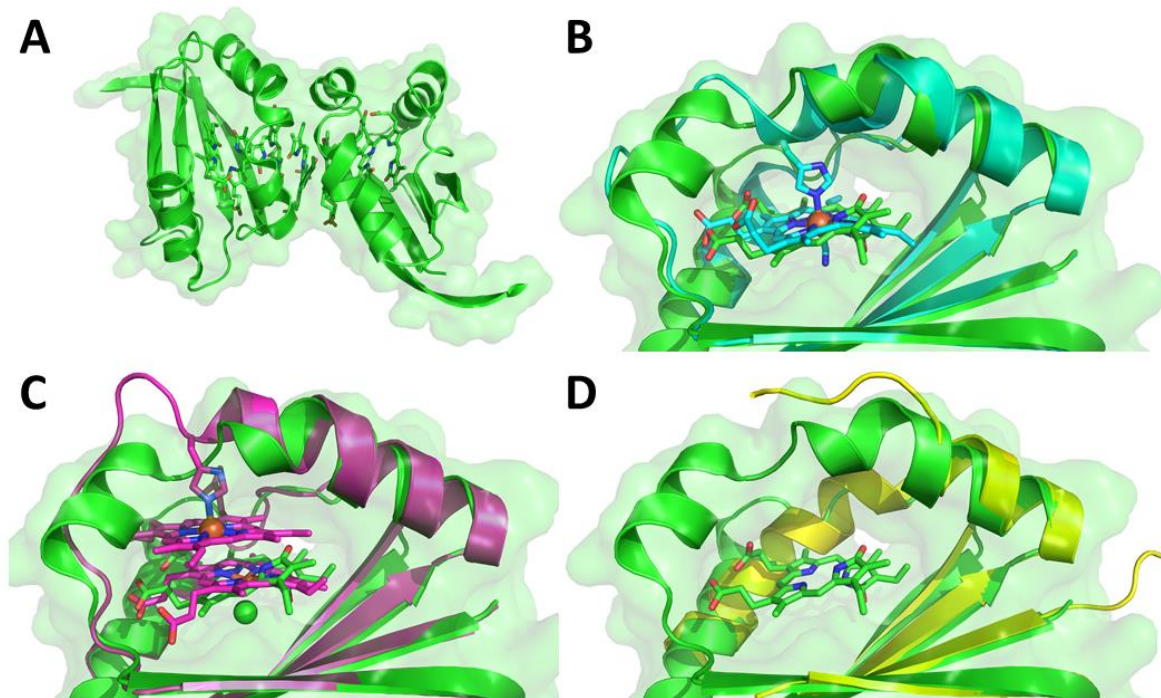


Figure 3.12 Ribbon representations of the full MhuD R26S-biliverdin structure (A). Structural comparison of the active sites of MhuD biliverdin (green) against active sites of MhuD heme-CN (cyan) (B), MhuD-diheme (purple) (C), and apo-MhuD WT (yellow) (D).

Table 3.2 X-ray data collection and refinement statistics for the structural determination of MhuD R26S diheme, MhuD R26S di-MnPPIX, and MhuD R26S biliverdin

	MhuD R26S diheme	MhuD R26S di-MnPPIX	MhuD R26S biliverdin
Space group	P2 ₁ 2 ₁ 2 ₁	P2 ₁ 2 ₁ 2 ₁	I222
Unit cell dimensions (Å)	38.21 × 68.57 × 74.09	39.02 × 68.70 × 74.49	37.2399 × 113.59 × 113.64
pH of crystallization conditions	5.5	7.5	6.5
Data Set			
wavelength (Å)	1.0	1.0	1.0
resolution range	37.05 - 1.90	50.50 - 2.40	35.93 - 2.5
unique reflections (total)	15858 (31671)	7868 (15636)	8413 (16206)
completeness (%) ^a	99.04 (96.54)	95.06 (93.60)	96.47
Redundancy	2.0 (2.0)	2.0 (2.0)	1.9 (1.9)
R _{merge} ^{a,b}	0.02947 (0.2111)	0.01736 (0.08277)	
I/σ	12.23 (2.67)	26.25 (7.58)	25.41 (10.64)
NCS copies	2	2	2
Model Refinement			
resolution range (Å)	37.05 - 1.90	50.50 - 2.40	35.93 - 2.5
no. of reflections (working/free)	15767 (1479)	7864 (760)	8409 (826)
no. of protein atoms	1495	1494	1449
no. of water molecules	127	24	16
no. of heme or MnPPIX or biliverdin/dimer	4	4	5
No. of chloride/dimer	2	2	0
missing residues	101-105	102-105	99-105
R _{work} /R _{free} (%) ^c	17.6/22.5	18.4/24.3	0.2211/0.3012
Average B-factor (Å²)			
protein	26.87	30.93	49.06
ligands	25.69	28.77	39.44
water	35.42	28.41	45.18
rms deviations			
bond lengths (Å)	0.015	0.012	0.011
bond angles (degrees)	1.75	1.45	1.47
Ramachandran Plot			
most favorable region (%)	95.88	95.88	90.53
additional allowed region (%)	4.12	4.12	7.89
disallowed region	0.00	0.00	0.00
PDB ID code	6DS7	6DS8	NA
^a Statistics for the highest-resolution shell are given in brackets.			
^b R _{merge} = Σ I - ⟨I⟩ / ΣI			
^c R _{work} = Σ F _{obs} - F _{calc} / ΣF _{obs} . R _{free} was computed identically to that of R _{work} except for where all reflections belong to a test set of 10% randomly selected data.			

UV/vis spectroscopy of MhuD R26S

Spectra of the wild type and R26S monoheme MhuD were collected to possibly observe differences in the heme binding environment. Both the wild and R26S monoheme complexes had Soret maxima at 399 nm. Furthermore, no spectra differences could be observed between the wild type and the R26S mutant.

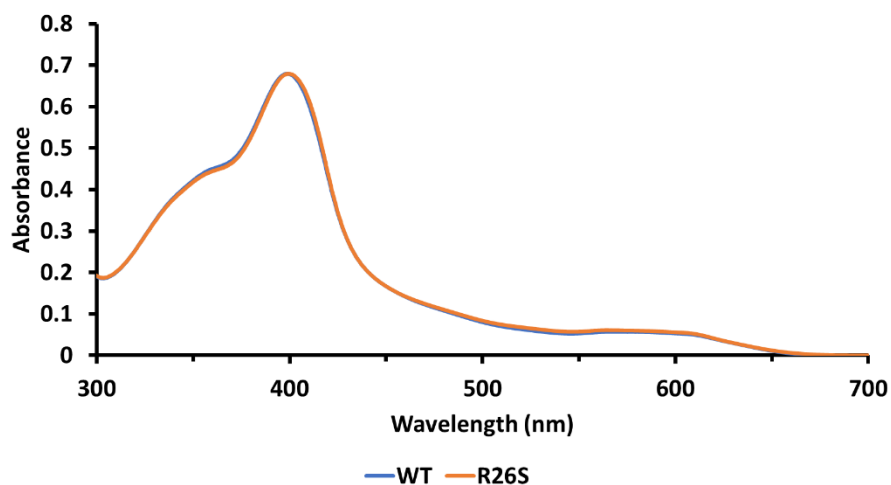


Figure 3.13 UV/vis spectra of wild type (blue) and R26S (orange) monoheme MhuD.

Resonance raman of MhuD R26S

Resonance raman spectroscopy of wild type and R26S MhuD monoheme (**Figure 3.14**). Frequency mode assignments were based on previous assignments from Heme-Nitric oxide/Oxygen binding domain from *Thermoanaerobacter tengcongensis*²⁴, which also has a ruffled heme. Reduced intensities corresponding to the symmetric pyrrole folding modes γ_{21} , γ_{15} , and ν_{15} were observed at 547, 685, and 749 cm^{-1} respectively in the spectra R26S monoheme, but not in the spectra of the WT monoheme. Additionally, the peak associated

with the symmetric pyrrole folding mode γ_{11} was upshifted by 2 cm^{-1} from 715 cm^{-1} in the wild type monoheme to 717 cm^{-1} in the R26S monoheme. These spectral differences suggest that heme ruffling is reduced in MhuD R26S.

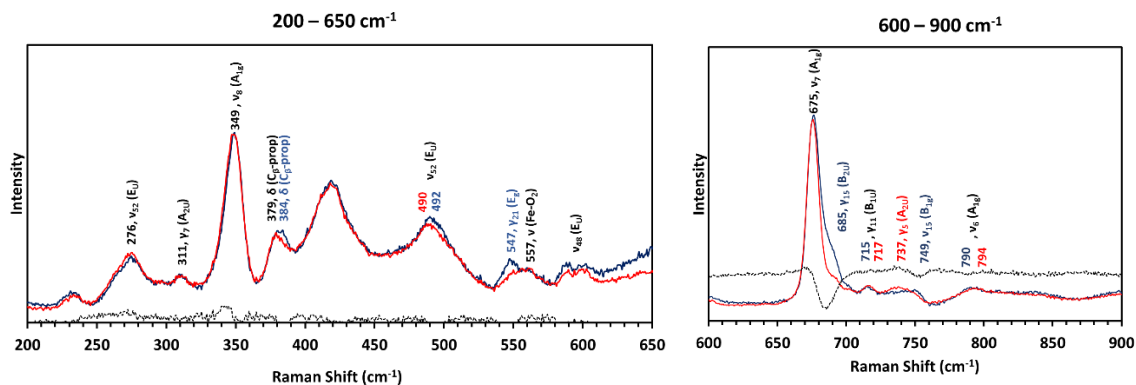


Figure 3.14 Raman spectra of MhuD WT-monoheme (blue) and MhuD R26S-monoheme (red). The difference spectra is also included (black dashes).

EPR spectroscopy of MhuD R26S

EPR spectroscopy was performed to tease out the electronic structure of monoheme MhuD R26S (**Figure 3.15**). EPR spectra of monoheme MhuD R26S were collected alongside with those of holo-hHO-1, MhuD WT monoheme, MhuD W66A monoheme, and holo-IsdI. The ruffled hemes of IsdI and MhuD WT both appeared low spin configuration. In sharp contrast, the EPR spectra of the ferric heme:hHO-1 complex at pH 7.4 exhibited a high spin ferric hemoprotein signal. The high spin state exhibits both an axially symmetric type of spectrum $g = 6$ and $g = 1.98$, previously observed for mammalian and bacterial HOs²⁵⁻²⁷. For IsdI, exhibited predominately low spin signal ($g = 2.57$, $g = 2.23$ and $g = 1.78$)²⁷ with slight high spin characteristics ($g = 6$ and $g = 1.98$), and wild-type MhuD also exhibited a similar EPR spectrum, however there appears to be a slightly larger percentage of a high

spin component, see **Table 3.3**. Interesting, the inactive MhuD W66A variant, in which heme ruffling has been shown to be diminished, exhibited a predominately high spin signal ($g = 5.96$ and $g = 1.97$), similar to hHO-1. Finally, the EPR spectra of the MhuD R26S variant suggests two separate populations of high spin ($g = 5.88$) and low spin ($g = 2.22$) heme complexes. These high and low spin populations could correspond to low to high degrees of heme ruffling. In the IsdI, MhuD WT and R26S MhuD samples, there is a $g = 4.20-4.28$, which may be attributed to trace iron in the samples – this has been observed previously in CcmE proteins²⁸.

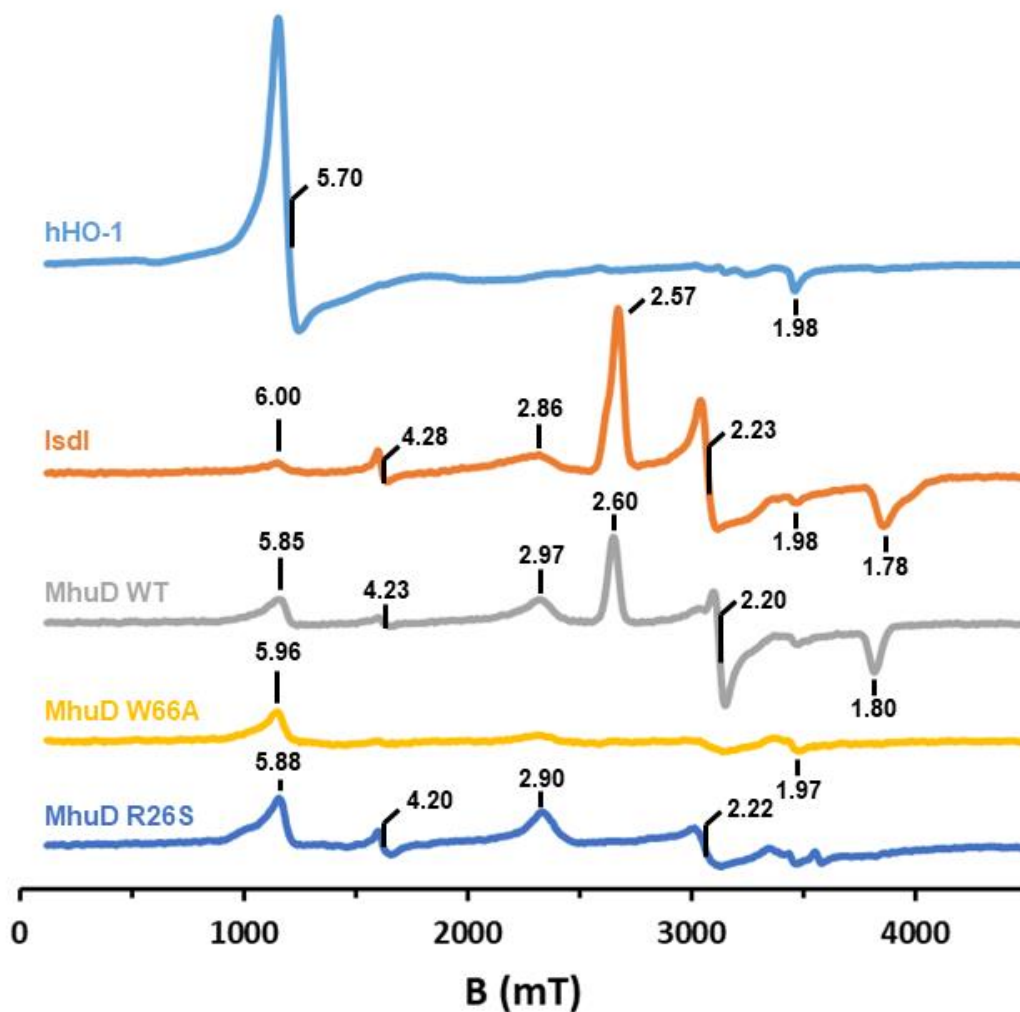


Figure 3.15 EPR spectra of holo-hHO-1 (light blue), holo-IsdI (orange), MhuD WT-mono-heme (gray), MhuD W66A-mono-heme (yellow), and MhuD R26S-mono-heme (dark blue).

Table 3.3 EPR values in this study.

Protein	Spin state		Liganding
	High -spin	Low-spin	
hHO-1	5.70	ND	His/Cl ⁻
IsdI	6.00/1.98	2.57/2.23/1.78	His/Cl ⁻
MhuD WT	5.85	2.60/2.20/1.80	His/Cl ⁻
MhuD W66A	5.96/1.97	ND	His/Cl ⁻
MhuD R26S	5.88	2.22	His/Cl ⁻

ND, not detected

Discussion

MhuD R26S generates biliverdin product

Previous it has been shown that MhuD WT degrades heme into distinct mycobilin isomers¹⁵. These mycobilin isomers are distinct from other heme degrading enzymes previously reported in the literature¹⁵. Furthermore, heme degradation by MhuD is achieved without the generation of a C1 product as observed in heme degradation by HOs and IsdG/I^{15, 17}. Initially, we thought that MhuD's differential heme orientation from that of IsdG/I was responsible for MhuD's unique heme degradation product. We identified two residues that were potentially responsible for MhuD's unique heme orientation inside the heme binding pocket, Arg-22 and Arg-26. Mutation of the Arg-22 residue into a serine did not appear to alter MhuD's heme degradation product. However, the R26S mutation changes MhuD's heme degradation product from mycobilin into biliverdin. Interestingly, unlike HOs which also produces biliverdin, our R26S variant does not generate CO upon heme degradation. Instead, MhuD R26S produces formaldehyde as its C1 product similar to IsdG/I¹⁷. This suggest that our R26S variant degrades heme in a mechanism different to that of HO and MhuD.

Proposed mechanism for MhuD heme binding and product release

Structural determination of the apo-MhuD revealed that apo-MhuD is highly disordered between residues 67 and 85. We propose residues Ala67-Thr85 are disordered when MhuD is in its apo form, allowing the now solvent exposed His75 residue to recognize and coordinate with either free heme or heme from a partner protein. Furthermore, the

propensity for MhuD R26S to crystallize in its diheme form suggests that the Arg26 residue prevents incorporation of the second heme into the binding site presumably unless the heme concentration is high. A closer look at the active site revealed that the Arg26 is perfectly positioned to sterically hinder accommodation of a second heme if heme passes through the opening between the $\alpha 1$ and the $\alpha 2$ helices in the heme incorporation process. After this, we postulate that the residues Ala67-His75 rearrange, stabilized by the presence of the heme ligand, in particular by the coordination of the heme iron and the His75 residue, resulting in an extended $\alpha 2$ helix as observed in the MhuD-heme-CN structure. Examination of the MhuD-biliveridin structure revealed the presence of a new $\alpha 3$ helix formed by residues His75 to Pro82. Interestingly, the His75 is oriented away from the biliverdin molecules and is solvent exposed, suggesting that this is the conformation adopted prior to product release post heme degradation after iron extraction. However, it is unclear if the MhuD-biliveridin conformation is an artifact of crystallization since it is uncertain whether iron is released from mycobilin before or during mycobilin release from the MhuD active site.

Accessibility of the MhuD R26S binding pocket and potential accommodation of water

To observe the ruffling state of the heme in the MhuD R26S active site, we attempted to crystallize the R26S variant with substoichiometric ratios of heme and with different heme analogs. However, despite our exhaustive attempts to crystallize MhuD R26S momoheme, we were only able to crystallize the mutant with two metalloprotoporphyrins per active site, suggesting that the R26S mutation decreases heme ruffling and thus increases susceptibility to

heme stacking. Additionally, initial EPR data of the MhuD R26S monoheme contains both high and low spin characteristics suggesting that heme ruffling is diminished in the mutant.

The EPR data of MhuD R26S and propensity of MhuD R26S crystallize as a diheme suggest that the MhuD R26S active site is flexible enough to accommodate water molecules on the distal side of the heme. In fact, in the cyanide derivative crystal structure of IsdI W66Y, in which heme ruffling is also diminished, there is a distal pair of water molecules forming a hydrogen bond network with the cyanide ligand and the Thr-55 residue²⁹. In a way analogous to the network of water molecules found in HOs, this purported distal water molecule in MhuD R26S may play a role in molecular oxygen activation as well as product specificity.

Proposed activation of R26S mutant

Previous work suggests that Isd-type heme degrading enzymes utilize ruffled or distorted heme, where the heme undergoes a out of plane distortion greater than 1 Å. This heme distortion is thought to enable the activation of molecular oxygen by decreasing the reduction potential of the heme, thus allowing for the production of a reactive ferric-oxy [Fe-OO-] species for heme degradation²⁹⁻³¹. Conversely, reductions in IsdG/I and MhuD heme ruffling have been shown to abolish heme degradation, which are thought to be attributed to a decreased heme reduction potential²⁹.

Paradoxically, despite evidence of diminished heme ruffling in the R26S variant, the R26S still retains its heme degradation properties. Examination of the MhuD WT monoheme

structure indicates that Arg-26 appears to immobilizes the negatively charged propionate-7 carboxyl group in close proximity of the heme iron. Previous work on the hHO-1 R183E mutant has shown that positive to negative charge reversal in the hHO-1 active site makes reduction of the heme substrate more difficult²². Conversely, mutation of the Arg-26 residue into serine may allow the propionate-7 carboxyl group to delocalize away from the heme iron increasing reduction potential in the heme iron and allowing for oxygen activation, and thus rescuing MhuD heme degradation in our R26S variant and possibly changing the degradation product into biliverdin.

Proposed mechanism

Degradation of heme by HOs into biliverdin has been shown to occur through three successive oxygenation steps⁶. In HO heme degradation, molecular oxygen is activated by the formation of a ferric-hydroxy [Fe-OOH] species with assistance from nearby network of water molecules in HO core after which the heme is hydroxylated at the α -meso carbon into α -hydroxyheme^{32, 33}. The α -meso-hydroxyheme undergoes a rapid, spontaneous auto-oxidation into α -verdoheme before undergoing another self-oxygenation into biliverdin^{34,35}. In the proposed heme degradation mechanism for MhuD, heme is hydroxylated at either the β/δ -meso carbon into β/δ -hydroxyheme, before undergoing a deoxygenation into mycobilin. Since the other meso carbons do not appear to be altered in R26S heme degradation, MhuD R26S likely degrades heme through the hydroxylation of a different site an instead of β/δ -meso carbon as is the case reported for wild type MhuD activity. This change in

hydroxylation site may be the result of the aforementioned of distal water molecule in R26S active site playing a role first in activation of molecular oxygen, forming a ferric-hydroxy [Fe-OOH] species, and secondly in orienting the oxygen away from the β/δ -meso carbon to favor hydroxylation at or near the α -meso carbon instead of at the β/δ -meso carbon. Because evidence suggest that heme ruffling is reduced in the MhuD R26S mutant, spin density may be delocalized onto the porphyrin pyrrole rings as observed in HOs instead of onto the α -, β -, γ -, and δ - meso carbons of the heme which is what is observed in IsdG/I and MhuD^{19, 30, 36}. As a result, we suspect that the heme is oxidized near the α -meso carbon at the 4- or 6- carbon position instead of at the α -meso carbon.

The fact that MhuD R26S does not produce CO as its C1 product suggest R26S heme degradation does not proceed through the formation of α -verdoheme. Production of formaldehyde by MhuD R26S suggest that ferric α -formyl-oxo-bilin is generated instead as an intermediate. As such, we propose that heme is converted into ferric α -formyl-oxo-bilin intermediate through a mechanism inspired by Wang et al. for hHO-1 (**Figure 3.16**)³⁷. In this mechanism, heme is hydroxylated at either the 4- or 6- carbon position by an activated oxygen molecule. Afterwards, the heme is hydrated before being oxidized at either the 4- or 6- carbon by another activated oxygen molecule resulting in a ferric α -formyl-oxo-bilin intermediate. Finally, similar to the final proposed step for IsdG/I production of staphylobilin, iron and formaldehyde leave resulting in the final biliverdin product.

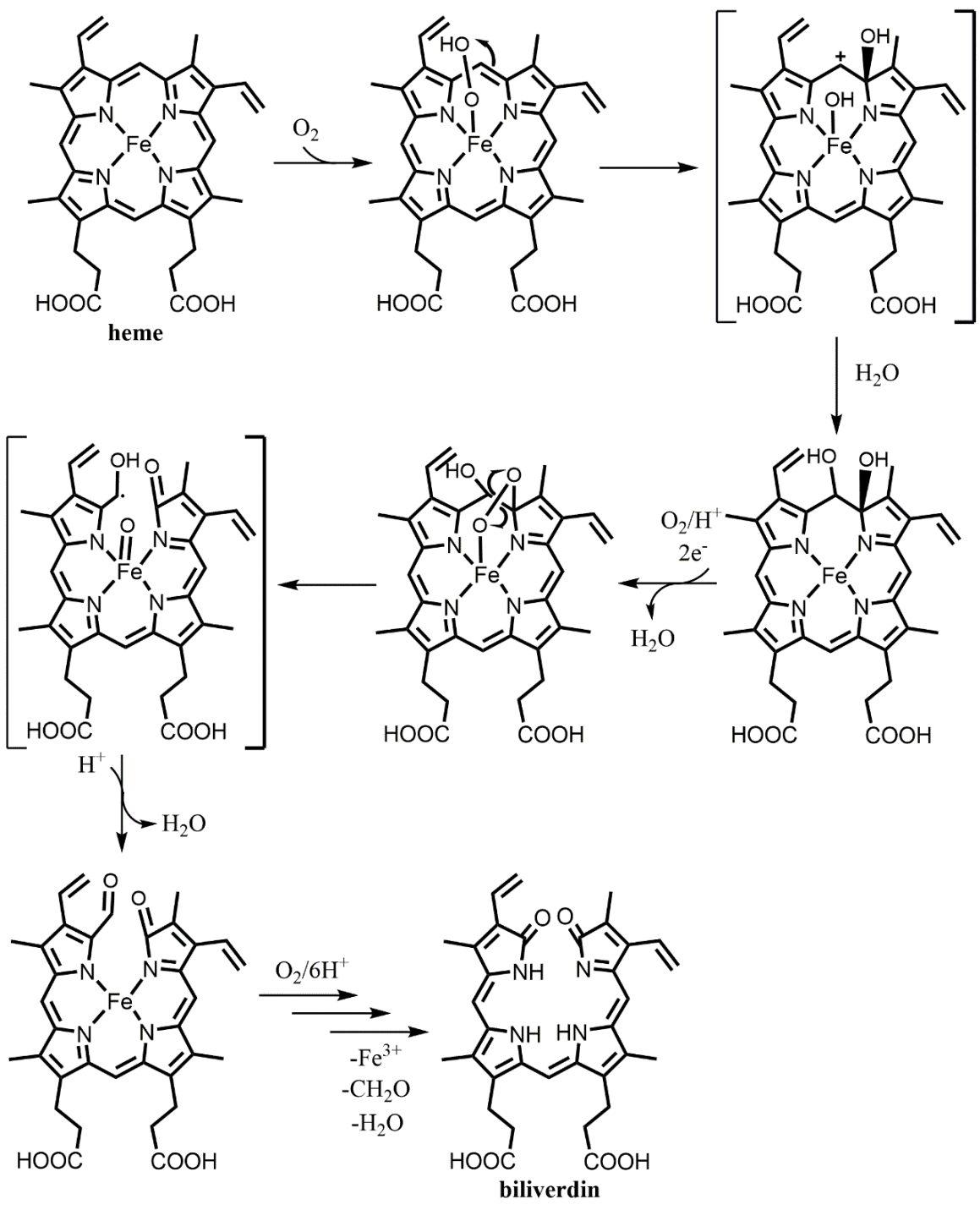


Figure 3.16 Proposed mechanism for MhuD R26S heme degradation.

Materials and Methods

Expression and purification of wild type Mtb MhuD and its mutants

Generation of pET22b vector for his-tagged wild type Mtb MhuD expression was achieved as previously described¹³ and the mutant constructs reported herein were prepared through site directed mutagenesis. Site directed mutagenesis using MhuD-R22S-fwd (5' - CGA GCT GGA GAA GTC GTT CGC TCA CCG - 3') and MhuD-R22S-rev (5' - CGG TGA GCG AAC GAC TTC TCC AGC TCG - 3') primers was used to introduce the R22S mutation. The MhuD R26S construct was produced via site directed mutagenesis using primers MhuD-R26S-fwd (5' - CGG TTC GCT CAC AGC GCG CAC GCG G - 3') and MhuD-R26S-rev (5' - CCG CGT GCG CGC TGT GAG CGA ACC G - 3'). The MhuD mutants were expressed and purified in the same manner as reported for the wild type variant. In brief, *E. coli* B21-Gold (DE3) cells transformed with pET22b-MhuD vector were grown in LB medium containing 50 µg/mL ampicillin at 37°C. Overexpression was induced at OD₆₀₀ of ~ 0.6 using 1 mM IPTG. The cells were harvested 4 hours post induction and resuspended in lysis buffer (50 mM Tris/HCl pH 7.4, 350 mM NaCl and 10 mM imidazole). Cells were lysed via sonication and the resulting lysate was centrifuged at 14,000 rpm and passed through a 1 µm filter. The cell supernatant was loaded onto a Ni²⁺-charged HiTrap chelating column (5 mL) and washed with lysis buffer. Bound protein was eluted from the column with increasing concentrations of imidazole. Next, MhuD, which elutes at 50 and 100 mM imidazole, was concentrated (Amicon, 5 kDa molecular mass cutoff) and was further purified on a S75 gel filtration column in 20 mM Tris, pH 8, and 10 mM NaCl. A final purification step was performed on an ion exchange column (HiTrap Q HP, 5 mL) with the pure MhuD eluting at 150 mM NaCl.

Preparation of MhuD-mono-heme

Reconstitution of wild type MhuD and its mutants with heme was achieved as previously described¹³. Briefly, a hemin solution was prepared by dissolving 4 mg of heme in 500 μ L 0.1 M NaOH. After the addition of 500 μ L 1 M tris, pH 7.4, the solution was diluted into 15 mL of 50 mM tris, pH 7.4, 150 mM NaCl. Heme was gradually titrated into 100 μ M apo-MhuD in a 0.9 heme: 1 MhuD ratio. The samples were incubated overnight at 4°C before being passed through a desalting column to remove unbound heme. Protein concentrations of the eluted samples were determined via lowry assay³⁸.

Single turnover heme degradation assays

Single turnover heme degradation assays of 5 μ M MhuD-mono-heme were performed in 50 mM tris, pH 7.4, 150 mM NaCl. To eliminate the possibility of non-enzymatic heme degradation, 2.5 μ M catalase from *Aspergillus niger* (Sigma Aldrich) was added to each reaction. Heme degradation reaction was initiated with 10 mM sodium ascorbate and the reaction was monitored spectrophotometrically (DU800, Beckman Coulter) for an hour with scans taken at 5-minute intervals.

Heme binding experiments

Heme was titrated in 1 μM increments into 5 μM apo-MhuD or buffer at room temperature. Spectra were collected after each titration after a 5-minute incubation period and the difference spectra obtained to determine absorbance change.

Heme off rate measurement

For the heme off rate measurement, MhuD-mono-heme of the wild type and its mutants were prepared as described above using the following heme to protein ratios: 1.2 heme:1 MhuD (wild type), 1.3 heme:1 MhuD (R22S), and 1.3 heme:1 MhuD (R26S). Preparation of apo-H64Y/V68F-Mb was achieved as previously reported³⁹. Hemechromogen and lowry assays were used to determine heme and protein concentration to ensure a near 1 to 1 heme protein ratio. To measure heme dissociation, 5 μM MhuD-mono-heme was mixed with a 5-fold excess of apo-H64Y/V68F-Mb. The reaction was monitored spectrophotometrically (DU800, Beckman Coulter) at 412 nm to completion.

MhuD product purification

Product purification was performed as previously reported with minor modifications¹⁵. MhuD mono-heme was prepared as described above. In this protocol, MhuD heme degradation was performed in 0.1 M MES, pH 6.0 at 37°C with 4 μM MhuD-mono-heme, 2.5 mM deferoxamine, 2 μM catalase, and 25 mM sodium ascorbate. Reaction mixtures were

incubated at 37°C for 50 minutes before termination with one half reaction volume of 8 M guanidinium chloride. Samples were incubated at 37°C for 10 minutes to ensure full protein denaturation. Products were purified via solid phase extraction using a C-18 column (Supelco). Initial sample analysis was done using a Hitachi 7000 series HPLC System equipped with a NUCLEODUR C-18 pyramid column. Sample separation was achieved using a linear gradient from 55% methanol, 45% 0.1 M ammonium acetate (v/v) to 65% methanol with a 0.25 mL/min flow rate. Product fractions were further analyzed via UV/vis spectroscopy (DU800, Beckman Coulter) and ESI-MS/MS (Micromass LCT Premier TOF, Waters). For further analysis samples were injected HPLC-MS/MS (Micromass Quattro Premier XE, Waters) on negative mode.

C1 product detection

C1 product detection was performed as previously described and outlined below.

CO detection^{15, 17}- For CO detection, heme degradation in 50 mM tris, pH 7.4, 150 mM NaCl of 5 μ M MhuD-mono-heme or of 5 μ M holo-hHO-1 was initiated with 10 mM sodium ascorbate in a sealed cuvette. After completion of heme degradation, 1 mM sodium dithionite was added to the reaction mixture before the addition of 5 μ M reduced Mb H64L for CO detection. Spectra were collected before and after addition of Mb H64L to monitor spectral changes. The experiment was repeated without initiation of heme degradation to eliminate spectral changes not due to CO association with the Mb H64L variant.

Formaldehyde detection¹⁷- Detection of formaldehyde was done using a modified Nash's method¹⁷. In this method, heme degradation of 20 μ M MhuD-mono heme was initiated with 10 mM sodium ascorbate in a 500 μ L of 50 mM tris, pH 7.4, 150 mM NaCl. At the completion of the reaction, 25 μ L of 10% trichloroacetic acid (w/v) was added to the reaction mixture. Samples were passed through an LC-18 SPE column (Supelco) before incubation with Nash's reagent (0.02 M acetyl acetone, 2 M ammonium acetate, and 0.05 M acetic acid) at 40°C for 30 min and at room temperature for 30 min. Formation of the yellow 3, 5-diacetyl-1,4-dihydrolutidine was quantified on a Hitachi 7000 series HPLC System equipped with a NUCLEODUR C-18 column on a 32% methanol (v/v) to 42% methanol (v/v) linear gradient. Control reactions were performed by adding trichloroacetic acid before reaction initiation.

Formic acid detection¹⁷- For formic acid detection, heme degradation of 50 μ M MhuD-mono heme was initiated with 10 mM sodium ascorbate in 50 mM tris pH 7.4, 150 mM NaCl. Formic acid dehydrogenase (R-Biofarm F-kit) was used to generate NADH. HPLC analysis of the NADH product was performed on a NUCLEODUR C-18 column with a 5%/methanol/95% mM triammonium (v/v) to 15% methanol (v/v) linear gradient.

Crystallization of MhuD-R26S heme-CN

A solution of cyanide derivatized heme (heme-CN) was prepared by dissolving 3.3 mg of hemin in 300 μ L 1 M NaOH before diluting into 50 mM sodium phosphate (NaPi), pH 7.4, 150 mM NaCl to 10 mL. Hydrochloric acid (1 M) was used to readjust the pH to pH 7.4, then several KCN crystals were added to derivatize the heme. Apo-MhuD-R26S (100 μ M) was

gradually titrated with a 1.3-fold excess of heme-CN and incubated overnight at 4°C. The mixture was concentrated and passed through a PD-10 column (GE Healthcare) to remove unbound heme. The MhuD R26S heme-CN was concentrated once again to 10 mg/mL in 50 mM NaPi, pH 7.4, 150 mM NaCl and crystallized in 1.6 M ammonium sulfate, 0.1 M sodium acetate, pH 5.5, 0.2 M NaCl. Crystals were flash frozen in 1:1 crystallization condition and 40% glycerol. A complete native data set was collected at a wavelength of 1.0 Å at 70 K and processed using iMOSFLM⁴⁰. Molecular replacement using the apo-MhuD-diheme structure as a search model (PDB ID 3HX9) was performed with the Phaser in the PHENIX suite⁴¹. Iterative rounds of structure refinement were completed with Coot⁴² and phenix.refine⁴¹.

Crystallization of MhuD-R26S Mn-PPIX

To prepare a Mn-PPIX solution, approximately 2 mg of Mn-PPIX was dissolved in 500 µL 0.1 M NaOH followed by 500 µL 1 M tris, pH 7.4 before dilution into 50 mM tris pH 7.4, 150 mM NaCl. Mn-PPIX was slowly added to 100 µM apo-MhuD R26S in a 0.9 Mn-PPIX to 1 MhuD molar ratio and incubated overnight at 4°C. The Mn-PPIX-protein complex was concentrated to 10 mg/mL and crystallized in 0.2 M ammonium sulfate, 0.1 M HEPES pH 7.5, 25% (w/v) Polyethylene glycol 3350. The crystals were mounted in a 1:1 mixture of crystallization buffer and 40% glycerol and diffracted to a resolution of 2.4 Å at 70 K. The collected data was indexed, integrated, and reduced using iMOSFLM⁴⁰. Initial phase determination was done with Phaser in the PHENIX suite using wild type MhuD-diheme structure with heme as a search model (PDB ID 3HX9)⁴¹. The initial model building was performed by Autobuild in

PHENIX⁴¹ and the preceding iterative structure refinement was done with Coot⁴² and phenix.refine⁴¹.

Crystallization of MhuD R26S biliverdin

A biliverdin solution was prepared as described above for Mn-PPIX and a ferric chloride was made by dissolving 27.3 mg of ferric chloride hexahydrate in 10 mL water. A 1.3 fold excess of biliverdin and ferric chloride mixture was gradually added to 100 μ M apo-MhuD R26S and incubated overnight at 4°C before concentration to approximately 10 mg/mL as estimated by the biliverdin Soret peak. Light blue crystals appeared in 0.1 HEPES pH 6.5, 4.6 M NaCl, 30 mM Glycyl-glycyl-glycine after 2 days. The crystals were flash frozen in 100% NVH oil and a 2.5 Å resolution data set was collected. The data was processed phaser before iterative rounds of refinement were completed with Coot⁴² and phenix.refine⁴¹.

Expression and purification of wild type hHO-1

Human HO-1 was prepared as previously described in the literature⁴³. In brief, the hHO-1-pBace plasmid for the expression of hHO-1 was transformed into *E coli* DH5 α cells, which were grown in LB medium containing 50 μ g/mL ampicillin at 37°C. Protein expression was induced at OD₆₀₀ of 0.3 – 0.5 with 1 mM IPTG after which cultures were incubated overnight at 18°C at 100 rpm for 12 -18 hours. After harvest, the greenish bacteria was lysed in 50 mM tris pH 8.0, 2 mM EDTA via microfluidization. Ammonium sulfate (250 mM) and 10%

polyethylenimine were added to the lysate, and after a 25 minute incubate period, the lysate was centrifuged at 14 krpm. Another round of ammonium sulfate precipitation was performed, this time using with a 40% ammonium sulfate concentration. The ammonium sulfate concentration of the supernatant was raised to 70% and centrifuged one last time. The precipitated green hHO-1 was resuspended into a minimal volume of 10 mM diaminopropane pH 9.0. Throughout the purification process 1 mM PMSF was constantly added to ensure minimal protein degradation. The sample was dialysed twice into fresh 10 mM diaminopropane. The protein was loaded onto an ion exchange column (HiTrap Q HP, 5 mL) and the pure protein was eluted with a KCl gradient.

Preparation of heme-protein complexes for EPR and Raman spectroscopy

MhuD WT-mono-heme, MhuD W66A-mono-heme, MhuD R26S-mono-heme, and holo-IsdI were prepared as described earlier for MhuD-mono-heme preparation however using a 0.6:1 heme to protein ratio and desalting into 100 mM MOPS pH 7.0, 5 mM EDTA. Holo-hHO-1 was prepared in a similar manner but using a 3-fold excess of heme to displace bound biliverdin. Samples were concentrated (Amicon, 5 kDa molecular mass cutoff) to a 1 mM heme concentration determined via a Hemochromogen assay⁴⁴. Protein concentrations were also measured using the Lowry assay³⁸ to ensure substoichiometric ratios of heme to protein for the MhuD samples.

Resonance Raman spectroscopy

Resonance Raman spectra of MhuD WT-mono-heme and MhuD R26S-mono-heme were acquired with TriVista 555 triple monochromator (900/900//2400 gr/mm; Acton Research, Acton, MA) equipped with a CCD camera (1,340 × 100 pixels; Princeton Instruments, Princeton, NJ). Samples were excited with a Krypton-ion laser (Innova 300C, Coherent, Santa Clara, CA) at a wavelength of 407 nm.

EPR spectroscopy

EPR spectra of holo-hHO-1, MhuD WT-mono-heme, MhuD W66A-mono-heme, MhuD R26S-mono-heme, and holo-IsdI were acquired from frozen samples with using a Bruker EMX-PLUS (9.2 GHz) EPR spectrometer at 10 K.

References

- [1] Ferris, C. D., Jaffrey, S. R., Sawa, A., Takahashi, M., Brady, S. D., Barrow, R. K., Tysoe, S. A., Wolosker, H., Baranano, D. E., Dore, S., Poss, K. D., and Snyder, S. H. (1999) Haem oxygenase-1 prevents cell death by regulating cellular iron, *Nat Cell Biol* 1, 152-157.
- [2] Brouard, S., Otterbein, L. E., Anrather, J., Tobiasch, E., Bach, F. H., Choi, A. M., and Soares, M. P. (2000) Carbon monoxide generated by heme oxygenase 1 suppresses endothelial cell apoptosis, *J Exp Med* 192, 1015-1026.
- [3] Dore, S., Takahashi, M., Ferris, C. D., Zakhary, R., Hester, L. D., Guastella, D., and Snyder, S. H. (1999) Bilirubin, formed by activation of heme oxygenase-2, protects neurons against oxidative stress injury, *Proc Natl Acad Sci U S A* 96, 2445-2450.
- [4] Tenhunen, R., Marver, H. S., and Schmid, R. (1969) Microsomal heme oxygenase. Characterization of the enzyme, *J Biol Chem* 244, 6388-6394.
- [5] Yoshida, T., Noguchi, M., and Kikuchi, G. (1980) Oxygenated form of heme - heme oxygenase complex and requirement for second electron to initiate heme degradation from the oxygenated complex, *J Biol Chem* 255, 4418-4420.
- [6] Matsui, T., Unno, M., and Ikeda-Saito, M. (2010) Heme oxygenase reveals its strategy for catalyzing three successive oxygenation reactions, *Acc Chem Res* 43, 240-247.
- [7] Schmitt, M. P. (1997) Utilization of host iron sources by *Corynebacterium diphtheriae*: identification of a gene whose product is homologous to eukaryotic heme oxygenases and is required for acquisition of iron from heme and hemoglobin, *J Bacteriol* 179, 838-845.
- [8] Wilks, A., and Schmitt, M. P. (1998) Expression and characterization of a heme oxygenase (Hmu O) from *Corynebacterium diphtheriae*. Iron acquisition requires oxidative cleavage of the heme macrocycle, *J Biol Chem* 273, 837-841.
- [9] Hirotsu, S., Chu, G. C., Unno, M., Lee, D. S., Yoshida, T., Park, S. Y., Shiro, Y., and Ikeda-Saito, M. (2004) The crystal structures of the ferric and ferrous forms of the heme complex of HmuO, a heme oxygenase of *Corynebacterium diphtheriae*, *J Biol Chem* 279, 11937-11947.
- [10] Friedman, J., Lad, L., Deshmukh, R., Li, H., Wilks, A., and Poulos, T. L. (2003) Crystal structures of the NO- and CO-bound heme oxygenase from *Neisseriae meningitidis*. Implications for O₂ activation, *J Biol Chem* 278, 34654-34659.
- [11] Zhu, W., Wilks, A., and Stojiljkovic, I. (2000) Degradation of heme in gram-negative bacteria: the product of the hemO gene of *Neisseriae* is a heme oxygenase, *J Bacteriol* 182, 6783-6790.
- [12] Wu, R., Skaar, E. P., Zhang, R., Joachimiak, G., Gornicki, P., Schneewind, O., and Joachimiak, A. (2005) *Staphylococcus aureus* IsdG and IsdI, heme-degrading enzymes with structural similarity to monooxygenases, *J Biol Chem* 280, 2840-2846.
- [13] Chim, N., Iniguez, A., Nguyen, T. Q., and Goulding, C. W. (2010) Unusual diheme conformation of the heme-degrading protein from *Mycobacterium tuberculosis*, *J Mol Biol* 395, 595-608.
- [14] Reniere, M. L., Ukpabi, G. N., Harry, S. R., Stec, D. F., Krull, R., Wright, D. W., Bachmann, B. O., Murphy, M. E., and Skaar, E. P. (2010) The IsdG-family of haem oxygenases degrades haem to a novel chromophore, *Mol Microbiol* 75, 1529-1538.

- [15] Nambu, S., Matsui, T., Goulding, C. W., Takahashi, S., and Ikeda-Saito, M. (2013) A new way to degrade heme: the Mycobacterium tuberculosis enzyme MhuD catalyzes heme degradation without generating CO, *J Biol Chem* 288, 10101-10109.
- [16] LaMattina, J. W., Nix, D. B., and Lanzilotta, W. N. (2016) Radical new paradigm for heme degradation in Escherichia coli O157:H7, *Proc Natl Acad Sci U S A* 113, 12138-12143.
- [17] Matsui, T., Nambu, S., Ono, Y., Goulding, C. W., Tsumoto, K., and Ikeda-Saito, M. (2013) Heme degradation by Staphylococcus aureus IsdG and IsdI liberates formaldehyde rather than carbon monoxide, *Biochemistry* 52, 3025-3027.
- [18] Schuller, D. J., Wilks, a., Ortiz de Montellano, P. R., and Poulos, T. L. (1999) Crystal structure of human heme oxygenase-1, *Nature structural biology* 6, 860-867.
- [19] Graves, A. B., Morse, R. P., Chao, A., Iniguez, A., Goulding, C. W., and Liptak, M. D. (2014) Crystallographic and spectroscopic insights into heme degradation by Mycobacterium tuberculosis MhuD, *Inorg Chem* 53, 5931-5940.
- [20] Lee, W. C., Reniere, M. L., Skaar, E. P., and Murphy, M. E. (2008) Ruffling of metalloporphyrins bound to IsdG and IsdI, two heme-degrading enzymes in Staphylococcus aureus, *J Biol Chem* 283, 30957-30963.
- [21] Friedman, J., Lad, L., Li, H., Wilks, A., and Poulos, T. L. (2004) Structural Basis for Novel δ -Regioselective Heme Oxygenation in the Opportunistic Pathgen Pseudomonas aeruginosa, *Biochemistry* 43, 5239-5245.
- [22] Wang, J., Lad, L., Poulos, T. L., and Ortiz de Montellano, P. R. (2005) Regiospecificity determinants of human heme oxygenase: differential NADPH- and ascorbate-dependent heme cleavage by the R183E mutant, *J Biol Chem* 280, 2797-2806.
- [23] Iwamori, S., Sato, E., Saigusa, D., Yoshinari, K., Ito, S., Sato, H., and Takahashi, N. (2015) A novel and sensitive assay for heme oxygenase activity, *Am J Physiol Renal Physiol* 309, F667-671.
- [24] Tran, R., Boon, E. M., Marletta, M. A., and Mathies, R. A. (2009) Resonance Raman spectra of an O₂-binding H-NOX domain reveal heme relaxation upon mutation, *Biochemistry* 48, 8568-8577.
- [25] Chu, G. C., Tomita, T., Sonnichsen, F. D., Yoshida, T., and Ikeda-Saito, M. (1999) The heme complex of Hmu O, a bacterial heme degradation enzyme from Corynebacterium diphtheriae. Structure of the catalytic site, *J Biol Chem* 274, 24490-24496.
- [26] Migita, C. T., Zhang, X., and Yoshida, T. (2003) Expression and characterization of cyanobacterium heme oxygenase, a key enzyme in the phycobilin synthesis. Properties of the heme complex of recombinant active enzyme, *Eur J Biochem* 270, 687-698.
- [27] Takahashi, S., Wang, J., Rousseau, D. L., Ishikawa, K., Yoshida, T., Host, J. R., and Ikeda-Saito, M. (1994) Heme-heme oxygenase complex. Structure of the catalytic site and its implication for oxygen activation, *J Biol Chem* 269, 1010-1014.
- [28] Garcia-Rubio, I., Braun, M., Gromov, I., Thony-Meyer, L., and Schweiger, A. (2007) Axial coordination of heme in ferric CcmE chaperone characterized by EPR spectroscopy, *Biophys J* 92, 1361-1373.
- [29] Ukpabi, G., Takayama, S. J., Mauk, A. G., and Murphy, M. E. (2012) Inactivation of the heme degrading enzyme IsdI by an active site substitution that diminishes heme ruffling, *J Biol Chem* 287, 34179-34188.

- [30] Takayama, S. J., Ukpabi, G., Murphy, M. E., and Mauk, A. G. (2011) Electronic properties of the highly ruffled heme bound to the heme degrading enzyme IsdI, *Proc Natl Acad Sci U S A* 108, 13071-13076.
- [31] Takayama, S. J., Loutet, S. A., Mauk, A. G., and Murphy, M. E. (2015) A Ferric-Peroxo Intermediate in the Oxidation of Heme by IsdI, *Biochemistry* 54, 2613-2621.
- [32] Wilks, A., Torpey, J., and Ortiz de Montellano, P. R. (1994) Heme oxygenase (HO-1). Evidence for electrophilic oxygen addition to the porphyrin ring in the formation of alpha-meso-hydroxyheme, *J Biol Chem* 269, 29553-29556.
- [33] Davydov, R. M., Tadashi, Y., Ikeda-Saito, M., and Hoffman, B. M. (1999) Hydroperoxy-Heme Oxygenase Generated by Cryoreduction Catalyzes the Formation of α -meso-Hydroxyheme as Detected by EPR and ENDOR, *Journal of the American Chemical Society* 121, 10656-10657.
- [34] Yoshida, T., Noguchi, M., and Kikuchi, G. (1982) The step of carbon monoxide liberation in the sequence of heme degradation catalyzed by the reconstituted microsomal heme oxygenase system, *J Biol Chem* 257, 9345-9348.
- [35] Saito, S., and Itano, H. A. (1982) Verdohemochrome IX alpha: preparation and oxidoreductive cleavage to biliverdin IX alpha, *Proc Natl Acad Sci U S A* 79, 1393-1397.
- [36] Chen, H., Moreau, Y., Derat, E., and Shaik, S. (2008) Quantum mechanical/molecular mechanical study of mechanisms of heme degradation by the enzyme heme oxygenase: the strategic function of the water cluster, *J Am Chem Soc* 130, 1953-1965.
- [37] Wang, J., Niemevz, F., Lad, L., Huang, L., Alvarez, D. E., Buldain, G., Poulos, T. L., and de Montellano, P. R. (2004) Human heme oxygenase oxidation of 5- and 15-phenylhemes, *J Biol Chem* 279, 42593-42604.
- [38] Lowry, O. H., Rosebrough, N. J., Farr, A. L., and Randall, R. J. (1951) Protein measurement with the Folin phenol reagent, *J Biol Chem* 193, 265-275.
- [39] Hargroves, M. S., Singleton, E. W., Quilling, M. L., Ortizfl, L. A., Phillips, G. N., John, S., and Mathews, A. J. (1993) His64(E7)-->Tyr apomyoglobin as a reagent for measuring rates of hemin dissociation, *Journal of Biological Chemistry* 269, 4207-4214.
- [40] Battye, T. G., Kontogiannis, L., Johnson, O., Powell, H. R., and Leslie, A. G. (2011) iMOSFLM: a new graphical interface for diffraction-image processing with MOSFLM, *Acta Crystallogr D Biol Crystallogr* 67, 271-281.
- [41] Adams, P. D., Afonine, P. V., Bunkoczi, G., Chen, V. B., Davis, I. W., Echols, N., Headd, J. J., Hung, L. W., Kapral, G. J., Grosse-Kunstleve, R. W., McCoy, A. J., Moriarty, N. W., Oeffner, R., Read, R. J., Richardson, D. C., Richardson, J. S., Terwilliger, T. C., and Zwart, P. H. (2010) PHENIX: a comprehensive Python-based system for macromolecular structure solution, *Acta Crystallogr D Biol Crystallogr* 66, 213-221.
- [42] Emsley, P., Lohkamp, B., Scott, W. G., and Cowtan, K. (2010) Features and development of Coot, *Acta Crystallogr D Biol Crystallogr* 66, 486-501.
- [43] Wilks, A., Black, S. M., Miller, W. L., and Ortiz de Montellano, P. R. (1995) Expression and characterization of truncated human heme oxygenase (hHO-1) and a fusion protein of hHO-1 with human cytochrome P450 reductase, *Biochemistry* 34, 4421-4427.
- [44] Anson, M. L., and Mirsky, A. E. (1928) On Hemochromogen, *J Gen Physiol* 12, 273-288.

CHAPTER 4

Inhibition of *In vivo Mycobacterium tuberculosis* Infection with Tin-Protoporphyrin

IX

This project was performed in collaboration with the Sher lab at the National Institute of Health

Abstract

Heme oxygenase-1 (HO-1) is a stress response antioxidant enzyme which catalyzes the degradation of heme released during inflammation. Also hHO-1 is a biomarker of active *Mycobacterium tuberculosis* (Mtb) infection. HO-1 expression is upregulated in both experimental and human Mtb infection suggesting that heme degradation plays an important role in Mtb pathogenicity. Adjunctive administration of a well-characterized HO-1 enzymatic inhibitor tin-protoporphyrin IX (SnPPIX) with an anti-TB drug cocktail resulted in accelerated pathogen clearance. Like humans, Mtb has its own heme degradation enzyme MhuD, which may also be a target for SnPPIX. We tested SnPPIX for both HO-1 and MhuD inhibitory activity. SnPPIX completely abolishes HO-1 activity, but SnPPIX failed to inhibit MhuD enzymatic activity. Together, the above findings demonstrate that SnPPIX may be used as an adjunctive therapy for tuberculosis and that the pharmacological target of SnPPIX is human HO-1 and not the Mtb heme degrading enzyme, MhuD.

Introduction

One novel strategy for the treatment of tuberculosis (TB) is through host directed therapies. Instead of targeting the pathogen directly, host directed treatments target host factors in host-pathogen interactions that aid or permit pathogen survival or augment factors involved in host immune response. By targeting or augmenting host factors, host directed therapies avoid the development of new drug-resistant strains since pathogens would have to evolve new mechanisms for drug-resistance. Furthermore, many drugs targeting host factors have already been approved and may be repurposed as host-directed therapies. Already, several host-directed treatments are in clinical use^{1, 2}. These include prednisone and erythromycin, which both act as anti-inflammatory agents in the treatment of *Streptococcus pneumoniae* infections¹. More promising therapies are in various stages of clinical testing^{1, 2}.

The current treatment for TB utilizes a battery of drugs, which must be consistently taken for at least 6 months for drug-sensitive Mtb strains. The treatment is considerably longer for multiple-drug resistant (MDR-TB) or extreme-drug resistant (XDR-TB) strains ranging from 18 to 24 months³. Due to the length of TB treatments and the rise of MDR-TB and XDR-TB strains, there is a dire need for new classes of anti-TB drugs. Host directed therapies offer a promising new approach to treat TB.

The causative agent of TB, *Mycobacterium tuberculosis* (Mtb), has evolved many mechanisms to use or modulate host-interactions in their favor. For example, Mtb has been shown to secrete proteins that inhibit phagosome maturation and acidification to allow for survival within the macrophage⁴. Additionally, Mtb has been found to induce the formation of lipid bodies for additional protection and as a source of nutrients⁵. Fortunately, drugs inhibiting

many of these host-pathogen interactions currently exist. For instance, the chemotherapeutic Imatinib has been shown in mice to restore phagosome acidification by indirectly increasing expression of the vacuolar proton pump vATPase^{6, 7}. Lipid body formation may be modulated with several different classes of drugs such as metformin, thiazolidinediones, and statins⁸. Numerous other potential targets for host directed treatments against TB have been identified and are currently being assessed (**Table 4.1**).

Table 4.1 Examples of novel anti-TB host directed therapies, their mechanism of action, and their stage in clinical development¹.

Drug class	Examples of host-directed therapy	Mechanism of action	Developmental stage
Repurposed drug	Imatinib, verapamil, metformin, ibuprofen	Modulation of inflammation and activation of intracellular antimicrobial defenses	Preclinical/clinical (early phase)
Cytokine therapy	Interleukin 2, GM-CSF, interferon γ , interleukin 12 (early stage)	Induction of pro-inflammatory cell signaling	Clinical (late phase)
Monoclonal antibody	Anti-TNF α , anti-interleukin 6, anti-VEGF	Reduction of tissue-destructive inflammation by cytokine neutralization	Preclinical/clinical (early phase)
	Anti-PD-1, anti-LAG3, anti-CTLA-4	Activation and mobilization of antigen-specific T cells by immune checkpoint inhibition	Preclinical
Vitamin	Vitamin D3	Activation and augmentation of intracellular defenses (via interferon γ and interleukin-15 signaling)	Clinical (late phase)
Cellular therapy	Autologous mesenchymal stromal cells, T cells	Neutralization of tissue-destructive inflammation, enhancement of organ repair, and potentiation of antigen-specific immune responses	Clinical (early phase)

One novel target for TB host directed therapies is human heme oxygenase-1 (hHO-1). hHO-1 is responsible for the degradation of heme into biliverdin, carbon monoxide (CO), and

ferrous iron, and has been implicated in the innate immune response^{9, 10}. Previous research has found that TB patients with reduced sera hHO-1 levels were more likely to have better prognoses post anti-TB therapy¹¹. This suggest that hHO-1 plays a significant role in Mtb survival within the host and that inhibition of hHO-1 is a possible strategy to treat TB. Here we evaluate the use of the hHO-1 inhibitor, tin protoporphyrin IX (SnPPIX), as a potential host directed therapy against TB¹². Additionally, we demonstrate that SnPPIX only inhibits mammalian and not the Mtb heme degradation enzyme. Together these results suggest that SnPPIX is host-directed anti-TB therapy, which targets hHO-1.

Results

Evaluation of adjunctive administration of SnPPIX for the treatment of TB (Sher Lab)

To evaluate whether adjunctive administration of SnPPIX could enhance the efficacy of conventional anti-TB drugs, mice were treated four weeks post infection with combined rifampin (R), isoniazid (H), and pyrazinamide (Z) therapy (RHZ) alone, SnPPIX alone, or a combination of SnPPIX and RHZ (**Figure 4.1A**). Similar experiments were performed on T-cell-deficient mice (TCR $\alpha^{-/-}$) to assess the role of host T-cells on TB infection. Bacterial burdens were quantified after 3 weeks by culturing serial dilutions of lung tissue homogenates. The RHZ and SnPPIX treatments of wild type mice each resulted in an approximate 1-log reduction in pulmonary bacterial loads below those in untreated infected animals, and when RHZ and SnPPIX are combined, this treatment resulted in an additive 2-

log reduction in mycobacterial burden (**Figure 4.1B**). Meanwhile, adjunctive treatment with SnPPIX failed to enhance RHZ efficacy in infected T cell-deficient mice (**Figure 4.1B**).

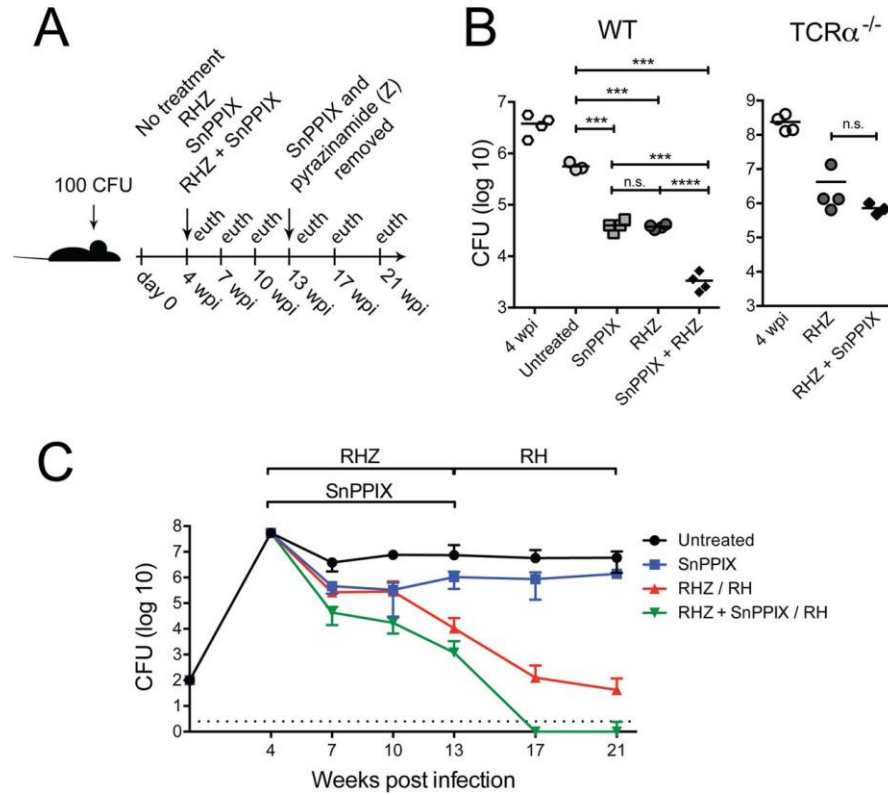


Figure 4.1 (Courtesy of Sher lab) Administration of SnPPIX in conjunction with conventional antibiotic treatment accelerates pulmonary bacterial clearance in Mtb -infected mice. (A) Diagram of the experimental protocol employed. (B) Quantification of CFU in lungs of Mtb-infected C57BL/6 (WT) mice at day 0 of treatment (4 wpi) and 3 weeks post-treatment initiation, in which animals were left untreated or were administered RHZ, SnPPIX, or RHZ plus SnPPIX, or in lungs of TCRα^{-/-} mice at day 0 of treatment (4 wpi) and 3 weeks post-treatment with RHZ or RHZ plus SnPPIX. (C) Quantification of CFU in lungs of Mtb-infected WT mice at the multiple time points described for panel A. The dotted line represents the limit of detection for the assay. Graphs show individual results or means ± standard deviations of the results. *, P ≤ 0.05; ***, P ≤ 0.001, n.s., nonsignificant. Each experimental group consisted of 4 to 5 mice. The experiment shown in panel B is representative of 2 to 3 performed, while the time course results shown in panel C are from a single experiment.

To evaluate the long-term effectiveness of the SnPPIX-RHZ therapy, time course experiments were also performed. In these experiments, mice were treated with either SnPPIX, RHZ, or both four weeks post Mtb infection. Colony forming units from lung tissue homogenates

were quantified every 3 weeks thereafter to assess long-term treatment effectiveness. Supplementation with SnPPIX improved RHZ treatment within the first three weeks. After 13 weeks of treatment, the combination treatment with SnPPIX and RHZ resulted in an undetectable bacterial load (**Figure 4.1C**). Meanwhile, in mice treated only with RHZ, Mtb was still detectable as late as 17-weeks after treatment (**Figure 4.1C**).

Pharmacological target of SnPPIX

In macrophages, hHO-1, which has been implicated in the innate immune response and degrades heme into biliverdin, carbon monoxide, and iron^{9, 13}. To study the effect of SnPPIX on hHO-1, we used the hHO-1 variant G139A whose heme degradation activity was attenuated by 58%, allowing for observation of heme degradation within a similar time period as MhuD¹⁴. When incubated with the electron donor sodium ascorbate, the hHO-1 variant was observed to degrade heme as evidenced by the observed soret peak decrease (**Figure 4.2D**). However, when the hHO-1 variant was incubated with 2 μ M SnPPIX, no Soret peak decrease was observed (**Figure 4.2A & 4.2B**), suggesting that hHO-1 heme degradation activity is completely inhibited by 2 μ M SnPPIX. In contrast, no inhibitory effect was observed when the SnPPIX concentration was lowered to 0.002 μ M (**Figure 4.2C**).

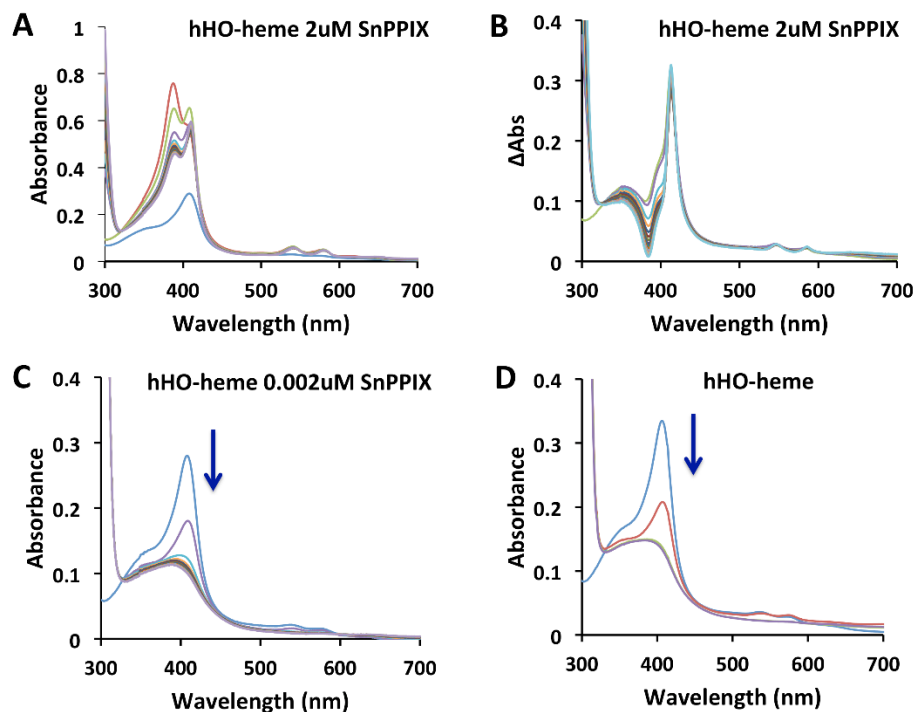


Figure 4.2 Heme degradation experiments were observed by the decrease of the soret peak (arrow) by monitoring the spectral changes from 300 – 700 nm every 5 mins where the hHO-1 G139A variant is called hHO1-G139A in the figure. (A) Heme degradation assay of 5 μ M hHO1-G139A-heme incubated in the presence of 2 μ M SnPPIX for 1 hr before reaction initiation with 10 mM ascorbate. No soret peak decrease was observed. (B) Difference spectra of experiment (A) where the 5 μ M apo-hHO1-G139A reaction spectra were subtracted from those of the 5 μ M hHO1-G139A-heme reaction. (C) Heme degradation assay of 5 μ M hHO1-G139A-heme incubated in the presence of 0.002 μ M SnPPIX for 1 hr before reaction initiation with 10 mM ascorbate. A soret peak decrease was observed similar to those of hHO1-G139A-heme in the absence of SnPPIX (D). (D) The heme degradation reaction of 5 μ M hHO1-G139A-heme alone was initiated by the addition of 10 mM ascorbate. All experiments were performed in triplicate.

Mtb has a heme-iron acquisition pathway^{15, 16}, and a previous study suggests that *Mycobacterium smegmatis*, a non-pathogenic mycobacterial strain, can uptake metalloporphyrins, such as Zn-mesoporphyrin¹⁷. Furthermore, Mtb has a cytosolic heme-degrading protein, MhuD, which breaks down heme to mycobilin isomers and iron¹⁸. As SnPPIX can competitively inhibit hHO-1, we asked the question whether MhuD may also play a role SnPPIX *in vivo* Mtb growth inhibition either by (1) degrading SnPPIX and liberating tin in the Mtb cytosol or (2) by interfering with the ability of MhuD to bind and degrade heme.

To determine if SnPPIX could also be degraded by Mtb MhuD, MhuD-SnPPIX and MhuD-mono heme complexes were incubated with the electron donor sodium ascorbate. Within an hour of incubation with sodium ascorbate, a soret peak decrease indicative of heme degradation was observed in the UV/vis spectra of the MhuD-mono heme complex (**Figure 4.3A**). Meanwhile, despite overnight incubation with ascorbate, no such soret peak decrease was observed in the spectra of the MhuD-SnPPIX complex demonstrating that SnPPIX is not cleaved by MhuD (**Figure 4.3B**).

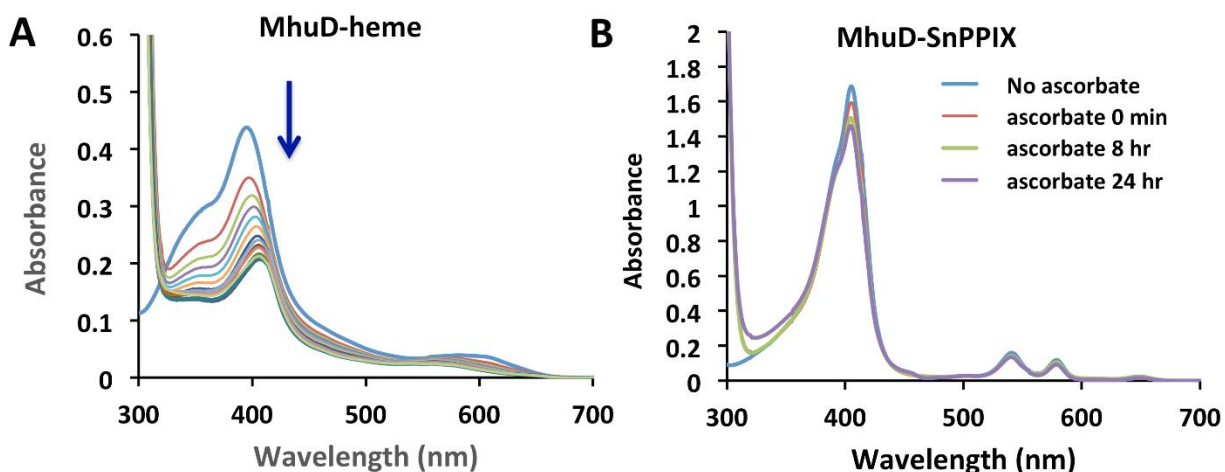


Figure 4.3 MhuD cannot degrade SnPPIX. Degradation of heme and SnPPIX by MhuD was monitored by UV/vis spectroscopy every 5 min for 1h for heme and for a period of 24h for SnPPIX. Each color represents a different time point. Degradation activity, as indicated by the soret peak decrease, was observed when sodium ascorbate was added to **(A)** MhuD-heme, but not when sodium ascorbate was added to **(B)** MhuD-SnPPIX. All experiments were performed in triplicate.

To assess if SnPPIX could inhibit MhuD heme degradation, MhuD heme degradation assays were performed in the presence of SnPPIX. Here, MhuD-mono heme was incubated in the presence of SnPPIX for an hour prior to the initiation of heme degradation with sodium ascorbate. A slightly diminished Soret peak was observed for the reaction suggesting that

heme degradation was occurring (**Figure 4.4A**). The difference spectra of this reaction (**Figure 4.4B**) was highly similar to those spectra of MhuD heme degradation in the absence of Sn-PPIX (**Figure 4.3A**), further reinforcing the results that SnPPIX does not competitively inhibit MhuD heme degradation.

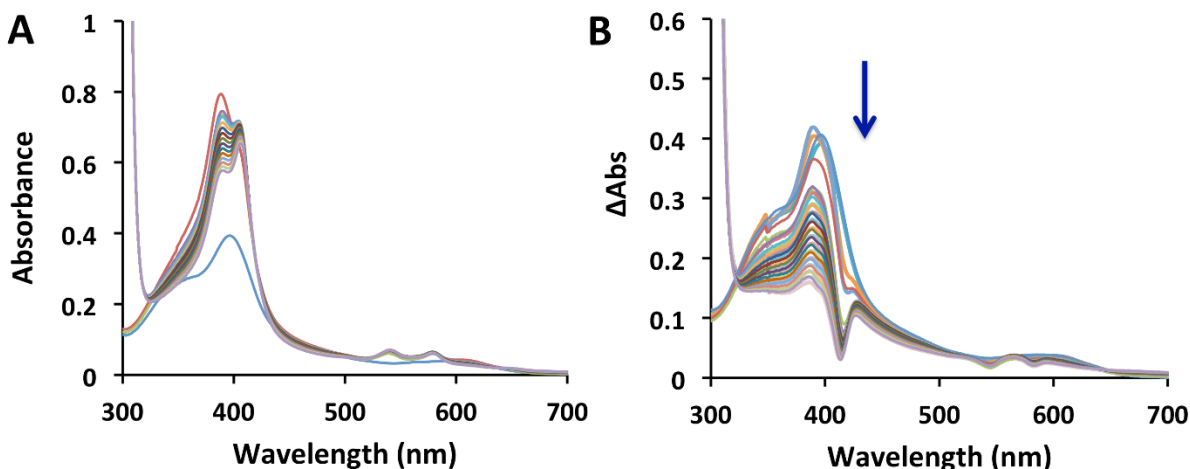


Figure 4.4 SnPPIX does not inhibit MhuD heme degradation. Heme degradation were observed by the decrease of the Soret peak (arrow) by monitoring the spectral changes from 300 – 700 nm every 5 mins. (A) Spectra of 5 μM MhuD heme degradation following an hour long incubation with 2 μM SnPPIX. (B) Difference spectra of (A) where the apo-MhuD reaction spectra were subtracted from those of the MhuD-heme reaction. The resulting difference spectra were very similar to those of the MhuD heme degradation in the absence of SnPPIX (**Figure 4.2A**). All experiments were performed in triplicate.

Discussion

Initial studies found that hHO-1 is expressed by host cells in response to oxidative stress and has several anti-inflammatory, anti-apoptotic and anti-proliferative effects. Bilirubin, a downstream product of biliverdin, has been shown to have potent antioxidant properties, while CO has been shown to have cryoprotective effects¹⁹. Additionally, the elimination of heme by hHO-1 may have anti-inflammatory effects²⁰. Despite the protective effects of hHO-1 in most infections, hHO-1 has been shown to paradoxically promote infections such as

*Leishmania chagasi*²¹ or *Salmonella enterica serovar Typhimurium*¹⁰. Whether hHO-1 expression during an Mtb infection is host protective is currently unclear. While it has been found that levels of hHO-1 in sera of TB patients is positively correlated to disease¹¹, deletion of HO-1 in mice resulted in increased susceptibility to Mtb infection²². Moreover, recent studies showed that inhibition of hHO-1 in Mtb-infected human macrophages resulted in a reduction in intracellular bacterial loads as well as decreased proinflammatory cytokine production²³.

Data presented in this study demonstrate that adjunctive treatment with known hHO-1 inhibitor SnPPIX reduces bacterial load in Mtb-infected mice and this reduction is T-cell response dependent (**Figure 4.1A-4.1C**). Experiments also showed that SnPPIX inhibited hHO-1 activity (**Figure 4.2B**) and not the activity of the Mtb heme degrader MhuD (**Figure 4.4B**). Lastly, we showed that the observed growth inhibition was not attributed to the release of tin upon the cleavage of SnPPIX by MhuD. While heme analog gallium protoporphyrin IX has been shown to inhibit Mtb growth possibly via the release of gallium upon cleavage by MhuD²⁴, our experiments show that MhuD is unable to degrade SnPPIX (**Figure 4.3B**). Together, this suggests that upregulation of hHO-1 expression has an overall host-detrimental effect during a Mtb infection.

SnPPIX acts mainly through the inhibition of hHO-1, although off-target effects are possible but unlikely. One possible way blockade of host heme degradation may suppress Mtb growth is by limiting the availability of free iron necessary for bacterial growth. Inhibition of hHO-1 may also reduce bacterial load via the generation of toxic reactive oxygen species as a result

of increased heme levels^{25, 26}. Additional experiments are required to delineate how the hHO-1 inhibition suppresses Mtb growth.

Although the exact mechanism of action is not understood, results from this study show that pharmacological inhibition of hHO-1 is a novel strategy for the treatment of TB. Inhibitors of hHO-1 such as SnPPIX have already been developed and are in the clinic to treat jaundice²⁷. While these inhibitors may potentially be repurposed to treat TB, more studies are necessary to assess the safety and efficacy compounds for host-directed therapy before initiation of human trials.

Materials and Methods

Recombinant MhuD and hHO-1 G139A protein expression and purification

Construction of the expression vector, pET22b-MhuD with a C-terminal His6tag, and the expression and purification of *M. tuberculosis* MhuD have been previously described²⁸. In brief, MhuD was overexpressed in BL21-Gold (DE3) *Escherichia coli*. Cells were resuspended in 50 mM Tris/HCl pH 7.4, 350 mM NaCl and 10 mM imidazole and lysed by sonication. The cell supernatant was loaded onto a Ni²⁺-charged HiTrap chelating column (5 mL) and washed with resuspension buffer. Fractions of eluted MhuD (between 50 and 100 mM imidazole) were collected and concentrated. Apo-MhuD was further separated on a S75 gel filtration column (GE Healthcare, Little Chalfont, UK) with 20 mM Tris, pH 8, and 10 mM NaCl before a final purification step with an ion exchange column (HiTrap Q HP, 5 mL) where homogeneous apo-MhuD eluted at 150 mM NaCl. Recombinant human heme oxygenase-1

variant G139A (hHO-1 G139A) clone was a gift from Dr. Thomas L. Poulos from the University of California, Irvine and was purified as previously described^{14, 29}.

MhuD-SnPPIX, MhuD-mono heme and hHO-1 G139A-heme / SnPPIX competition assays

For these assays, SnPPIX was dissolved in 300 μ l of 0.1 M NaOH before dilution into 50 mM Tris pH 7.4, 150 mM NaCl. The pH was readjusted back to 7.4 with 1 M HCl. Hemin was prepared by dissolving hemin chloride (Sigma-Aldrich) in 0.1 M NaOH before the addition of 1 M Tris pH 7.4 and dilution into 50 mM Tris pH 7.4, 150 mM NaCl. To produce the MhuD-SnPPIX complex, SnPPIX was gradually added to 0.1 M Apo-MhuD in a 1:1 molar ratio. The mixture was incubated overnight at 4°C and exchanged into 50 mM Tris pH 7.4, 150 mM NaCl via a desalting column (HiTrap desalting, 5 mL). The protein concentration post-desalting was determined by Lowry assay. MhuD-mono heme was prepared as previously reported²⁸. Briefly, heme was gradually added to 0.1 M MhuD in a 1.2:1 molar ratio before overnight incubation at 4°C. Excess heme was removed using a desalting column (HiTrap desalting, 5 mL) and the eluted protein concentration was determined by Lowry assay. The human HO-1 variant G139A (hHO-1 G139A) was used as a positive control for heme degradation by the host enzyme as its reaction rate is attenuated by 58%¹⁴, allowing for the observation of single turnover heme degradation within a similar time period as MhuD²⁸. The heme degradation reaction for hHO-G139A-heme was carried out in a similar manner as that for MhuD-mono heme. In all assays, sodium ascorbate was added as an electron donor to initiate the heme degradation process, as previously described²⁸. The reaction was monitored by UV/vis spectroscopy by collecting spectra between 300 – 700 nm at various time intervals and

observing the decrease of the Soret peak over time to determine heme degradation. For the SnPPIX/heme competition assays, 2 μM SnPPIX was incubated with either 5 μM MhuD-mono heme or 5 μM apo-MhuD as well as 5 μM hHO G139A-heme or 5 μM apo-hHO-1 G139A for 1 hr before addition of 10 mM sodium ascorbate to initiate the reaction. The difference spectra ($\Delta\text{Absorbance}$) were calculated by subtracting the reaction spectra without enzyme from those of the 5 μM enzyme-heme reaction to remove the absorbance interference of SnPPIX.

References

- [1] Zumla, A., Rao, M., Wallis, R. S., Kaufmann, S. H., Rustomjee, R., Mwaba, P., Vilaplana, C., Yeboah-Manu, D., Chakaya, J., Ippolito, G., Azhar, E., Hoelscher, M., Maeurer, M., and Host-Directed Therapies Network, c. (2016) Host-directed therapies for infectious diseases: current status, recent progress, and future prospects, *Lancet Infect Dis* 16, e47-63.
- [2] Wallis, R. S., and Hafner, R. (2015) Advancing host-directed therapy for tuberculosis, *Nat Rev Immunol* 15, 255-263.
- [3] Winston, C. A., and Mitruka, K. (2012) Treatment duration for patients with drug-resistant tuberculosis, United States, *Emerg Infect Dis* 18, 1201-1202.
- [4] Rohde, K., Yates, R. M., Purdy, G. E., and Russell, D. G. (2007) Mycobacterium tuberculosis and the environment within the phagosome, *Immunol Rev* 219, 37-54.
- [5] Singh, V., Jamwal, S., Jain, R., Verma, P., Gokhale, R., and Rao, K. V. (2012) Mycobacterium tuberculosis-driven targeted recalibration of macrophage lipid homeostasis promotes the foamy phenotype, *Cell Host Microbe* 12, 669-681.
- [6] Bruns, H., Stegelmann, F., Fabri, M., Dohner, K., van Zandbergen, G., Wagner, M., Skinner, M., Modlin, R. L., and Stenger, S. (2012) Abelson tyrosine kinase controls phagosomal acidification required for killing of Mycobacterium tuberculosis in human macrophages, *J Immunol* 189, 4069-4078.
- [7] Napier, R. J., Rafi, W., Cheruvu, M., Powell, K. R., Zaunbrecher, M. A., Bornmann, W., Salgame, P., Shinnick, T. M., and Kalman, D. (2011) Imatinib-sensitive tyrosine kinases regulate mycobacterial pathogenesis and represent therapeutic targets against tuberculosis, *Cell Host Microbe* 10, 475-485.
- [8] Hawn, T. R., Shah, J. A., and Kalman, D. (2015) New tricks for old dogs: countering antibiotic resistance in tuberculosis with host-directed therapeutics, *Immunol Rev* 264, 344-362.
- [9] Tenhunen, R., Marver, H. S., and Schmid, R. (1969) Microsomal heme oxygenase. Characterization of the enzyme, *J Biol Chem* 244, 6388-6394.
- [10] Mitterstiller, A. M., Haschka, D., Dichtl, S., Nairz, M., Demetz, E., Talasz, H., Soares, M. P., Einwallner, E., Esterbauer, H., Fang, F. C., Geley, S., and Weiss, G. (2016) Heme oxygenase 1 controls early innate immune response of macrophages to Salmonella Typhimurium infection, *Cell Microbiol* 18, 1374-1389.
- [11] Andrade, B. B., Pavan Kumar, N., Mayer-Barber, K. D., Barber, D. L., Sridhar, R., Rekha, V. V., Jawahar, M. S., Nutman, T. B., Sher, A., and Babu, S. (2013) Plasma heme oxygenase-1 levels distinguish latent or successfully treated human tuberculosis from active disease, *PLoS One* 8, e62618.
- [12] Drummond, G. S., and Kappas, A. (1981) Prevention of neonatal hyperbilirubinemia by tin protoporphyrin IX, a potent competitive inhibitor of heme oxidation, *Proc Natl Acad Sci U S A* 78, 6466-6470.
- [13] Woo, J., Iyer, S., Cornejo, M. C., Mori, N., Gao, L., Sipos, I., Maines, M., and Buelow, R. (1998) Stress protein-induced immunosuppression: inhibition of cellular immune effector functions following overexpression of haem oxygenase (HSP 32), *Transpl Immunol* 6, 84-93.
- [14] Liu, Y., Koenigs Lightning, L., Huang, H., Moenne-Loccoz, P., Schuller, D. J., Poulos, T. L., Loehr, T. M., and Ortiz de Montellano, P. R. (2000) Replacement of the distal glycine 139 transforms human heme oxygenase-1 into a peroxidase, *J Biol Chem* 275, 34501-34507.
- [15] Tullius, M. V., Harmston, C. A., Owens, C. P., Chim, N., Morse, R. P., McMath, L. M., Iniguez, A., Kimmey, J. M., Sawaya, M. R., Whitelegge, J. P., Horwitz, M. A., and Goulding, C. W. (2011) Discovery and characterization of a unique mycobacterial heme acquisition system, *Proc Natl Acad Sci U S A* 108, 5051-5056.

- [16] Jones, C. M., and Niederweis, M. (2011) Mycobacterium tuberculosis can utilize heme as an iron source, *J Bacteriol* 193, 1767-1770.
- [17] Owens, C. P., Chim, N., Graves, A. B., Harmston, C. A., Iniguez, A., Contreras, H., Liptak, M. D., and Goulding, C. W. (2013) The Mycobacterium tuberculosis secreted protein Rv0203 transfers heme to membrane proteins MmpL3 and MmpL11, *J Biol Chem* 288, 21714-21728.
- [18] Nambu, S., Matsui, T., Goulding, C. W., Takahashi, S., and Ikeda-Saito, M. (2013) A new way to degrade heme: the Mycobacterium tuberculosis enzyme MhuD catalyzes heme degradation without generating CO, *J Biol Chem* 288, 10101-10109.
- [19] Gozzelino, R., Jeney, V., and Soares, M. P. (2010) Mechanisms of cell protection by heme oxygenase-1, *Annu Rev Pharmacol Toxicol* 50, 323-354.
- [20] Lee, T. S., and Chau, L. Y. (2002) Heme oxygenase-1 mediates the anti-inflammatory effect of interleukin-10 in mice, *Nat Med* 8, 240-246.
- [21] Luz, N. F., Andrade, B. B., Feijo, D. F., Araujo-Santos, T., Carvalho, G. Q., Andrade, D., Abanades, D. R., Melo, E. V., Silva, A. M., Brodskyn, C. I., Barral-Netto, M., Barral, A., Soares, R. P., Almeida, R. P., Bozza, M. T., and Borges, V. M. (2012) Heme oxygenase-1 promotes the persistence of Leishmania chagasi infection, *J Immunol* 188, 4460-4467.
- [22] Silva-Gomes, S., Appelberg, R., Larsen, R., Soares, M. P., and Gomes, M. S. (2013) Heme catabolism by heme oxygenase-1 confers host resistance to Mycobacterium infection, *Infect Immun* 81, 2536-2545.
- [23] Scharn, C. R., Collins, A. C., Nair, V. R., Stamm, C. E., Marciano, D. K., Graviss, E. A., and Shiloh, M. U. (2016) Heme Oxygenase-1 Regulates Inflammation and Mycobacterial Survival in Human Macrophages during Mycobacterium tuberculosis Infection, *J Immunol* 196, 4641-4649.
- [24] Stojiljkovic, I., Kumar, V., and Srinivasan, N. (1999) Non-iron metalloporphyrins: potent antibacterial compounds that exploit haem/Hb uptake systems of pathogenic bacteria, *Mol Microbiol* 31, 429-442.
- [25] Dutra, F. F., and Bozza, M. T. (2014) Heme on innate immunity and inflammation, *Front Pharmacol* 5, 115.
- [26] Akaki, T., Tomioka, H., Shimizu, T., Dekio, S., and Sato, K. (2000) Comparative roles of free fatty acids with reactive nitrogen intermediates and reactive oxygen intermediates in expression of the anti-microbial activity of macrophages against Mycobacterium tuberculosis, *Clin Exp Immunol* 121, 302-310.
- [27] Kappas, A., Drummond, G. S., Manola, T., Petmezaki, S., and Valaes, T. (1988) Sn-protoporphyrin use in the management of hyperbilirubinemia in term newborns with direct Coombs-positive ABO incompatibility, *Pediatrics* 81, 485-497.
- [28] Chim, N., Iniguez, A., Nguyen, T. Q., and Goulding, C. W. (2010) Unusual diheme conformation of the heme-degrading protein from Mycobacterium tuberculosis, *J Mol Biol* 395, 595-608.
- [29] Wilks, A., and Ortiz de Montellano, P. R. (1993) Rat liver heme oxygenase. High level expression of a truncated soluble form and nature of the meso-hydroxylating species, *J Biol Chem* 268, 22357-22362.

CHAPTER 5

Towards the Identification and Characterization of MhuD Interaction Partners for Electron Donation and Product Release

Abstract

While the heme degradation protein MhuD has been extensively characterized, little is known about its interaction partners. Of particular interest is the electron donor(s) for MhuD which currently remains unidentified. Through a BLAST search, we have identified several candidate electron donors and have begun purifying and testing them for MhuD electron donor activity. Unfortunately, of the two candidate proteins tested thus far neither demonstrated electron donor activity with MhuD. Also unknown is the mechanism for MhuD product release. We hypothesize that LpqF, which is encoded on the same operon as MhuD, is crucial for MhuD product release. We have been able to express and solubilize LpqF, however attempts to purify LpqF in a native buffer for biochemical characterization has thus far proven unsuccessful. In this chapter, we document our ongoing efforts to identify the MhuD electron donor(s) as well as our attempts to express and purify a candidate protein for MhuD product release.

Introduction

The mechanism of *Mycobacterium tuberculosis* (Mtb) MhuD heme degradation has been quite extensively studied; however there remains a large knowledge gap with regards to protein partners that ensure fully functional MhuD *in vivo*. For instance, while an electron source is essential for MhuD-dependent heme cleavage, the MhuD electron donor protein(s) remain elusive. Notably, electron donors for other heme degradation proteins have been identified. In humans, NADPH cytochrome P450 reductase donates electrons from NADPH to human heme oxygenase (hHO-1)¹. More recently, *Staphylococcus aureus* proteins NtrA and IruO have been shown to donate electrons to IsdG and IsdI, both homologs of MhuD^{2,3}. IruO is a FAD-containing NADPH-dependent reductase². NtrA is thought to be a novel nitroreductase capable of S-nitrosoglutathione activity and is believed to be involved in nitrofuran activation as well as protection against transnitrosylation⁴. Additionally, NtrA has also been shown to play a role in staphyloferrin A mediated iron uptake in *S. aureus*³. While both NtrA and IruO can participate in heme utilization, they appear to serve redundant roles in *S. aureus* heme degradation^{2,3}. In fact, deletion of either NtrA or IruO does not appear to inhibit growth of *S. aureus* when heme is the sole iron source, while deletion of both genes debilitates Mtb ability to grow in heme alone².

While the by-products of MhuD have been identified, mycobilin isomers, the fate of these by-products is unknown. Because of the harsh, denaturing conditions required to extract mycobilin isomers from MhuD⁵, we speculate that MhuD requires a protein partner to release and shuttle mycobilins from its active site. Other heme degradation by-products have been shown to be secreted. Biliverdin in humans is converted into bilirubin by biliverdin

reductase before excretion⁶. In *Pseudomonas aeruginosa*, products resulting from *P. aeruginosa* HO heme degradation, β - and δ -biliverdin, are both secreted^{7,8}. However, similar to MhuD, the fate of *S. aureus* IsdG/I staphylobilin products is unknown.

Thus, there are several questions that remain to be resolved regarding the protein factors that are important for the MhuD function within the Mtb heme utilization pathway. In this chapter, we will describe the on-going research to identify of the MhuD electron donor(s). Several candidate proteins have been identified and are being tested. Furthermore, we have identified a potential protein partner required for product release, and we will discuss our progress thus far.

Results

Evidence of a MhuD electron donor

To demonstrate the existence of a mycobacterium MhuD electron donor, we utilized *Mycobacterium smegmatis*, the non-pathogenic Mtb model organism⁹. We grew *M. smegmatis* in iron deplete media and used its cytosolic fraction to test for MhuD heme degradation *in vitro*. For this reaction, we used NADPH as the electron source. Upon addition of 100 μ M NADPH to MhuD-mono heme and the *M. smegmatis* cytosol, a decrease in the Soret peak was observed, indicating that heme was being degraded (**Figure 5.1B**). However, when NADPH was added to MhuD-mono heme alone, no heme degradation activity was observed (**Figure 5.1A**). These results demonstrate that there is an electron donor for MhuD in mycobacterium.

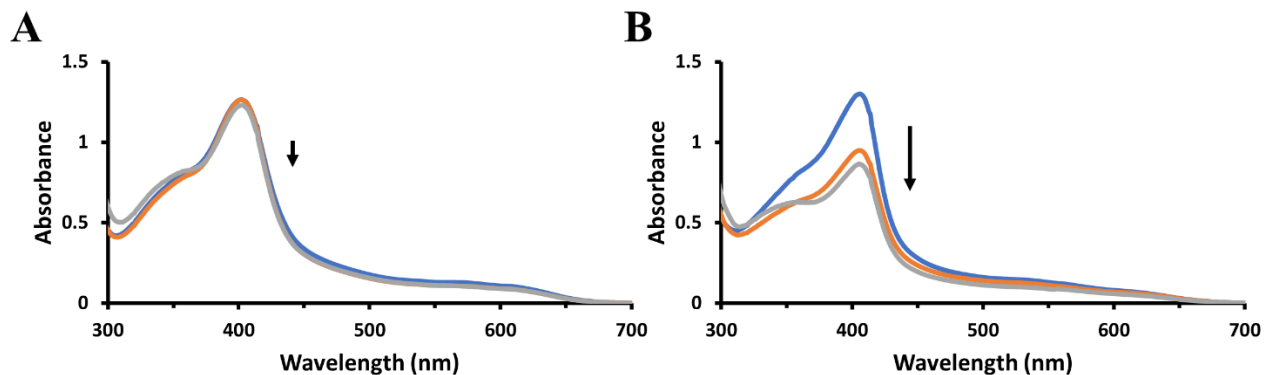


Figure 5.1 Demonstration of the presence of a MhuD electron donor in mycobacterium. NADPH was added to MhuD-mono-heme in the absence of **(A)** and presence of **(B)** the cytosolic fraction from *M. smegmatis*. UV/vis spectra were collected between 300 to 700 after each titration of NADPH. Heme degradation, as evidenced by the decrease in the Soret peak at around 410 nm, was observed when NADPH was added to MhuD-mono-heme in the presence of *M. smegmatis* cytosol **(B)**. No such decrease was observed for MhuD-mono-heme in the absence of mycobacterium cytosolic fraction **(A)**.

Previous studies have identified IruO and NtrA as *S. aureus* IsdG/I electron donors. Blast searches of IruO and NtrA with the Mtb proteome have identified IruO homologs Rv0628c (27% sequence identity), LpdB (Rv0794c, 24% sequence identity), Rv1432 (27% sequence identity), GorA (Rv2855, 24% sequence identity), Rv2997 (33% sequence identity), and TrxB2 (Rv3913, 25% sequence identity) and an NtrA homolog Rv0306 (21% sequence identity) as possible MhuD electron donors (**Figures 5.2, 5.3, and 5.S1-5.S4**). Because TrxB2 is essential for Mtb survival, we decided to test TrxB2 for electron donor activity¹⁰⁻¹². Rv0306 was also tested since it was the only homolog of NtrA in Mtb.

```

IruO      1 . . . . . MKDVTIIGGGPSGLYASFYAGLRDMSVRLIDVQSELGGKMRIY 43
Rv3913    1 MTAPPVHDRAHHPVRDVIIVIGSGPAGYTAALYAARAQLAPLVFEGTSTFGGALMTT 58

IruO      44 PEKI IWD IGGIAPKPCH EILKDTIKQGLYFKPEVHLNERVVDIRKKAERHFETE 99
Rv3913    57 DVENYPGFRNGITGP - - ELMDREMREQALRFGADLRMED - - VESVSLHGPLKSVVTA 108

IruO      100 AGEIYTSKAVIIAIGAGIINPKQLDVKGVERYQLTNLHYVVQSY-RRFKDKDVLIS 154
Rv3913    109 DGQTHRARAVILAMGA - - AARYLQVPGEQELLGRGVSSCATCDGFFFRDQDI AVI 181

IruO      155 GGGNTALDWAHDIAKIAKSVTVVYRKEDVSGHEAMKTLVTDLNVKLCPKTRIKYLV 210
Rv3913    162 GGGDSAMEEATFLTRFARSVTLVHRRDEF RASKIMLDRARNNDKIRFLTN - - HTVV 215

IruO      211 GNDDETHISEVVLEHVESGDRHTVKFDDVVISHGFDRCNTLLSETSSKLDMHDDCR 266
Rv3913    216 AVDGDTTVTGLRVRDNTNTGAETTL PVTGVFVAIGHEPRSGLVREA - - IDVDPDGY 268

IruO      267 VKGFG - NTTTSTIPGIYACGDIVYHDAKSHLIASAFSDGANAANLAKTYIQPDANAE 321
Rv3913    269 VLVQGRTTSTSLPGVFAAGDLVDRTYRQAVTAAG - - SGCAA AIDAERWLAEHAATG 322

IruO      322 GYVSSHHEVFKEANKTIVNKHLY 344
Rv3913    323 - - EADSTDALIGAQR - - - - - 335

```

Figure 5.2 Sequence alignment of IruO with Mtb homolog TrxB2 (Rv3913).

```

NtrA      1 . . . . . MELQQA IANRRSVKKF KRD MHIDDALLYQAIEKAADAPNHGMREPWRV 48
Rv0306    1 MFSAPERRAVYRVIAERRDMRRFVPGGVVSEDLARLLHAAHAAPSVGLMQPWRV 55

NtrA      49 VHVPKDRLG - - - DMSKD I SKFAFPNELDKQQCHYDAVTKLG - - - GMLLLILKTD 96
Rv0306    56 IRITDETLKRR I HALVD DERLLTAEALGAREEEFLALKVEGILDCAELLVVALCD 110

NtrA      97 PR - - - - - QRQNDENYFAFGAYAQNLM LLLYEAGIGTCWKSPLYIYDP - KVRKT 143
Rv0306    111 RRGSYIFGRRTL PQMDLASVSCAIQNLWLAARSEGLGMGWVS - - - LFD PQR LAAL 162

NtrA      144 LGIKKDEVLAGFLYLTDLLEGDMPKAPRKNRN - - - - - LITLY - - - - - 179
Rv0306    163 LAMPADAEPVA I LCLGPVP - EFPDRPALELDGWAYARPLAEFVSEN RWSYPSALA 216

NtrA      . . . . .
Rv0306    217 TDHHHGE 223

```

Figure 5.3 Sequence alignment of NtrA with Mtb homolog Rv0306.

Assaying candidate proteins for MhuD electron donor activity

To determine if IruO homolog TrxB2 was a MhuD electron donors, heme degradation assays were performed with MhuD-mono heme in the presence of TrxB2. In these assays, NADPH and NADH were added into a mixture of MhuD-mono heme and TrxB2. UV/vis spectra were collected between 300 nm and 700 nm to monitor the reaction. No Soret peak decrease was

observed upon the addition of either NADPH or NADH indicating that heme degradation had not occurred and suggesting that the IruO homolog TrxB2 is unable to act as a MhuD electron donor (**Figure 5.4A & 5.4B**).

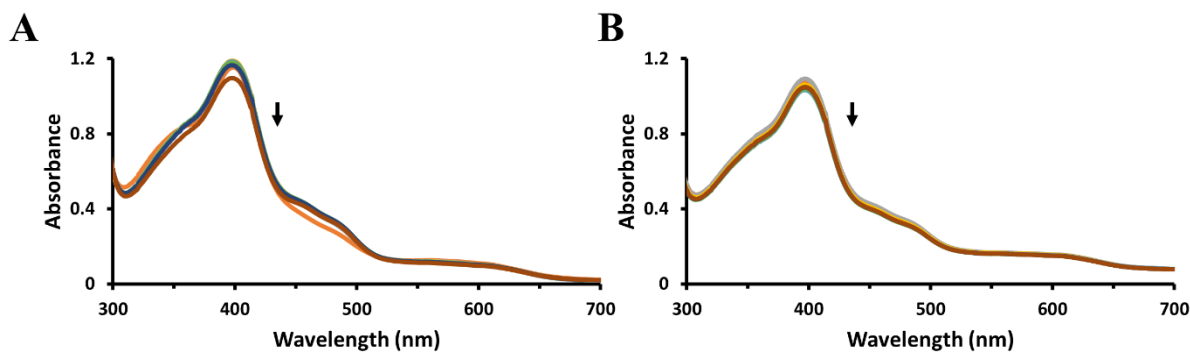


Figure 5.4 UV/vis spectra of MhuD heme degradation assay of 10 μ M MhuD-mono heme performed in the presence of 10 μ M candidate electron donor TrxB2 with 200 μ M of either NADPH (**A**) or NADH (**B**) added. No Soret peak decrease was observed upon the addition of either NADPH or NADH.

NtrA homolog Rv0306 was also tested to assay for MhuD electron donor activity. In these assays, NADPH was added to a mixture of MhuD-mono heme and Rv0306. As before, the reaction was monitored over time spectrophotometrically between 300 and 700 nm. Similar to TrxB2, there was an absence of a Soret peak decrease indicating MhuD heme degradation did not occur (**Figure 5.5A & 5.5B**). This suggests that the protein Rv0306 is not MhuD's cognate electron donor.

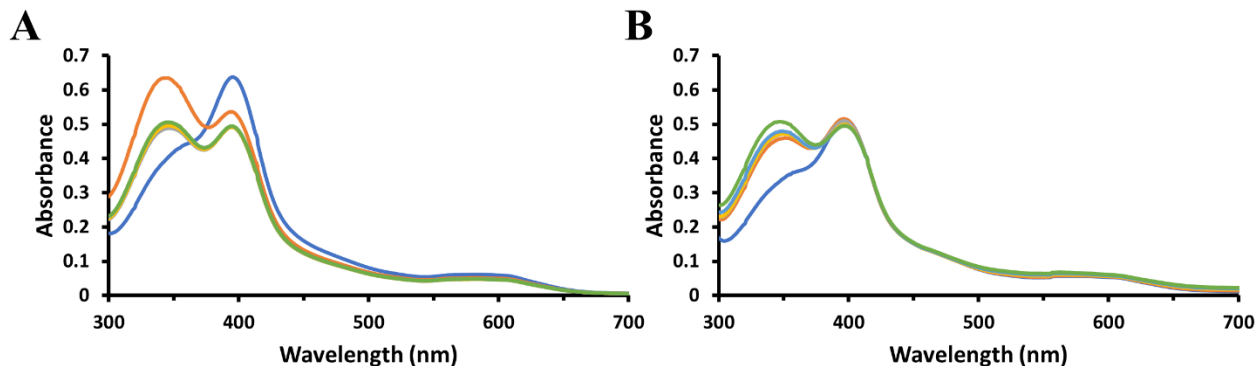


Figure 5.5 MhuD heme degradation assays in the absence (A) and presence (B) of candidate electron donor Rv0306. MhuD-mono-heme (5 μ M) was mixed with 1 μ M Rv0306 prior to the addition of 200 μ M of NADPH. The reaction was monitored using UV/vis spectrometry.

Assaying a candidate protein for MhuD product release

Examination of the MhuD operon revealed a 2-gene operon where the gene encoding for LpqF (Rv3593) that partially overlaps with the one that encodes for MhuD. This MhuD opeonic structure is highly conserved amongst mycobacteria, and suggests that MhuD interacts with LpqF. The LpqF gene is predicted to encode a two-domain protein that is directed to the periplasm. One domain of the protein product is predicted to share homology to β -lactamase and penicillin-binding proteins (PBP), which are known antibiotic targets. Since genes on the same operon are often functionally linked, we suspected that like MhuD, LpqF is involved in Mtb heme-iron metabolism. While LpqF function is unknown, we currently postulate that LpqF facilitates the difficult process of MhuD product release.

To study LpqF, several different constructs of truncated LpqF were cloned and inserted into expression vectors. For these constructs, based on prior literature and predicted domain boundaries, LpqF³⁴⁻⁴⁵², LpqF⁴⁴⁻⁴⁵², and LpqF⁵²⁻⁴⁵² truncation mutants were generated and inserted into pET22a and/or pET28a vectors (**Table 5.1**). Constructs were transformed into

several different *E. coli* strains for expression studies at 37°C or 18°C. The best expression of LpqF was the pET28a 34-452 amino acid truncation construct in BL21 Gold, RIPL, and Rosetta *E. coli* cells when the cells are grown to an O.D. of 0.6 at 37°C and induced with 1 mM IPTG for either 4 h at 37°C or 18 h at 18°C (**Figure 5.6**).

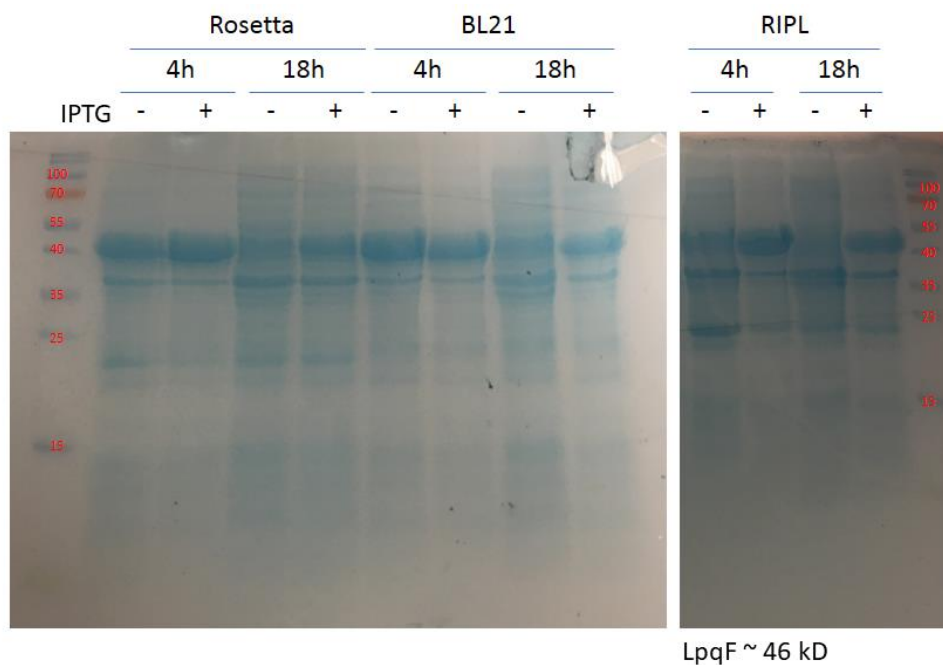


Figure 5.6 SDS-PAGE gel of LpqF expression in BL21 Gold, RIPL, and Rosetta *E. coli* after incubation for 4 h at 37°C or 18 h at 18°C post IPTG induction. Expression from uninduced cultures included for comparison.

LpqF³⁴⁻⁴⁵² was then tested for solubility in 8 different buffers. To test for solubility in a given buffer, *E. coli* cells were spun down and pelleted after expression of our truncated LpqF. Following lysis in the buffer, the lysate was centrifuged and the supernatant run in a SDS-PAGE gel. The LpqF³⁴⁻⁴⁵² construct appear most soluble in 6.0 M urea, 50mM Tris, pH 7.4, 350 mM NaCl, 10% glycerol. Partial protein solubility was observed in the similar buffers with

reduced urea concentrations (**Figure 5.7**). Despite partial or full protein solubility in urea based buffers, efforts to refold LpqF purified proved unsuccessful.

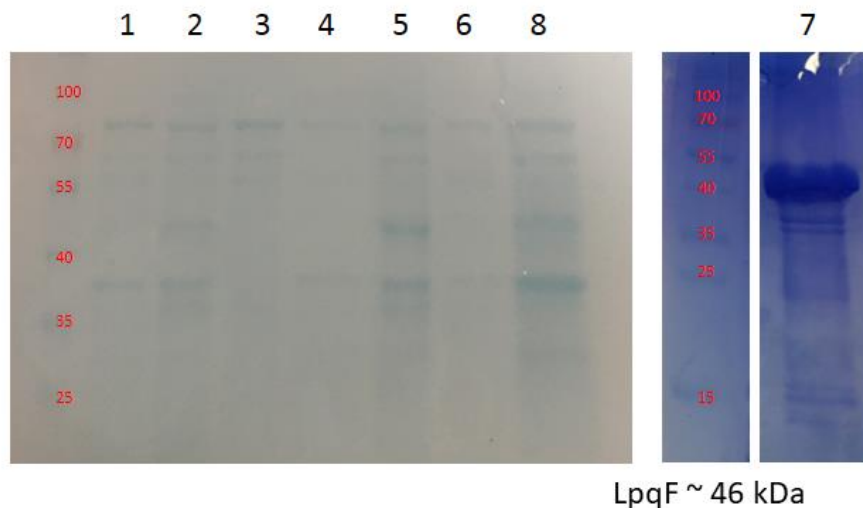


Figure 5.7 SDS-PAGE gel of solubility test of LpqF. LpqF was overexpressed in BL21 (DE3) Gold *E coli* cells and lysed in one of the buffers: (1) 50 mM Tris, pH 7.4, 350 mM NaCl, 10% glycerol; (2) 0.5 M Urea, 50 mM Tris, pH 7.4, 350 mM NaCl, 10% glycerol; (3) 0.2% NP40, 50 mM Tris, pH 7.4, 350 mM NaCl, 10% glycerol; (4) Bugbuster (1x), 50 mM Tris, pH 7.4, 350 mM NaCl, 10% glycerol; (5) 2.0 M Urea, 50 mM Tris, pH 7.4, 350 mM NaCl, 10% glycerol; (6) LDAO 0.2%, 50 mM Tris, pH 7.4, 350 mM NaCl, 10% glycerol; (7) 6.0 M Urea, 50 mM Tris, pH 7.4, 350 mM NaCl, 10% glycerol; (8) 50 mM Tris, pH 7.4, 350 mM NaCl, 2% dodecyl-maltoside. Lysate was centrifuged and the supernatant was run on an SDS-PAGE gel.

Because attempts to purify and refold LpqF³⁴⁻⁴⁵² proved unsuccessful, we attempted to purify folded LpqF³⁴⁻⁴⁵² in 50 mM Tris, pH 7.4, 350 mM NaCl, 10% glycerol via Ni²⁺ affinity chromatography in the presence of 25 μ M heme (**Figure 5.8**). Eluted protein was concentrated and passed through a S75 size exclusion column (**Figure 5.9**). Unfortunately, we were unable to purify LpqF³⁴⁻⁴⁵² truncation construct to a purity sufficient for protein characterization.

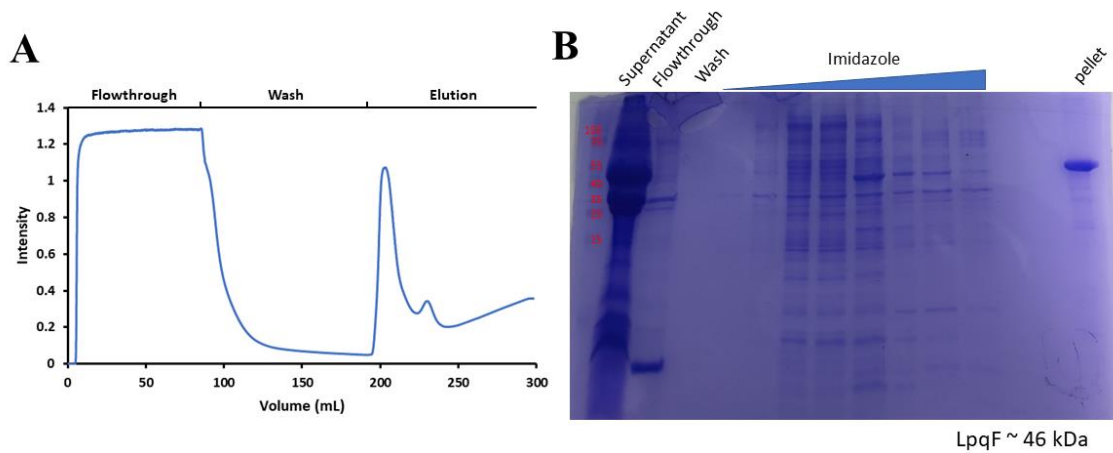


Figure 5.8 Chromatogram (A) and SDS-PAGE gel (B) from LpqF³⁴⁻⁴⁵² Ni²⁺ affinity purification.

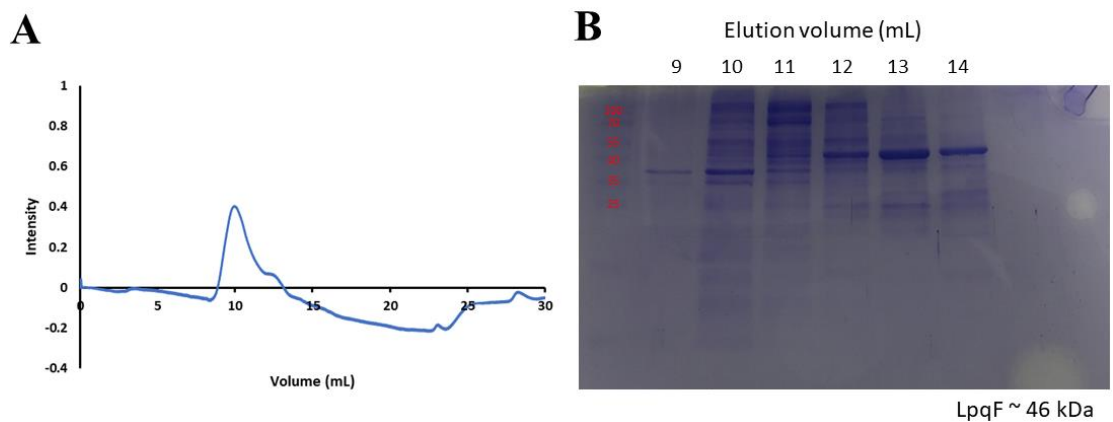


Figure 5.9 Purification of LpqF³⁴⁻⁴⁵² via size exclusion chromatography. (A) Chromatogram of elutions from the size exclusion column. (B) SDS-PAGE of selected elution from LpqF³⁴⁻⁴⁵² size exclusion purification.

Future directions

Further research is needed to identifying the MhuD electron donor and towards understanding the role of LpqF in MhuD function. Prior work in *S. aureus* identified IruO and NtrA as electron donors for MhuD homologs IsdG/I. Based on sequence homology, we identified IruO homologs Rv0628c, LpdB, Rv1432, GorA, Rv2997, and TrxB2 and NtrA

homolog Rv0306 as potential MhuD electron donors. Of the 7 of candidate MhuD electron donors identified, only TrxB2 and Rv0306 have been tested for electron donor activity. Unfortunately, neither TrxB2 nor Rv0306 demonstrated MhuD electron donor activity. Although the rest of the candidate MhuD electron donors have been cloned into vectors, their expression and purification remains to be optimized before testing for electron donor activity.

Because LpqF is located in a two-gene operon with MhuD, we suspect that LpqF plays a role in MhuD function and that it may play a role in MhuD product release. Work is ongoing to optimize expression and purification of LpqF for biochemical and structural characterization. Thus far, the expression and purification of LpqF has proven difficult. In this study, several truncation mutants were generated based on prior literature, structural alignment models, and leader peptide prediction. Of these constructs, only the LpqF³⁴⁻⁴⁵² truncation mutant when cloned into a pET28a vector appeared to express in *E. coli*. While LpqF was soluble under denaturing conditions, removal of the denaturing agent resulted in substantial protein aggregation. We were able to partially purify LpqF in the presence of heme in a native buffer. This suggests that LpqF is capable of binding heme and might not be responsible for MhuD product release, but may instead facilitate the transfer of heme from inner membrane proteins in the heme uptake pathway onto MhuD. This is consistent with the fact that LpqF is predicted to be a two-domain periplasmic protein and would be ideally positioned to interact with the transmembrane proteins of the heme uptake pathway. More work will need to be done to identify suitable purification protocol for the eventual characterization of LpqF.

Materials and Methods

Expression and purification of wild type Mtb MhuD

Purification of his-tagged wild type Mtb MhuD expression was achieved as previously described. In brief, *E. coli* B21-Gold (DE3) cells transformed with pET22b-MhuD vector were grown in LB medium containing 50 µg/mL ampicillin at 37 °C. Overexpression was induced at OD₆₀₀ of ~ 0.6 using 1 mM IPTG. The cells were harvested 4 hours post induction and resuspended in lysis buffer (50 mM Tris/HCl pH 7.4, 350 mM NaCl and 10 mM imidazole). Cells were lysed via sonication and the resulting lysate was centrifuged at 14 krpm and passed through a 1 µm filter. The cell supernatant was loaded onto a Ni²⁺-charged HiTrap chelating column (5 mL) and washed with lysis buffer. Bound protein was eluted from the column with increasing concentrations of imidazole. Next, MhuD, which elutes at 50 and 100 mM imidazole, was concentrated (Amicon, 5 kDa molecular mass cutoff) and was further purified on a S75 gel filtration column in 20 mM Tris, pH 8, and 10 mM NaCl. A final purification step was performed on an ion exchange column (HiTrap Q HP, 5 mL) with the pure MhuD eluting at 150 mM NaCl.

Preparation of MhuD-monoheme

Reconstitution of wild type MhuD with heme was achieved as previously described. Briefly, a hemin solution was prepared by dissolving 4 mg of heme in 500 µL 0.1 M NaOH. After the addition of 500 µL 1 M tris, pH 7.4, the solution was diluted into 15 mL of 50 mM tris, pH 7.4, 150 mM NaCl. Heme was gradually titrated into 100 µM apo-MhuD in a 0.9 heme: 1 MhuD

ratio. The samples were incubated overnight at 4°C before being passed through a desalting column to remove unbound heme. Protein concentrations of the eluted samples were determined via Lowry assay¹³.

Verification of the presence of a MhuD electron donor

The non-pathogenic Mtb model organism *Mycobacterium smegmatis* was cultured in iron deleted 7H9-0.01% tyloxapol for 3 days. Cells were centrifuged and the pelleted cells were washed with prechilled PBST (PBS, 0.05% Tween 20). The washed cells were lysed using glass beads in 50 mM tris pH 7.4, 150 mM NaCl. The resultant lysate was spun down at 14 krpm and the supernatant containing the *M. smegmatis* cytosolic fraction was collected. MhuD-mono-heme (5 µM) was added to the *M. smegmatis* cytosolic fraction prior to the titration of NADPH up to 100 µM in 10 µM increments. Spectra were collected between 300 and 700 nm (DU800, Beckman Coulter) after each titration to monitor the reaction.

Construction of expression vectors

Generation of expression vector was achieved as previously outlined. Primers listed in **Table 5.2** were used to PCR amplify Mtb genes encoding NtrA (Rv0306), Rv0628c, IpdB (Rv0794c), Rv1432, GorA (Rv2855), Rv2997, LpqF (Rv3593), and TrxB2 (Rv3913). PCR products were ligated into pCR-BluntII-TOPO. The resultant plasmids were transformed into E. coli OneShot TOP10 cells for plasmid expression. Restriction enzyme digestions were performed to excise

the gene inserts as well as to cut the target vector, which were ligated together using T4 DNA ligase (NEB).

Table 5.1 Primers used in vector construction

Gene	Construct	Primer Sequence
Rv0306	pET28a::NtrA	Fwd: 5' - GGC ATA TGT TTA GTG CAC CAG AAC GAC GGG - 3' Rev: 5' - GGG GAT CCC TAT TCG CCG TGA TGG TGA TCT GTG GCC - 3'
Rv0628c	pET28a::Rv0628c	Fwd: 5' - GGC ATA TGC GGA TCG GAG TCG GGG TTT CCA CCG C - 3' Rev: 5' - GGA AGC TTT CAG TCG ACG AAC AGC GCC ATC GAC GCG G - 3'
lpdB (Rv0794c)	pET28a::lpdB	Fwd: 5' - GGC ATA TGA CCG CGG CCC AAC AGG ACC AGG CG - 3' Rev: 5' - GGA AGC TTG GCG CGG CGG CGG GTT GGC TAT AC - 3'
Rv1432	pET28a::Rv1432	Fwd: 5' - GGC ATA TGA CGA CCG CGG TCG TCG TCG GAG CC - 3' Rev: 5' - GGA AGC TTT CAA CGT CGC TTG CGC AGC CAC CTC AGC G - 3'
GorA (Rv2855)	pET28a::GorA	Fwd: 5' - GGC ATA TGG AAA CGT ACG ACA TCG CGA TCA TCG GAA CCG GTT CGG G - 3' Rev: 5' - GGA AGC TTT CAA CGC AGG CCA AGC AGC GCG TTT TCC ACC ACC - 3'
Rv2997	pET28a::Rv2997	Fwd: 5' - GGC ATA TGG ACG TCA CCG TCG TCG GCA GCG GAC C - 3' Rev: 5' - GGG AGC TCT TAT GGC CTC AGC TCA TGG CCC AAA GGG GGC ATG C - 3'
LpqF (Rv3593)	pET21a::LpqF ³⁴⁻⁴⁵²	Fwd: 5' - GCC ATA TGT CAG CTC CGA CGC CGT CCG CGA ACG CGG C - 3' Rev: 5' - CGC TCG AGT TGT GGC GCT ATC AAC GCA AAG ACT TGC CTG GCG ACC TGC - 3'
	pET22a::LpqF ³⁴⁻⁴⁵²	Same as the primers for pET21a::LpqF ³⁴⁻⁴⁵²
	pET28a::LpqF ³⁴⁻⁴⁵²	Same as the primers for pET21a::LpqF ³⁴⁻⁴⁵²
	pET28a::LpqF ⁴⁴⁻⁴⁵²	Fwd: 5' - CGC CAT ATG AAT CAC GGG CAC CGG ATC GAC ACC AGA ACT CCG C - 3' Rev: 5' - CCC AAG CTT TTG TGG CGC TAT CAA CGC AAA GAC TTG CCT GGC GAC C - 3'
	pET28a::LpqF ⁵²⁻⁴⁵²	Fwd: 5' - GCC ATA TGA GAA CTC CGC CTG GTC TGC GGG CGC AAC AG - 3' Rev: Same as the Rev primer for pET28a::LpqF ⁴⁴⁻⁴⁵²
TrxB2 (Rv3913)	pET28a::TrxB2	Fwd: 5' - GCC ATA TGA CCG CCC CGC CTG TCC ATG - 3' Rev: 5' - GCA AGC TTT CGT TGT GCT CCT ATC AAT GCG TCG GTA CTG - 3'

Expression and purification of TrxB2

TrxB2 was expressed and purified as previously reported¹⁴. In brief, *E. coli* B21(DE3)-Gold cells with pET22b-TrxB2 vector was grown in Terrific broth with 50 µg/mL ampicillin at 37 °C. Overexpression was induced at OD₆₀₀ of ~ 0.6 using 1 mM IPTG. The cells were harvested

4 hours post induction and resuspended in lysis buffer (50 mM phosphate buffer pH 8, 300 mM NaCl, 5% glycerol, 20 mM imidazole). Cells were lysed via sonication and the resulting lysate was centrifuged at 14 krpm and passed through a 1 μ m filter. The cell supernatant was loaded onto a Ni²⁺-NTA column (5 mL) and the column was washed with lysis buffer. Bound protein was eluted from the column with increasing concentrations of imidazole.

Expression and purification of NtrA

B21-Gold (DE3) cells were transformed with pET28a-NtrA vector and grown in Luria broth with 30 μ g/mL kanamycin at 37°C to an OD₆₀₀ of ~ 0.6 before induction with 1 mM IPTG. Cells were harvested following overnight expression of NtrA for approximately 18 hours at 18°C for lyse in 50 mM tris, 350 mM NaCl, 10% glycerol, 2 M urea via sonication (Lysis buffer). The resulting lysate was clarified via centrifugation at 14 krpm and passage through a 1 μ m filter for purification with Ni²⁺-NTA gravity column. After loading the protein onto the Ni²⁺-NTA column, the column was thoroughly washed with lysis buffer and the bound protein was eluted with increasing concentrations of imidazole. Urea was gradually removed and 5 mM DTT and 0.5 mM EDTA was added with the pure protein fractions via dialysis. Imidazole was gradually dialyzed out of the sample before stepwise dialysis into buffer containing 150 mM NaCl. Lastly, dialysis was used to remove DTT and EDTA from the sample.

Binding FAD to TrxB2 and NtrA

To ensure near 1: 1 stoichiometric ratio of FAD to protein, a two-fold excess of FAD was incubated with TrxB2 or Rv0306 for 1 hour. Protein samples were passed through a desalting column to remove unbound FAD. Protein and FAD concentrations of the desalted samples were measured to ensure near 100 percent FAD loading. Protein concentration was determined using the Lowry assay¹³. SDS denaturation was used to measure FAD concentrations¹⁵. In brief, spectra of a 10 μM TrxB2 or Rv0306 (1mL) in 10 mM tris-HCl, pH 7.5 were collected after addition of a 10% SDS solution (20 μL). FAD concentrations were calculated using $\epsilon_{450} = 11,300 \text{ M}^{-1}\text{cm}^{-1}$.

Testing TrxB2 and NtrA for electron donor activity

To test TrxB2 and Rv0306 for electron donor activity, heme degradation assays were performed in the presence of a candidate electron donor. In these assays, 10 μM of TrxB2 was mixed with 10 μM of MhuD-mono-heme, to which 200 μM of either NAPDH or NADH was added. Similar reactions were performed using 1 μM of Rv0306 and 5 μM of MhuD-mono-heme. The reactions were monitored spectrophotometrically between 300 and 700 nm with spectra collected at regular intervals for 30-45 minutes.

Expression of LpqF

Vectors encoding the LpqF truncation mutants were transformed into BL21 (DE3)-Gold, BL21 (DE3)-C41, BL21 (DE3)-C43, BL21 (DE3)-Rosetta-gami B, and BL21 CodonPlus (DE3)-RIPL *E. coli* cells. Transformed cells were grown in Luria broth with 30 µg/mL kanamycin at 37°C to an OD₆₀₀ of ~ 0.6 before induction with 1 mM IPTG. Duplicate cultures were also grown concurrently without the addition of IPTG. Following incubation either for 4 hours at 37°C or overnight at 18°C, 1 mL aliquots of cells were pelleted and lysed via sonication in 6.0 M Urea, 50 mM Tris, pH 7.4, 350 mM NaCl, 10% glycerol. Lysates were loaded and run on SDS-PAGE gels for analysis.

Testing the solubility of LpqF

B21-Gold (DE3) cells containing vectors for LpqF expression were grown in Luria broth with 30 µg/mL kanamycin at 37°C to an OD₆₀₀ of ~ 0.6 before induction with 1 mM IPTG. Following overnight expression of NtrA for approximately 18 hours at 18°C, 1 mL aliquots of cells were pelleted and lysed in 200 µL of various lysis buffers. The lysates were centrifuged and supernatants were run on an SDS-PAGE gel.

Expression and partial purification of LpqF

B21-Gold (DE3) cells transformed with the pET28a-LpqF³⁴⁻⁴⁵² vector were grown in LB medium containing 30 µg/mL kanamycin at 37 °C. Overexpression was induced at OD₆₀₀ of

~ 0.6 using 1 mM IPTG. The cells were harvested 18 hours post induction and resuspended in lysis buffer (50 mM Tris/HCl pH 7.4, 350 mM NaCl and 10% glycerol) supplemented with 25 μ M of heme. Cells were lysed via sonication and the resulting lysate was centrifuged at 14 krpm and passed through a 1 μ m filter. The cell supernatant was loaded onto a Ni²⁺-charged HiTrap chelating column (5 mL) and washed with lysis buffer. Bound protein was eluted from the column with increasing concentrations of imidazole. Next, the eluted protein was concentrated (Amicon, 5 kDa molecular mass cutoff) and passed through a S75 gel filtration column equilibrated with lysis buffer.

References

- [1] Schacter, B. A., Nelson, E. B., Marver, H. S., and Masters, B. S. (1972) Immunochemical evidence for an association of heme oxygenase with the microsomal electron transport system, *J Biol Chem* 247, 3601-3607.
- [2] Loutet, S. A., Kobylarz, M. J., Chau, C. H., and Murphy, M. E. (2013) IruO is a reductase for heme degradation by IsdI and IsdG proteins in *Staphylococcus aureus*, *J Biol Chem* 288, 25749-25759.
- [3] Hannauer, M., Arifin, A. J., and Heinrichs, D. E. (2015) Involvement of reductases IruO and NtrA in iron acquisition by *Staphylococcus aureus*, *Mol Microbiol* 96, 1192-1210.
- [4] Tavares, A. F., Nobre, L. S., Melo, A. M., and Saraiva, L. M. (2009) A novel nitroreductase of *Staphylococcus aureus* with S-nitrosoglutathione reductase activity, *J Bacteriol* 191, 3403-3406.
- [5] Nambu, S., Matsui, T., Goulding, C. W., Takahashi, S., and Ikeda-Saito, M. (2013) A new way to degrade heme: the *Mycobacterium tuberculosis* enzyme MhuD catalyzes heme degradation without generating CO, *J Biol Chem* 288, 10101-10109.
- [6] McDonagh, A. F., Palma, L. A., and Schmid, R. (1981) Reduction of biliverdin and placental transfer of bilirubin and biliverdin in the pregnant guinea pig, *Biochem J* 194, 273-282.
- [7] Barker, K. D., Barkovits, K., and Wilks, A. (2012) Metabolic flux of extracellular heme uptake in *Pseudomonas aeruginosa* is driven by the iron-regulated heme oxygenase (HemO), *J Biol Chem* 287, 18342-18350.
- [8] Caignan, G. A., Deshmukh, R., Wilks, A., Zeng, Y. H., Huang, H. W., Moenne-Loccoz, P., Bunce, R. A., Eastman, M. A., and Rivera, M. (2002) Oxidation of heme to beta- and delta-biliverdin by *Pseudomonas aeruginosa* heme oxygenase as a consequence of an unusual seating of the heme, *Journal of the American Chemical Society* 124, 14879-14892.
- [9] Barry, C. E., III. (2001) *Mycobacterium smegmatis*: an absurd model for tuberculosis?, *Trends in Microbiology* 9, 473-474.
- [10] Harbut, M. B., Vilcheze, C., Luo, X., Hensler, M. E., Guo, H., Yang, B., Chatterjee, A. K., Nizet, V., Jacobs, W. R., Jr., Schultz, P. G., and Wang, F. (2015) Auranofin exerts broad-spectrum bactericidal activities by targeting thiol-redox homeostasis, *Proc Natl Acad Sci U S A* 112, 4453-4458.
- [11] Zhang, Y. J., Ioerger, T. R., Huttenhower, C., Long, J. E., Sasseti, C. M., Sacchettini, J. C., and Rubin, E. J. (2012) Global assessment of genomic regions required for growth in *Mycobacterium tuberculosis*, *PLoS Pathog* 8, e1002946.
- [12] Griffin, J. E., Gawronski, J. D., Dejesus, M. A., Ioerger, T. R., Akerley, B. J., and Sasseti, C. M. (2011) High-resolution phenotypic profiling defines genes essential for mycobacterial growth and cholesterol catabolism, *PLoS Pathog* 7, e1002251.
- [13] Lowry, O. H., Rosebrough, N. J., Farr, A. L., and Randall, R. J. (1951) Protein measurement with the Folin phenol reagent, *J Biol Chem* 193, 265-275.
- [14] Akif, M., Chauhan, R., and Mande, S. C. (2004) Expression, purification, crystallization and preliminary X-ray crystallographic studies of *Mycobacterium tuberculosis* thioredoxin reductase, *Acta Crystallogr D Biol Crystallogr* 60, 777-779.
- [15] Aliverti, A., Curti, B., and Vanoni, M. A. (1999) Identifying and Quantitating FAD and FMN in Simple and in Iron-Sulfur-Containing Flavoproteins, In *Flavoprotein*

Protocols (Chapman, S. K., and Reid, G. A., Eds.), Humana Press Inc., Totowa, New Jersey.

Supplemental information

```

IruO          1 MKDVTIIGGGPSGLYASFYAGLR...DMSVRLIDVQSELGGKMRIYPEKIIWDI 51
Rv0628c      1 MRIGVGVSTAPDVRRAAAEAAAHAAREELAGGTPALAVLLG...SRSHTDQAVDLL 52

IruO          52 GG IAPKPCHEILKDTIKQGLYFKPEVHLNERVVDIRKKAERHFE...VETE 99
Rv0628c      53 AAVQASVEPAALIGCVAQGIVAGRHELENEPAVAVWLASGPPAETFHLDFVRTG 106

IruO          100 AGEIYT...SKAVIIAIGAGIINPKQLDVKGVER...YQLTNLHYVVQSYR 144
Rv0628c      107 SGALITGYRFDRTAHLHLHLLLPDPYSFSPNLLIEHLNTDLPQTTVVGGVVSGGR 160

IruO          145 R...FKDKDVLISGGNTALDWAHDIAKIAKSVTVVYRKEDVSGHEAMKTL 192
Rv0628c      161 RRGDTRLFRDRDVLTSGLVGVRLPGAHSVSVVSQGCRI GEPYIVTGADGAVIT 214

IruO          193 VTDLNVKLCPKTRIKYLVGNDDETHISEVVLEHVESGDRHTVKFDDVISHGF 246
Rv0628c      215 ELGGRPPLHRLREIVLGMAPDEQELVSRGLQIGIVVDEHLAVPGQGDFLIRGLL 268

IruO          247 RCN...TLLSETSSKLDMHDDCRVKG...FGNTTTSIPGIYACGD 285
Rv0628c      269 GADPTTGAIGIGEVVEVGATVQFQVRDAAAADKDLRLAVERAAAELPGPPVGG 322

IruO          286 IVYHDAKS-HL IASAFSDGANAANLAKTYIQP...DANAEGYVSSHHEVFKEAN 335
Rv0628c      323 LFTCNGRGRRMFGVTDHDASTIEDLLGGIPLAGFFAAGEIGPVAGHNALHGF 376

IruO          336 KTI VNKHLY 344
Rv0628c      377 SMALFVD - 383

```

Figure 5.S1 Sequence alignment of *IruO* with *Mtb* homolog *Rv0628c*.

```

IruO          1 .....MKDVTIIGGGPSGLYASFYAGLRDMSVRLID...V 32
Rv0794c      1 MTAAQQDQAPMATPGCREGETYDVVVVLGAGPVGQNVADRARAGGLRVAVVERELV 55

IruO          33 QSELGGKMRIYPEKIIWDIGG IAPKPCHEILKDTIKQGLYFKPEVHLNERVVDIR 87
Rv0794c      56 GGECSYWACVPSKALLRPVIAISDARRVDGAREAVDGSINTAGVFGRNRVVAHW 110

IruO          88 KKAER...HFEVETEAGEIYTSKAVIIAIGAG...IINPKQLDVKGVERY 131
Rv0794c      111 DDTGQADWVSGIGATLIRGDGRLDGPRRVVVTKSSGESVALTARHAVVIC TGSRP 165

IruO          132 QLTNLHYVVQS...YRRFKD...KDVLSGGNTALDWAHDIAKIAKSVTVV 177
Rv0794c      166 ALPDLPGITEARPWTNRQATDNSTVDPDLAIVGAGGVGVEMATAWQGLGASVTLL 220

IruO          178 YRKEDVSG...HEAMKTLVTDLNVKLCPKTRIKYLVGNDDETHISEVVLEHVESGD 230
Rv0794c      221 ARGSGLLPRMEPFV GELIGRGLADAGVDVRVGVSVRALGRPNPTGPPVLELDDG 274

IruO          231 RHTVKFDDVISHG-FDRCNTLLSETS...SKLDMHDDCRVKGFGN... 272
Rv0794c      275 -TELRVDEVLFATGRAPRTDDIGLETIGLTPGSWLDVDDTCRVRVAVDDGWLYAAG 328

IruO          273 .....TTTSSIPGIYACG.....DIVYHDAKSHLIASAFSD 302
Rv0794c      329 DVNHRALLTHQGKYQARIAGTAIGARAAGRPLD TTSWGMHATTADHHA VPQAFFT 383

IruO          303 GANAANLAKTYIQPDAN.....AEGYVSSHHEVFKEAN 336
Rv0794c      384 DPEAAAVGLTADQAAQAGHR IKAIDVEIGDVVMGAKLFA DGYTGRARMVVDVDRG 438

IruO          337 TIVNKHLY..... 344
Rv0794c      439 HLLGVMTMVGPGAAELLHSATVAVAGQVPIDRLWHAVPCFPTISELWLRLLLESYRD 493

IruO          ..... 344
Rv0794c      494 SFYLLV 499

```

Figure 5.S2 Sequence alignment of *IruO* with *Mtb* homolog *IpdB* (*Rv0794c*).

```

IruO          1 MKDVT I IGGGPSGLYASFYAGLRDMSVRLIDVQSELGGKMR..... 41
Rv1432       1 MTTAVVVVAGP NGLAAA IHLARHGVDVQVLEARDT IGGGARSGELTVPGV IHDHCS 58

IruO          42 ..... IYP 44
Rv1432       57 AFHPLGVGSPFWAAIDLQRYGLTWKWPDVDCAHPLDDGTAGVLYRSIEATAAGLGP 112

IruO          45 EK I IWD - - IGG IAP - - - KPCHEILKDT I KQG - - - - - LYFKPEVHLNERVVDIRKK 89
Rv1432       113 DGKRWQRAVGD LAAGFDELAEDLLRPV L NMPRHP IRLARFGPRAALPATAMARRFH 168

IruO          90 AERHFVEVET - EAGEIYT - - SKAV I I A I G A G I I N P K Q L D - - - - V K G V E R Y Q L T N L H Y 138
Rv1432       169 TERARALFGGAAAHVYTR LDRPLTASLGLMILASGHRHGWPVARGGSGSITKALAA 224

IruO          139 VVQSYRRFKDKDVLISGGGNTALDWAHDI AKI AKSVTVVYRKEDVS - - - GHEAMK 190
Rv1432       225 ALDAYGGTVATGVTVTSRRDIPDADIVMLDLSPAAVLGIYGDVMPTRINRSYRRYR 280

IruO          191 TLVTDLNLVKLCPKTRIKYLVGNDDETHISEVVLEHVESGDRHTVKFDDVVIISHGF 246
Rv1432       281 AGSSAFKVDFAIEGDVGTWNPDCRRAGTVHLGGTFAE IADTERQRAQGT MVQRPFV 336

IruO          247 RC - NTL LSETSSKLDMHDDCRVKG - - - FGNTTTSIPGIYACGDIVYHDAKSHL IAS 298
Rv1432       337 LVGQQYLADPSRSVGNINPIWAYAHVVPFGYTGDATAAVIDQIERFAPGFRDRIVAT 392

IruO          299 AFSDGANAA NLAKTYIQ - - - - - PDANAEGYVSSHHEVFK EANKTI 338
Rv1432       393 VSTSTTELQTYNRF IGGDI IGGANDRLQVIFRPRVAVDPYAIGVPGVYLCSQSAP 448

IruO          339 VNKHLY - - - - - 344
Rv1432       449 PGAGIHGLCGYHAAESALRWLRKRR 473

```

Figure 5.S3 Sequence alignment of IruO with Mtb homolog Rv1432.

```

IruO          1 .. MKDVT I IGGGPS ..... GLYASFYAGLRDMSVRLIDVQSEL 36
Rv2855       1 METYDIA I IGTGSGNS ILDERYASKRAAICEQGTFGGTCLNVGCIPTKMFVYAAEV 58

IruO          37 G G K M R - - - - - I Y P E K I I W D I G G I A P K P C H E I L K D T I K Q G L Y F K P E V H L N E R V V 84
Rv2855       57 A K T I R G A S R Y G I D A H I D R V R W D D V V S R V F G R I D P I A L S G E D Y R R C A P N I D V Y R T H T 112

IruO          85 D I R - K K A E R H F E V E T E A G E I Y T S K A V I I A I G A G I I N P K Q L D V K G V E R Y Q L T N L H Y V 139
Rv2855       113 R F G P V Q A D G R Y L L R T D A G E E F T A E Q V V I A A G S R P V I P P A I L A S G V D Y H T S D T V M R I 168

IruO          140 V Q S Y R R F K D K D V L I S G G G N T A L D W A H D I A K I A K S V T V V Y R K E D V S G H E A M K T L V T D 195
Rv2855       169 A E L P - - - - - E H I V I V G S G F I A A E F A H V F S A L G V R V T L V I R G - S C L L R H C D D T I C E R 218

IruO          196 L N V K L C P K T R I K Y L V G N D D E T H I S E V V L E H V E S G D R H T V K F D D V I I S H G F D R C N T L 251
Rv2855       219 F T R I A S T K W E L R T H R N V V D G Q Q R G S G V A L R L D D G - - C T I N A D L L L V A T G R V S N A D L 272

IruO          252 L S E T S S K L D M H D D C R V K G F G N T T T S I P G I Y A C G D I V Y ..... 288
Rv2855       273 L D A E Q A G V D V E D - G R V I V D E Y Q R T S A R G V F A L G D V S S P Y L L K H V A N H E A R V V Q H N L 327

IruO          289 ..... H D A K S H L I A S A F S D G A N A A N ..... 308
Rv2855       328 L C D W E D T Q S M I V T D H R Y V P A A V F T D P Q I A A V G L T E N Q A V A K G L D I S V K I Q D Y G D V A 383

IruO          309 ..... L A K T Y I Q P D A N A E G Y V S S H H E V F K - 332
Rv2855       384 Y G W A M E D T S G I V K L I T E R G S G R L L G A H I M G Y Q A S S L I Q P L I Q A M S F G L T A A E M A R G 439

IruO          333 - - - - - E A N K T I V N K H L Y - - - 344
Rv2855       440 Q Y W I H P A L P E V V E N A L L G L R 469

```

Figure 5.S4 Sequence alignment of IruO with Mtb homolog GorA (Rv2855).

```

IruO          1 MKDVT I IGGGPSGLYASFYAGLRDMSVRLIDVQSELGGKMR - - - - IYPEKI IWDI 51
Rv2997       1 -MDVTVVVGGSPNGLATAVICARAGLNVQVVEAQATFGGGARSAADEFEPVLDHVC 55

IruO          52 GGIAP - - - - - KPCHEILKDTIKQGLYFK 74
Rv2997       56 SAVHPLALASPFFAEFDLPARGVTLTVPDIAYANPLPGRPAAIAYHDLAHTCAKLD 111

IruO          75 PEVHLNERVVDIRKKAERHFEEVETEAG - EIYTSKAVIIAIGAGIINPKQLDVKGV E 129
Rv2997      112 DGASWRRLLGPLVAHSETVVEFMLS DKRSLPTALGSLRLGLRMLAQGTPAWRSLA 167

IruO          130 RYQLTNLHYVVQSYRRFKDKDVLISGGGNTALDWAHDI - - - - - 167
Rv2997      168 GEDARALFTGVAAHAISPLPSLVSAGAGLMLATLAHSVGPWPVPVGGTQAIADALIA 223

IruO          168 - - - - - AKIAKSVTVVYRKEDVSGHEAMKTLVTDLNVKLCPKTRIKYLVGN - - - - 212
Rv2997      224 DLRAHGGRLAAGVEITEPQRSVVVFDTAPTALLRVYRDKLP HRYAKALRRYRFRA G 279

IruO          213 - - - - - DDETHISEV VLEHVE - - - - SDRHTVKFDDVIISHGFDRCNTLLSETS 256
Rv2997      280 IAKVDFVLSDEIPWSDPRLRRAATLHLGGTRDQMARAEADVAAGRHADWPMVLAAC 335

IruO          257 SKLDMHDDCRVKG - - - - - FGNTTTSIPGIYACGDIVYHDAKSHLIASAFS 301
Rv2997      336 PHVADPGRIDETGRRPFWTYAHVPSGSTLDATETVTSVLERFAPGFRDIVVAARAV 391

IruO          302 DGANAANLAKTYIQPDANAEG - - - - YVSSHHEVFK EANKTIVNKHLY - - - - 344
Rv2997      392 PAARMADHNANYVGGDITVGANSTWRAIAGPTPRLNPWRTPIPKVYLC SAATPPGA 447

IruO          - - - - -
Rv2997      448 GVHGMCGWYAARTLLRTEFGITRMPPLGHEL RP 480

```

Figure 5.S5 Sequence alignment of IruO with Mtb homolog Rv2997.

CHAPTER 6

Closing Remarks and Future Directions: Understanding MhuD and its Role in Mtb Heme Uptake

Summary

The enzyme MhuD is an integral part of iron metabolism in *Mycobacterium tuberculosis* (Mtb)^{1,2}. Within the Mtb cytosol, MhuD is responsible for the degradation of heme and the liberation of iron resulting in distinct mycobilin products^{2,3}. While much has been reported in the literature about MhuD, much remains unknown about Mtb's heme degrading enzyme MhuD. Here we present work to both biochemically and structurally characterize MhuD in an effort to better understand the factors behind MhuD heme degradation and product uniqueness as well as preliminary work towards the identification and characterization of MhuD's protein partners.

Role of heme ruffling in MhuD reactivity

While the crystal structure of MhuD in its inactive diheme form has previously been solved², the structure of MhuD in its monoheme form has remained elusive. Though derivatization of the heme with cyanide, we were able to solve the crystal structure of MhuD in its monoheme form. Close examination of the heme molecule within the MhuD-monoheme structure

revealed that similar to MhuD homologs IsdG/I the heme is ruffled^{4, 5}. Previous studies of IsdG/I suggest that this heme ruffling in fact is important in IsdG/I reactivity⁵⁻⁸. Mutations to apparent heme ruffling residues Phe23 and Trp66 abolished MhuD's heme degradation activity suggesting that heme ruffling is important in MhuD heme degradation. This research has allowed us to understand the factors important for non-canonical MhuD heme degradation.

Single mutation alters MhuD's heme degradation product

Close examination of the active site of the MhuD-mono-heme structure also revealed that the heme molecule is rotated $\sim 90^\circ$ about the tetrapyrrole plane from the heme molecules in MhuD homologs IsdG/I^{4, 5}, which may be responsible for MhuD's distinct mycobilin products. Two arginine residues potentially responsible of MhuD's altered heme orientation were identified. Interestingly, mutation of one the arginines, Arg26, to serine resulted in new heme degradation products, biliverdin and formaldehyde, instead of the MhuD mycobilin isomers. Despite our best attempts, we could only the MhuD R26S mutant in its di-heme form and not its mono-heme form. This propensity to crystalize as a di-heme along with spectroscopic characterization suggests heme ruffling is reduced in the MhuD R26S mutant, which may be the cause for the mutant's altered degradation products. The single residue mutation is also suspected to alter the electrostatic environment of the active site thus changing the reduction potential of the heme iron; however, this speculation remains to be tested. Additional experiments are required to understand the role of the Arg26 residue in product specificity.

Role of heme degradation enzymes in pharmacological inhibition of Mtb growth by tin-protoporphyrin IX

Prior work has implicated the heme degrader human heme oxygenase-1 (hHO-1) as a potential target for host directed therapy against Mtb⁹. Here, we show that adjunctive administration of known hHO-1 inhibitor and heme analog tin-protoporphrin IX (SnPPIX) can inhibit Mtb growth *in vivo*¹⁰. Because the precise mechanism of action for SnPPIX-mediated Mtb growth inhibition in a mouse model was unknown, activity assays were performed to determine if SnPPIX inhibited MhuD in addition to inhibiting hHO-1. Results show that whereas SnPPIX inhibits hHO-1, it does not inhibit MhuD, demonstrating SnPPIX acts through a host directed mechanism. Although the work is just starting, the results presented here may represent the initial steps towards a novel class of effective anti-TB treatments.

Towards the identification of MhuD interaction partners

To date, the protein partners of MhuD are unknown. We hypothesize that the existence of a MhuD electron donor as well as a protein partner involved in MhuD product release. We've identified several candidate electron donors as well as a potential product release protein. Thus far, we've expressed, purified, and tested two candidate electron donors, neither of which demonstrated electron donor activity with MhuD. Meanwhile, our attempts at expression, solubilization, and purification of a potential product release protein LpqF have

proven unsuccessful. More work will need to be done to identify and eventually characterize MhuD's protein partners.

Concluding Remarks

The research documented in this work has led to a better understanding the fundamentals of MhuD heme degradation and possibly of aerobic heme degradation in general. Additionally, we have identified several residues important for MhuD heme degradation or product uniqueness. Of note, we have shown that heme ruffling is important for normal MhuD heme degradation and we found that the R26S mutation alters the heme degradation product of MhuD. We have also begun work towards the identification of MhuD's elusive protein partners. The identity and nature of these protein partners represent a massive gap in knowledge that must be filled before MhuD and the heme uptake pathway can be fully understood.

References

- [1] Tullius, M. V., Harmston, C. A., Owens, C. P., Chim, N., Morse, R. P., McMath, L. M., Iniguez, A., Kimmey, J. M., Sawaya, M. R., Whitelegge, J. P., Horwitz, M. A., and Goulding, C. W. (2011) Discovery and characterization of a unique mycobacterial heme acquisition system, *Proc Natl Acad Sci U S A* 108, 5051-5056.
- [2] Chim, N., Iniguez, A., Nguyen, T. Q., and Goulding, C. W. (2010) Unusual diheme conformation of the heme-degrading protein from *Mycobacterium tuberculosis*, *J Mol Biol* 395, 595-608.
- [3] Nambu, S., Matsui, T., Goulding, C. W., Takahashi, S., and Ikeda-Saito, M. (2013) A new way to degrade heme: the *Mycobacterium tuberculosis* enzyme MhuD catalyzes heme degradation without generating CO, *J Biol Chem* 288, 10101-10109.
- [4] Graves, A. B., Morse, R. P., Chao, A., Iniguez, A., Goulding, C. W., and Liptak, M. D. (2014) Crystallographic and spectroscopic insights into heme degradation by *Mycobacterium tuberculosis* MhuD, *Inorg Chem* 53, 5931-5940.
- [5] Lee, W. C., Reniere, M. L., Skaar, E. P., and Murphy, M. E. (2008) Ruffling of metalloporphyrins bound to IsdG and IsdI, two heme-degrading enzymes in *Staphylococcus aureus*, *J Biol Chem* 283, 30957-30963.
- [6] Ukpabi, G., Takayama, S. J., Mauk, A. G., and Murphy, M. E. (2012) Inactivation of the heme degrading enzyme IsdI by an active site substitution that diminishes heme ruffling, *J Biol Chem* 287, 34179-34188.
- [7] Takayama, S. J., Loutet, S. A., Mauk, A. G., and Murphy, M. E. (2015) A Ferric-Peroxo Intermediate in the Oxidation of Heme by IsdI, *Biochemistry* 54, 2613-2621.
- [8] Takayama, S. J., Ukpabi, G., Murphy, M. E., and Mauk, A. G. (2011) Electronic properties of the highly ruffled heme bound to the heme degrading enzyme IsdI, *Proc Natl Acad Sci U S A* 108, 13071-13076.
- [9] Andrade, B. B., Pavan Kumar, N., Mayer-Barber, K. D., Barber, D. L., Sridhar, R., Rekha, V. V., Jawahar, M. S., Nutman, T. B., Sher, A., and Babu, S. (2013) Plasma heme oxygenase-1 levels distinguish latent or successfully treated human tuberculosis from active disease, *PLoS One* 8, e62618.
- [10] Costa, D. L., Namasivayam, S., Amaral, E. P., Arora, K., Chao, A., Mittereder, L. R., Maiga, M., Boshoff, H. I., Barry, C. E., 3rd, Goulding, C. W., Andrade, B. B., and Sher, A. (2016) Pharmacological Inhibition of Host Heme Oxygenase-1 Suppresses *Mycobacterium tuberculosis* Infection In Vivo by a Mechanism Dependent on T Lymphocytes, *MBio* 7.